Developmental neurodegeneration requires axoplasmic Ca^{2+} influx via TrpV1

Aaron Johnstone
Integrated Program in Neuroscience
McGill University, Montreal

A thesis submitted to McGill University in partial fulfillment
of the requirements of the degree of PhD Neuroscience

Table of Contents

Abstract

Plasticity of neural structures, from synapses to neurites to entire neurons and networks, depends on tightly regulated equilibrium between cytoskeleton polymerization and depolymerisation mediated by protease activity. The conservation of signaling pathways governing cytoskeletal plasticity raises the prospect that understanding apoptotic-like degeneration can be leveraged to guide hypotheses exploring non-lethal sub-neuronal plasticity events in both the normal physiological functioning of the nervous system, and also in the earliest changes during neurodegenerative disease to halt their progression. Neurite pruning and neuronal cell death that occur normally during embryonic development establish and refine nervous systems into their mature patterning. Components of the same destructive signaling pathways appear to underlie neurodegenerative diseases such as Alzheimer's, Parkinson's and ALS when aberrantly reactivated in adulthood. The emerging overlap between developmental and pathological mechanisms of neurodegeneration suggests that therapeutic opportunities will be revealed by understanding the sequence of molecular events culminating in degeneration of neurites and entire neurons. Developmental axon degeneration can be modeled *in vitro* by nerve growth factor (NGF) withdrawal from dorsal root ganglion (DRG) neurons. We have used this model system together with a novel method of quantification to examine the role of Ca^{2+} influx in developmental axonal degeneration. We find that NGF deprivation from DRG sensory neurons induces a robust increase in axonal Ca^{2+} prior to membrane blebbing and degeneration. Chelation of divalent cations using EDTA rescues axons from degeneration when present for the final phase of NGF deprivation, indicating that cation influx plays a key role late in the degeneration cascade. Axon degeneration is significantly rescued by pharmacological inhibitors of Ca^{2+} channels, including capsazepine, an antagonist of transient receptor potential family member vanilloid 1 (TrpV1)-mediated Ca^{2+} flux, whereas inhibition of Na^{+} action potentials does not rescue axons. Cultured sensory neurons

derived from TrpV1-null mouse embryos are partially rescued from degeneration, indicating a pro-degenerative role for TrpV1 *in vitro*. We hypothesized that reactive oxygen species (ROS) mediate the activation of TrpV1 in this setting and consistent with this, ROS-scavengers and Nox complex inhibitors rescue axons from degeneration. Nox complexes are typically activated by PKC and we show that PKC inhibitors block degeneration whereas PMA, a PKC activator, induces potent NOX- and ROS- dependent activation of TrpV1-dependent Ca^{2+} currents in DRG axons. We conclude that a PKC>Nox>ROS>TrpV1 axis induces toxic Ca^{2+} overload to drive developmental axon degeneration.

Résumé

La plasticité des structures neuronales -des synapses aux neurites jusqu'aux neurones et réseaux neuronaux- dépends d'une balance finement régulée entre polymérisation et dépolymérisation du cytosquelette par les protéases. La conservation des voies de signalisations gouvernant la plasticité du cytosquelette suggère que la compréhension des mécanismes de dégénération de type apoptotique peut être un levier à de nouvelles hypothèses. Celles-ci pourraient permettre d'explorer les événements de plasticité au niveau sub-neuronale et non létale tant au niveau physiologique qu'au niveau des maladies neurodégénératives.

Dans le but d'établir un système nerveux mature, le raffinement des neurites et la mort cellulaire neuronales sont des événements communs pendant le développement embryonnaire. Cependant, les mêmes composants de ces voies de signalisation destructrices sont impliqués dans les maladies neurodégénératives comme la maladie d'Alzheimer et la maladie de Parkinson ou encore lors de sclérose latérale amyotrophique. Les points communs entre les mécanismes de dégénération neuronale aux niveaux physiologiques et pathologiques suggèrent que des opportunités thérapeutiques vont être dévoilées si nous parvenons à comprendre la séquence des événements moléculaires qui aboutissent à la dégénération des neurites et des neurones. La dégénération axonale pendant le développement peut être réalisée *in vitro* en privant les neurones ganglionnaires de la racine dorsale (DRG) du facteur de croissance neuronal (NGF). Nous avons utilisé ce model en plus d'une nouvelle méthode de quantification pour examiner le rôle de l'influx calcique dans la dégénération axonale. Nous avons trouvé que la privation de NGF des neurones ganglionnaires de la racine dorsale induit une forte augmentation du calcium dans les axones, juste avant l'apparition de bourgeonnement et de la dégénération. La chélation des ions divalent par l'EDTA dans la phase finale de la privation du NGF protège les axones de la dégénération, indiquant que l'influx de cation joue un rôle majeur tardivement

dans la cascade dégénérative. De plus, la dégénération axonale est significativement protégée par des inhibiteurs de canaux calciques dont la capsazepine – un antagoniste des canaux dit potentiel transitoire récepteur (Trp) de la famille vanilloid 1 (TrpV1) - alors que l'inhibition des canaux sodiques sensibles au voltage ne protège pas les axones. Les neurones sensoriels provenant de souris knock-out pour *TrpV1* sont partiellement protégés contre la dégénération, indiquant un rôle pro dégénératif à TRPV1 *in vitro.*

Nous avons fait l'hypothèse que les espèces réactives de l'oxygène (ROS) provoquent l'activation de TrpV1 dans ce système. Consistant avec cette hypothèse, des chélateurs de ROS et des inhibiteurs des complexes Nox protègent contre la dégénération axonale. Les complexes Nox sont activés par la protéine kinase C (PKC) et nous avons démontré que des inhibiteurs de la PKC bloquent la dégénération axonale alors que le PMA –un activateur de la PKC- induit l'influx de calcium via l'activation de TrpV1 de manière NOX et ROS dépendante. Nous concluons qu'un axe PKC>Nox>ROS>TrpV1 induit un enrichissement toxique de calcium au niveau de l'axone conduisant à sa dégénération durant le développement embryonnaire.

Acknowledgements

I would like to thank Dr Philip Barker for guiding and supervising this thesis work. The patience and good faith that I received from Phil in his lab are greater than what I know how to offer to others. Phil's ability to make cell signaling appear simple with clear communication is an ideal for me to strive for in years to come. Thanks to Dr Julien Gibon, whose hard work and conscientiousness got the new lab running after the move to Kelowna. I appreciated our rigorous discussions and his editorial input in shaping our projects was essential. I thank Julien also for the French translation of the thesis abstract. Thanks to Andrés de León, the gentleman scientist and renaissance man, for good discussion and company over all these years in Montreal and Kelowna. I would like to thank my advisory committee, Dr Alyson Fournier and Dr Heidi McBride for the suggestions and interesting conversations that I always looked forward to in our committee meetings. Finally, thanks to my parents, Karen and Dave, for their constant and essential support during these adventures.

Abbreviations

6-OHDA	6-hydroxydopamine
AD	Alzheimer's disease
ALS	Amyotrophic Lateral Sclerosis
Apo	Apocynin
Aβ42	Amyloid beta 42 mutant protein
CNS	Central nervous system
Caspase	Cysteine-dependent aspartate-directed protease
CNTF	Ciliary neurotrophic factor
CPZ	Capsazepine
Cryo-EM	Cryogenic electron microscopy
DAG	Diacylglycerol
DkTx	Double-knot toxin
DMSO	dimethylsulphoxide
DPI	Diphenyleneiodonium
DRG	Dorsal root ganglia
EDTA	Ethylenediaminetetraacetic acid
EGTA	Ethylene glycol-bis(β-aminoethyl ether)-N,N,N',N'-tetraacetic acid
ES	Embryonic stem
R-GECO	Red genetically encoded Ca^{2+} indicator for optical imaging
G-GECO	Green genetically encoded Ca^{2+} indicator for optical imaging
HBSS	Hank's balanced salt solution
HCN	Hyperpolarization-activated, cyclic nucleotide-gated
IP3(R)	1,4,5-triphosphate (receptor)
HSV	Herpes simplex virus
JNK	c-Jun kinase
LPA	Lysophosphatidic acid
LTD	Long-term depression
LTP	Long-term potentiation
MOMP	Mitochondrial outer membrane permeabilization
MPTP	1-methyl-4-phenyl-1,2,3,6-tetrahydropyridine
NAC	N-acetylcysteine
NGF	Nerve growth factor
NT-3	Neurotrophin 3
$p75^{NTR}$	p75 neurotrophin receptor
PD	Parkinson's disease
PFA	Paraformaldehyde
PI3K	Phosphoinositide 3-kinase
PI(4,5)P2	Phosphatidylinositol 4,5-bisphosphate
PKC	Protein kinase C
PLC	Phospholipase C
PNS	Peripheral nervous system
RGC	Retinal ganglion cell
ROS	Reactive oxygen species
RTX	Resiniferotoxin
TNFR	Tumour necrosis factor receptor

TrkA	tropomyosin receptor kinase A
TrpV1	Transient receptor potential vanilloid family member 1
TTX	Tetrodotoxin
XIAP	X-linked inhibitor of apoptosis

Contributions of Authors

Chapter 2. A novel method of quantifying axon degeneration

Aaron Johnstone conceived of and prototyped the quantification method as a macro for ImageJ, contributed R coding, performed experiments and data analyses and wrote the text. Robin Hallett adapted the image processing workflow for EBImage and wrote R script. Andrés de León contributed micrographs to Figure 2.1. Bruno Carturan provided edits to R script. Julien Gibon contributed essential discussion and edits to text, and Philip Barker directed experiments and edited the text.

Chapter 3. Developmental neurodegeneration requires axoplasmic Ca^{2+} influx via TrpV1

Aaron Johnstone planned performed experiments, data analyses and wrote the text. Andrés de León contributed experiments to Figures 3.2 and 4.1. Julien Gibon conceived of Figure 3.4 and contributed essential discussion and edits to text, and Philip Barker directed experiments and edited the text.

Chapter 4. Ca^{2+} influx is mediated by a PKC > Nox complex > ROS > TrpV1 axis

Aaron Johnstone planned and performed experiments, data analyses and wrote the text. Genevieve Dorval and Svetlana performed molecular cloning and mutagenesis of TrpV1-GECO constructs. Julien Gibon contributed essential discussion and edits to text, and Philip Barker directed experiments and edited the text.

Chapter 1. General introduction and background from literature

1.1 Developmental neurodegeneration of sensory neurons of the dorsal root ganglia

1.1.1 NGF activates a TrkA/p75^{NTR} complex to signal neuronal survival in the developing sensory system

Neurodegeneration occurs normally during embryonic development to establish and refine the maturing nervous system. Genetically-encoded components of the same destructive signaling pathways (including apical tumor necrosis factor receptors (TNFRs), Bax, caspases and microtubule-associated proteins) also appear to underlie neurodegenerative diseases such as Alzheimer's, Parkinson's and amyotrophic lateral sclerosis (ALS) when they are aberrantly reactivated in adulthood due to interactions between genetic and environmental factors that are only partially understood (1–4). The emerging overlap between developmental and pathological mechanisms of neurodegeneration suggests that understanding the sequence of molecular events comprising physiological neurite degeneration and cell death programs during development will reveal therapeutic opportunities that interrupt disease.

Initially, greater numbers of sensory neurons of the dorsal root ganglia (DRG) are generated early in development than will persist in the mature nervous system. Surviving neurons are those that arrive at their targets and receive adequate neurotrophic support from a limited pool secreted from their targets (schematic of the neurotrophic support hypothesis of NGF/TrkA signaling shown in Figure 1 A, and DRG explants provided with or deprived of NGF for 24 hours are shown in B) (1,5). A majority of DRG axons respond to trophic support from target-derived nerve growth factor (NGF), which binds to its high-affinity surface receptor tropomyosin related kinase A (TrkA) on axons to activate its cytoplasmic tyrosine kinase domain, initiating a pro-survival signaling cascade that depends on retrograde signaling (8,9). Besides NGF, neurotrophins NT-3 (TrkC) and BDNF and NT-4 (TrkB) mediate diverse effects in the developing and adult central and peripheral nervous systems

(6,7). Upon NGF binding to TrkA a survival signal is generated; three possible mechanisms were at one time proposed to accomplish this retrograde signal: i) activated NGF-TrkA complexes are endocytosed to form signaling endosomes that are transported retrogradely via microtubule association, and signal throughout their lifespan, ii) activated TrkA generates signaling endosomes even if NGF is no longer associated and iii) and NGF signal may be transduced without transport of either NGF or TrkA (10). It has now been well-established that the active NGF-TrkA complex is endocytosed dependent on clathrin and dynamin to generate retrogradely-transported signaling endosomes that activate the Ras-MAP kinase pathway resulting in Erk1/2-mediated activation of pro-survival transcription factors Elk and CREB (8,11,12). NGF-TrkA survival signaling depends on direct interaction with the tumour necrosis factor receptor (TNFR) superfamily member and neurotrophin receptor p75 ($p75^{NTR}$), which possesses relatively low affinity for NGF on its own, but enhances NGF binding and signal transduction when complexed with TrkA (Figure 1.1 C) (9,13). It was long assumed that the degeneration of those axons that fail to reach their targets and acquire sufficient access to a limited neurotrophin pool was due simply to a deficiency in survival signaling initiated by NGF, but it is now clear that degeneration is an active, regulated process, and is reversible at several stages upstream of a commitment to cysteine-dependent aspartate-directed protease (caspase) activation and fragmentation and/or retraction of axons (14). Intriguingly, TrkA expression in engineered embryonic stem (ES) cell-derived neurons was reported to induced caspase-3 activation and neurite degeneration in the absence of NGF, yet control neurons not expressing TrkA survive, indicating that death following NGF withdrawal from TrkA is not due simply to lack of survival signals from the receptor but also depends on some yet-unknown death-inducing activity of unliganded TrkA (15). Mouse embryos derived from TrkA-overexpressing ES cells generate a peripheral nervous system by E11.5 but this is almost entirely lost by degeneration two days later; interestingly,

sympathetic neurons deprived of NGF largely survive when lacking TrkA expression (15). In this study TrkA was overexpressed from the Tau promotor (mapt) and thus the system may be vulnerable to unintended effects of accumulation of overexpressed protein in Golgi, and it will be valuable to learn whether TrkA expressed at endogenous levels also generates this effect. The apical molecular mechanism by which TrkA induces death when NGF is withdrawn remains one of the key open questions in the field.

1.1.2 NGF deprivation activates prodegenerative signaling via JNK, Bax and caspase activation

Though it is unclear how NGF deprivation from TrkA is transduced to downstream effectors, it is established that the latter phases of the pathway require c-Jun kinase (JNK) activation, Bax-dependent pore formation and mitochondrial outer membrane permeabilization, cytochrome c release and caspase cascade activation (Figure 1.1C) (16–19). Neurons that normally degenerate in the absence of NGF-TrkA survival signaling are rescued from apoptosis by genetic knockout of Bax (19), and Bax requires activation by JNK to activate mitochondrial-mediated programmed cell death (17,20). Release of cytochrome c from mitochondria in response to NGF withdrawal, a prerequisite for caspase activation, is also blocked in Bax null sympathetic neurons (16,18). Although Bax knockout blocks peripheral neuron loss, cutaneous innervation is severely deficient in these animals, highlighting the importance of NGF signaling in establishing proper innervation of targets in addition to survival (19). Following Bax- and mitochondria-dependent release of cytochrome c, a caspase activation cascade initiated by caspase-9 ultimately results in effector caspase activation (16,21–23). Although caspases had originally been overlooked or discounted in neurite degeneration, more recent work has firmly established that caspase-3 is a major effector of destructive events downstream of NGF deprivation signaling (16,21,24,25). Caspase-3 null DRGs derived from embryonic mice are strongly protected

from NGF withdrawal-induced degeneration, and degeneration is suppressed by overexpression of its endogenous inhibitor X-linked inhibitor of apoptosis protein (XIAP) (25).

1.1.3 Non-lethal executioner caspase activity is emerging as a core regulator of neural plasticity and disease

For decades, caspase activation was viewed as a cell-wide, catastrophic event occurring chiefly during cell death, but mounting evidence places non-lethal caspase activity at the center of essential non-apoptotic cytoskeletal remodeling events in neural plasticity (26–28). Intriguingly, signals and effectors of apoptosis, from receptor to caspase, appear to have been co-opted during evolution to allow for remodeling or removal of distinct neuronal subdomains (synapses, spines, and neurites) to regulate developmental pruning and learning & memory (Figure 1.2) (25,28–30). Normal development and adult functioning of the nervous system requires caspase activity to remodel the cytoskeleton supporting fine and course neural structures. However, dysregulated protease activity by caspases leads to a loss of structural responsiveness to normal plasticity-inducing stimuli when underactive, or degeneration and apoptosis. In this paradigm, knowledge of the molecular machinery of apoptosis gained by decades of study may be leveraged to generate hypotheses in order to understand normal synaptic and developmental plasticity, and thus the earliest events of neurodegenerative disease that begin at the finest neural structures and spread to destroy entire neurites, neurons and networks.

1.1.4 NGF withdrawal from DRG explants is an *in vitro* model of developmental degeneration

Developmental degeneration can be modeled *in vitro* by removal of NGF from cultured *ex vivo* DRG (Figure 1.1 B). Ganglia from embryos, typically isolated between 12 and 14 embryonic days, extend an array of axons onto the culture substrate in the presence of NGF that degenerate asynchronously within 15-40 hours of NGF withdrawal from the growth media (31). This *in vitro* system allows experimental dissection of the molecular pathway that underpins developmental degeneration by

pharmacological inhibition and genetic deletion of candidate proteins, using axonal membrane and cytoskeletal integrity and biochemical markers of degenerative signaling as quantifiable experimental outputs. Although the *in vitro* neurotrophic support phenomenon was first reported by Nobel laureate Rita Levi-Montalcini in 1951, many aspects of the signaling process underlying degeneration remain obscure (Figure 1.1 C) (32,33).

1.1.5 Ca^{2+} stress is a hallmark of neurodegeneration but its role in developmental degeneration of DRG neurons is unreported

Chronic Ca^{2+} stress and toxicity, amplified by feedback loops with sources of cellular oxidative stress, is established as a key mediator of synapse loss, neurite degeneration and apoptotic neuron death in neurodegenerative disease (Figure 3) (34–42). Recently, axonal Ca^{2+} influx has gained attention as a key mediator of injury-induced degeneration of sensory axons, but the role of Ca^{2+} in developmental degeneration has been unclear (43–46). This thesis explores the previously unreported role of Ca^{2+} influx via the transient receptor potential vanilloid family member 1 (TrpV1) during developmental degeneration in the sensory system.

1.2 TrpV1 is a tetrameric cation channel with complex polymodal activation

The founding member of the Trp (**t**ransient **r**eceptor **p**otential, sometimes **t**ransient **r**esponse **p**otential) superfamily of cation channels was first described in 1969 as a Drosophila mutant that displayed time-dependent desensitization of photoreceptors during sustained light exposure and decay of Ca^{2+} tone (47,48). Subsequently, 7 vertebrate Trp subfamilies were identified that have physiological roles in sensing and processing temperature, pain, pressure, stretch, osmolarity, acidity, taste, olfaction, vision and hearing information, and that function in memory and learning (49). The first characterized member of the vanilloid subfamily of channels (TrpV) was TrpV1, identified by an expression cloning quest by a group led by David Julius to identify the gene product underlying the Ca^{2+} influx-response

to the pungent compound capsaicin, produced by some plants, used by riot police, and responsible for the heat-like sensation of hot peppers (50). This study, published in Nature in 1997, found that TrpV1 is activated by noxious heat above ~42°C. In the intervening 20 years, TrpV1 has been confirmed to also be activated by protons, reactive oxygen species and oxidized lipids, ethanol, an array of noxious pest-defence compounds produced by vipers, spiders, scorpions and plants, as well as endogenous compounds N-arachidonoyl dopamine (NADA) and anandamide (51–54). Extensive mutant analyses have identified key regulatory residues within TrpV1, some which are multimodal while others are activation mode-specific (55–57).

1.3 TrpV1 structure

Functional TrpV1 channels are homotetrameric protein complexes formed by four subunits each with 6 membrane-spanning helices that assemble to form a central pore (though heterotetrameric complexes have also been described formed by TrpV1 and other Trp family members, suggesting potential for nuance of activation and function not fully understood) (58–60). The highest-resolution structural models of TrpV1 homotetramers, recently generated via cryo-EM, have provided insight into the rich versatility of activation modes of TrpV1 (61–63). A central ion-permeable pore is controlled by two gates: an upper selectivity filter and a lower gate (58). The channel was resolved in its closed conformation in the absence of activating compounds, but no single activator ligand tested stably maintained both the extracellular selectivity filter and the intracellular lower gate in an open conformation in these studies; the spider-derived double-knot toxin (DkTx) opened the latter while the former was dilated by resiniferatoxin (RTX) upon binding to the vanilloid binding site (shared by capsaicin) in the intracellular portion proximal to the membrane interface (61,62). When both compounds were complexed with TrpV1 simultaneously, both the selectivity filter and lower gate were found to be maintained in an open position with a wider diameter than either compound alone (61,62).

Intriguingly, capsaicin alone failed to provide a stable structural conformation of TrpV1, though it is has potent effects on cell systems expressing TrpV1 and is a bona fide activator, suggesting that its binding to TrpV1 may induce an unstable "flickering" effect of pore opening that technically confounds cryo-EM which requires stable conformations to estimate protein structure with confidence (61). A stable, open lower gate conformation was established by capsaicin with simultaneous maintenance of an open state of the selectivity filter by DkTx (61). New evidence indicates that the vanilloid binding site recognized by agonists capsaicin and RTX, as well as antagonist capsazepine, is a site of endogenous regulation by lipids, with functional consequences for physiological activation by heat, and exogenous oxidation and enzymatic lipid products (37,47–49).

1.4 Redox regulation of TrpV1

Multiple lines of evidence indicate that reactive cysteine residues in multiple TrpV1 domains contribute to its sensitization and activation. Allicin, a pro-oxidant molecule that gives pungency to onions and garlic, activates TrpV1 entirely via cysteine 157 (in rat TrpV1), while the C157A mutation did not impact activation by capsaicin (66,67). Mutation of this residue (C158 in human TrpV1) significantly reduced the pool of homocomplexed TrpV1 versus monomer, suggesting an important role for disulphide linkages in assembling TrpV1 monomers and creating functional pores (68). Intraplantar injection of H_2O_2 increased TrpV1-dependent pain sensitivity, indicating that elevated oxidative status sensitizes TrpV1 activation (69,70). In HEK293 cells expressing TrpV1, H_2O_2 potentiated the capsaicin response in whole-cell electrophysiological recordings, and H_2O_2 dose-dependently induced TrpV1-mediated Ca^{2+} influx (71). Oxidized lipids are emerging as key physiological activators of inflammatory pain that work by targeting specific residues with TrpV1 (72,73). Phosphatidylinositol 4,5-bisphosphate (PI(4,5)P2), an established regulator of apoptosis, binds directly to TrpV1 and agonizes Ca^{2+} flux (74). The naturally-occurring omega-9 oleic acid

competitively attenuated TrpV1 activation by capsaicin *in vitro*, while cyclic phosphatidic acid and lysophosphatidic acid (LPA), a bioactive lysophospholipid, directly activated the channel, arguing that the binding site exploited for pharmacological agonism and antagonism is directly involved in lipid-mediated redox regulation (75,76).

1.4.1 Nox complex-derived ROS are intimately linked to TrpV1 activation

Reactive oxygen species (ROS) were once thought of primarily as a toxic consequence of aerobic respiration, but a large number of studies published in the past two decades have firmly established ROS as second messengers that transduce signals from activated cytokine receptors (77–81). Since ROS are highly reactive small molecules capable of modifying a vast range of macromolecules, its usefulness as a specific signal requires that it be spatially restricted and attenuatable (82). These requirements are met by NADPH oxidase (Nox) complexes, membrane-associated protein complexes that reduce NADPH to generate superoxide from molecular oxygen, have been found to be a major source of signaling ROS in a wide range of signaling contexts, including the immune response by neutrophils, control of vascular tone and regulation of survival, plasticity and degeneration in the nervous system (83–85).

Seven mammalian NADPH oxidase catalytic subunits are known: Nox1-5 and Duox 1 & 2. Nox1-3 depend on regulation by cytosolic activators including Rac1 GTPase, $p67^{phox}$ and core Nox complex organizer $p47^{phox}$, allowing for strict regulation of ROS production in response to upstream signaling events (80,86). Because ROS react with a vast range of biological macromolecules, spatial restriction of signaling ROS is believed critical for its functional specificity. A growing body of evidence, in particular from a group led by John Engelhardt, suggests that receptor activation of Nox complexes occurs within redox-active signaling endosomes, or "redoxosomes" (86). In a series of studies, the Engelhardt group fractionated endosomes and identified a high-oxidative status fraction

containing Rab5, an early endosome marker, but lacked Rab11, and downstream signaling to NF-kB and IKK required Nox complex activity (78,82,86). Nox-dependent redoxosomes have been best characterized in response to tumour necrosis factor receptor 1 (TNFR1) and interleukin-1 receptor (IL-1R1) activation by their respective cytokine ligands; inhibition of Rac1 or the Nox complex organizer $p47^{phox}$ prevents H_2O_2 production and downstream signaling (80,87–89).

Post-natal sympathetic neurons were reported to be rescued from apoptosis *in vitro* by treatment with diphenyleneiodonium (DPI), a pharmacological Nox complex inhibitor that prevents NADPH (the electron source for superoxide production) from binding to the activated Nox complex (90). The same study also reported that neurons derived from NOX2 null mice were protected from apoptosis following NGF deprivation. DPI treatment reduced ROS production induced by NGF withdrawal in these cells, which like DRG sensory neurons depend on NGF for survival, implicating Nox complex activation as a major source of oxidative signaling in NGF deprivation- induced degeneration (90). However, it has not been reported whether degeneration of sensory neurons is Nox-dependent following NGF withdrawal.

Nox complexes are stimulated to produce a ROS burst upon phosphorylation of the core complex organizer $p47^{phox}$ by protein kinase C (PKC) in response to direct activation by endogenous diacylglycerol or pharmacological activator phorbol 12-myristate 13-acetate (PMA) (91). In isolated Nox1-null DRG neurons treated with PMA, the Ca^{2+} influx response after capsaicin addition was attenuated compared to the wild-type, indicating that Nox complexes downstream of PKC modulate TrpV1 sensitivity in this model (77). In a model of mechanical inflammatory hyperalgesia in DRG, inhibition of Nox1 and Nox4 reduced cytosolic oxidative status, while TrpV1 antagonist SB366791 and antioxidant N-acetylcysteine (NAC) reduced intracellular free calcium during challenge by pro-inflammatory oxidized protein products, indicating that Ca^{2+} influx downstream of Nox complex

activation depends on TrpV1 (73). TrpV1 expressed on DRG neurons innervating the renal pelvis was reported to be involved in mechanosensation for monitoring of urine production, which was defective upon Nox complex inhibition by apocynin, or sensitized by exogenous H_2O_2 in rat (92). It has not been reported whether PKC and Nox complexes have a role in developmental degeneration of sensory neurons after NGF deprivation, and this topic is explored further in this thesis.

1.6 TrpV1: More than just a pain

1.6.1 TrpV1 is widely expressed outside of nociceptors

Research into TrpV1 has largely focused on its role in pain transduction, particularly as interest in developing non-opioid anti-pain therapeutics has grown with an addiction epidemic. But as TrpV1 expression has been revealed also in non-nociceptive neurons, in glial cells in both the central and peripheral nervous systems, in keratinocytes, adipose tissue, epithelium, in vasculature in heart, and in kidney. It has become clear that TrpV1 regulates Ca^{2+} entry required for downstream functions as diverse as immune response, energy metabolism and memory and learning (70,93–97). In sensory neurons of the DRG, TrpV1 expression detectable by immunohistochemistry is restricted chiefly to the nociceptive subset of sensory neurons of the DRG in adults, but during embryonic development its expression is widespread in DRG neurons regardless of ultimate functional fate as nociceptors (98). A study of the expression pattern of TrpV1 in DRG neurons found that earliest detectable expression begins at embryonic day 12.5 and increases over the next two days before decreasing, a window of expression that has particular relevance to this thesis as it coincides with the phase of programmed death of sensory neurons that normally occurs during development (98,99).

1.6.2 TrpV1 in synaptic plasticity

TrpV1 is implicated in plasticity and cytoskeletal dynamics in response to Ca^{2+} (100). TrpV1 knockout mice were reported to display decreased anxiety-linked behaviour during an elevated maze and light-dark test, and reduced freezing response to a tone after fear-conditioning training, implicating TrpV1 in hippocampal learning in both innate and learned fear contexts (101). In this study, TrpV1 knockout was found to reduce long-term potentiation (LTP) in the Schaffer collateral–commissural pathway to CA1 hippocampal neurons. TrpV1 is widely expressed in hippocampus (102), and enriched at dendritic post-synaptic spines (103). The effect of TrpV1 activation by capsaicin on long-term depression (LTD) and LTP was investigated in CA1 hippocampal slices, and the authors reported enhanced LTP but defective LTD upon TrpV1 activation, which was reversed in the presence of TrpV1 inhibitors capsazepine and SB366791, consistent with published genetic data using TrpV1-null rodents (104,105). This effect appears to depend, in part, on the GABAergic system in hippocampus (97) and glutamate receptor GluA1 in LTP in the amygdala (106). TrpV1 stimulation by capsaicin in sensory neurons induced increased glutamate release and action potentials in post-synaptic neurons, indicating that plasticity mediated by TrpV1, when taken together with evidence in the CNS, occurs in diverse neuron types in both peripheral and central nervous systems (107).

1.6.3 Non-physiological TrpV1 activation can be pro-degenerative

Capsaicin application to sensory neuron endings induces a degeneration phenotype. Ablation of innervating fibres using capsaicin is of interest as a potential treatment for chronic pain and itch caused by hyperalgesia or hyper-innervation (108–114). In cultured embryonic rat DRG neurons, capsaicin application induced Ca^{2+} influx and degeneration that was accompanied by mitochondrial Ca^{2+} stress and fission (115). While exogenous TrpV1 activation can induce degeneration of neurons *in vivo* and *in vitro,* it has not been reported whether TrpV1 does so under physiological conditions in developmental degeneration.

1.6.4 TrpV1 in models of neurodegenerative disease

A growing number of published studies have investigated the role of TrpV1 in neurodegenerative disease (discussed below). Evidence is sporadic and comes from studies in disparate models, and experimentally reversing hypo- or hyperactivation of TrpV1 appears to either ameliorate or worsen degenerative phenotypes depending on the disease modeled; no clear mechanistic model of TrpV1 function on neurons or neuroimmune cells has yet emerged. Studies *in vivo* using TrpV1 genetic knockout or pharmacological ant/agonists have been difficult to integrate and interpret due to apparently simultaneous and possibly opposing roles of distinct pools of TrpV1 in neurons and neuroimmune cells, as well as system-wide effects of thermoregulation on the rate of progression of disease (reviewed below). To make matters more complicated, studies that rely on TrpV1 agonism with capsaicin can be difficult to interpret since activation of TrpV1 can lead to desensitization and removal from the membrane, so the biological effects of chronic TrpV1 activation may actually result from loss of TrpV1 function rather than the hyperactivation often assumed in some models of how TrpV1 contributes mechanistically to disease (116). Nevertheless, a growing body of evidence implicates TrpV1 in both healthy and diseased nervous system function.

In Alzheimer's disease models

Alzheimer's disease has been modeled in mice by injection of amyloid β-protein 1-42 (Aβ42) to induce AD-like behavioural and cognitive deficits and synapse loss (117). In a recent study, defective spatial learning and memory accompanied by hippocampal synapse loss and impaired hippocampal long-term potentiation (LTP) was confirmed in mice two weeks after Aβ42 injection; however intraperitoneal injection of TrpV1 agonist capsaicin significantly reduced behavioural deficits in the Morris water maze and in a novel object recognition test (118). Electrophysiological assessment of LTP in hippocampal slices and rescued synapse density showed that capsaicin ameliorated the effect of Aβ42

(118). It is unclear whether this protection is due to increased TrpV1 activity stimulated by its agonist, or underactivity of TrpV1 due to subsequent desensitization of the channel that accompanies its chronic activation.

Defective insulin signaling in the brain is a consequence of type-II diabetes and is a risk factor for Alzheimer's disease. In a rat model of diabetes (119), the TrpV1 agonist capsaicin, provided orally, reduced Alzheimer's-associated tau phosphorylation It is impossible without further study to reasonably claim that neuronal TrpV1 is responsible for the effect since somatic TrpV1 inhibition has effects on insulin resistance independent of the CNS (95) and it is not known whether TrpV1 expressed by neurons contributes to Alzheimer's disease-associated neurodegeneration.

In Parkinson's disease models

Parkinson's disease has been modeled in rat by intracerebroventricular injection of 6-hydroxydopamine (6-OHDA) to induce degeneration of dopaminergic neurons of the substantia nigra. In one study, motor and cognitive function was partially restored by injection of TrpV1 antagonist AMG9810 early after 6-OHDA injury, but chronic TrpV1 inhibition worsened its effect(120). Thus, TrpV1 may contribute to disease progression but may also be required for normal maintenance of motor and cognitive function (120). In a Parkinson's-like rat model (injection of neurotoxin precursor 1-methyl-4-phenyl-1,2,3,6-tetrahydropyridine, MPTP), systemic injection of capsaicin improved dopaminergic neuron survival and behavioural deficits via astrocyte-expressed TrpV1 (121). In this model, stimulation of astrocyte-expressed TrpV1 enhanced release of ciliary neurotrophic factor (CTNF) from astrocytes, promoting survival of CTNF receptor expressing neurons (121,122). In another study using the same experimental model, nigrostriatal dopaminergic neurons were also rescued from excitotoxic death and microglial oxidative and neuroinflammatory statuswas reduced

(123).Whether TrpV1 expressed by neurons themselves contributes to degeneration of dopaminergic neurons cell-autonomously remains unknown.

In optic nerve degeneration and glaucoma models

Several studies have investigated TrpV1 in ocular hydrostatic pressure-induced degeneration of retinal ganglia cells (RGCs), a sensory neuron type, though conclusions drawn *in vivo* and *in vitro* appear contradictory. Cultured RGC neurons underwent apoptosis when subjected to high hydrostatic pressure (an *in vitro* glaucoma model), but were rescued from apoptosis by TrpV1 inhibitor capsazepine (124). The same group reported that while TrpV1 mRNA is enriched in rat retina in response to elevated intraocular pressure, RGCs in $TrpV1^{-/-}$ rats displayed accelerated degeneration of the optic projection to the superior colliculus, a result replicated by pharmacological TrpV1 inhibition in wild-type rats, contradicting *in vitro* data suggesting TrpV1 inhibition to be neuroprotective (124,125).

These reports may be reconciled if TrpV1 has opposing roles in neurons themselves versus non-cell autonomous effects on neurons mediated by astrocytes in the retina and optic nerve, adding complexity that is not yet understood. For example, a role for TrpV1 in CNS neurodegeneration may be due in part to a contribution, as a Ca^{2+} channel, to Ca^{2+}-mediated cytoskeletal remodeling necessary for astrocyte migration to lesions after injury; TrpV1 inhibition with capsazepine or Ca^{2+} chelation with EGTA was reported to significantly slow astrocyte motility *in vitro*, while its activator capsaicin had an opposite effect (126). It remains unknown whether an analogous neuroinflammatory response of Schwann cells in the PNS is similarly influenced by TrpV1 activity during physiological or pathological sensory neurodegeneration.

In models of hypoxic-ischemic stroke

While clinically-induced hypothermia offers bona fide reduction in the ischemic umbra after stroke if applied within the appropriate therapeutic window, there are unintended consequences to the patient such as cold-induced tissue damage (127). Systemic TrpV1 activation has been reported to induce "pharmacological hypothermia" via dysregulation of its role in thermoregulation in rodents, thus achieving lowered temperature in the brain while avoiding the need for exposure of the animal to external cooling systems (128). TrpV1 activation by capsaicin-derivative dihydrocapsaicin reduced the size of the brain infarct in a rat model of hypoxic ischemia, though not necessarily via action on pro-degenerative TrpV1 activation itself but rather by confounding somatic temperature sensing and regulating systems (128,129).

Hippocampal and DRG neurons isolated and cultured from rats after middle cerebral artery occlusion-induced stroke showed reduced Ca^{2+} influx upon application of the TrpV1 activator capsaicin when rats were also injected with antioxidant, linking elevated oxidative status after injury to TrpV1 sensitivity (130). The study did not explore the effect of inhibiting TrpV1 *in vivo* after injury, and the precise effect of cerebral occlusion (which severely reduces blood flow to the brain ipsilateral to injury) on peripheral sensory neurons like DRG is difficult to interpret.

In axon regeneration after axotomy

Surgical transection or crush of sciatic nerve is a model of mechanical axon injury in rodents. In the days and weeks following injury, distal axon segments no longer connected to cell bodies degenerate through a process termed Wallerian degeneration, followed by limited regeneration of new fibres (24). It has been reported that sciatic nerve crush in rats induced an upregulation of TrpV1 expression in injured axons, but that injection of TrpV1 inhibitor AMG517 significantly increased the number of axons present in the nerve two weeks after injury compared to controls without TrpV1 inhibition (131).

The authors concluded that the increased axonal density in distal nerve is due to improved regenerative capability when TrpV1 is inhibited, i.e. enhanced regrowth of new axons after injury, but neglected to test the possibility that axons existing prior to injury are rescued from Wallerian degeneration in the first place by hypoactive TrpV1. Whether distal axons are protected from degeneration by TrpV1 antagonism remains to be reported. Since TrpV1 inhibitors resulted in lowered TrpV1 expression in longitudinal sections of nerve prepared for immunofluorescence, it remains a distinct possibility (131).

1.7 Research rationale and original contribution to knowledge

A major gap remains in our understanding for how TrkA/$p75^{NTR}$ prodegenerative signaling is transduced to downstream events ultimately leading to JNK/Bax activation, mitochondrial permeabilization and cytochrome c-dependent effector caspase activation (Figure 1.1 C). Understanding the molecular events linking early and late events is key to understanding degenerative signaling and identifying strategies to impede its progression in disease states. No definitive model for the role of TrpV1 in neurodegeneration has yet emerged. We hypothesize that developmental degeneration is mediated by Ca^{2+} toxicity via activation of TrpV1 downstream of ROS generated by Nox complexes activated by PKC.

The *in vitro* developmental degeneration model utilized in this work provides several advantages not available to those in the disease-model studies summarized above; DRG explant morphology provides fields of essentially pure axons for biochemical and morphological analysis separated from neuroimmune or myelination-related-factors. In this setting, neurite degeneration can be objectively quantified without interference from cell bodies, and it does not depend on the inherently imperfect rodent models of human neurodegenerative disease in animals or *in vitro.*

Major original contributions of this thesis are:

i. the development of a novel method for objective, automated quantification of neurodegeneration of DRG axons *in vitro,*

ii. the determination that developmental degeneration of DRG neurons requires the TrpV1 Ca^{2+} channel during NGF withdrawal-induced degeneration of sensory neurons, and

iii. that TrpV1 is activated by a PKC > Nox > ROS axis during developmental neurodegeneration.

1.8 Figures and figure legends

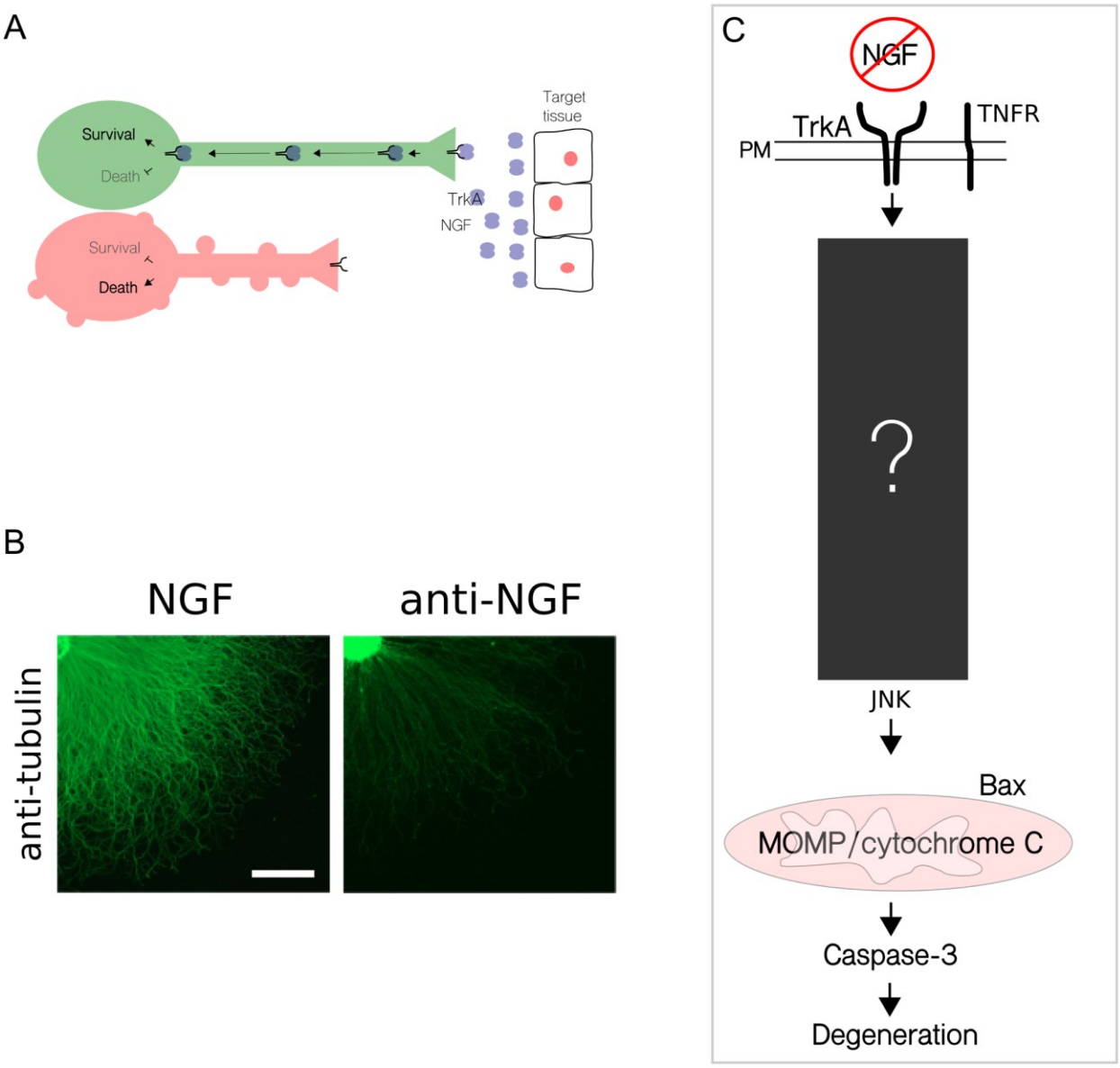

Figure 1.1. Neurodegeneration normally occurs during embryonic development but remains poorly understood.

Axons of the DRG extend during development to establish connectivity between peripheral tissues and the central nervous system. Target-derived nerve growth factor (NGF) activates its receptor TrkA in concert with $p75^{NTR}$ and perhaps other members of the tumor necrosis factor receptor (TNFR) family on the neurite plasma membrane to transduce a pro-survival signal via internalization and retrograde

transport; those axons which fail to reach their targets within the normal developmental window degenerate (A). Developmental degeneration is modeled *in vitro* with explanted DRG either provided with NGF to promote survival, or NGF deprivation using an anti-NGF antibody to induce degeneration (B; scale bar indicates 1 mm). Early and late signaling events have been identified during several decades of study, yet major gaps in our understanding of how NGF deprivation from TrkA and associated TNFRs is transduced to catastrophic mitochondrial outer membrane permeabilization and caspase activation (C).

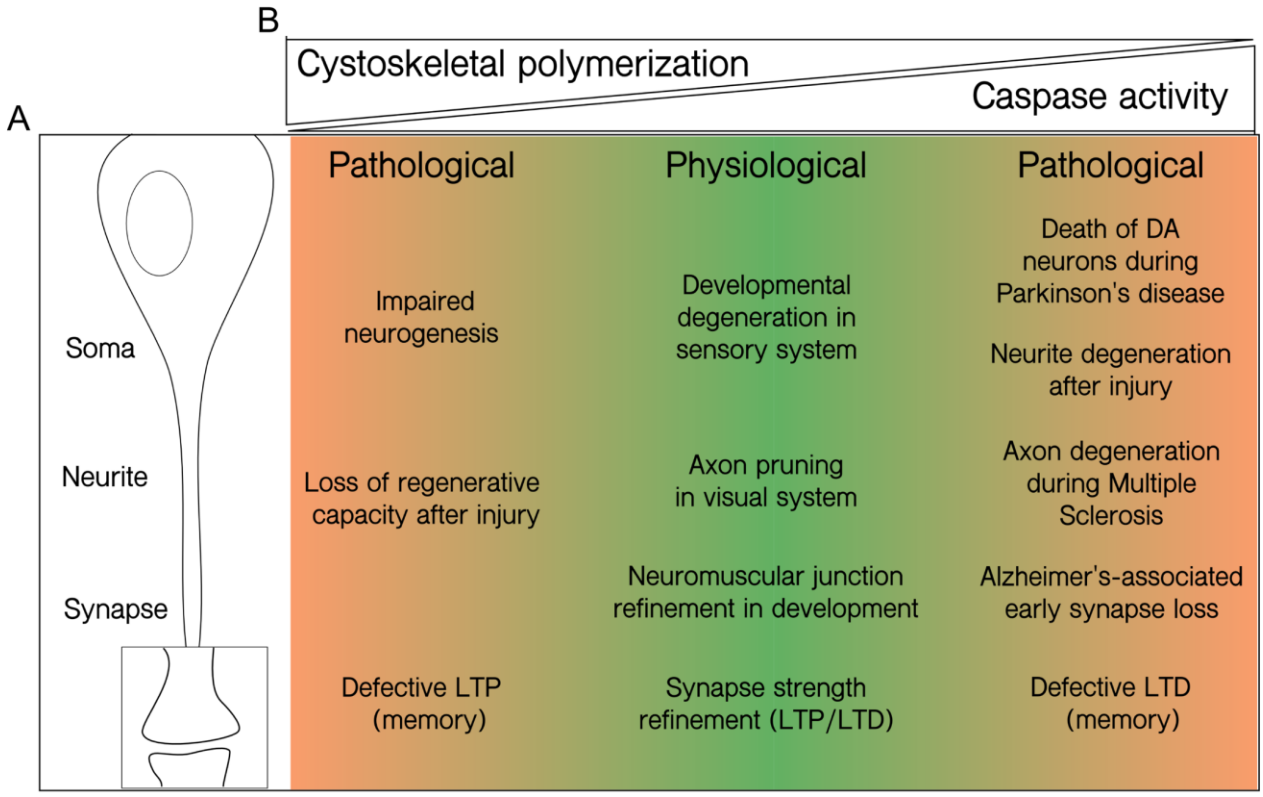

Figure 1.2. Structural plasticity in the healthy nervous system requires a regulated balance between maintenance and remodeling of the cytoskeleton.

Structural plasticity occurs at all levels of neural organization, from changes at minute synaptic structures in response to activity or disease, to pruning of neurites and removal of entire neurons and networks (A). Normal development and adult functioning of the nervous system requires regulated caspase activity to disassemble and remodel cytoskeleton with a high degree of spatial and temporal regulation, but over- or under-activity of the protease outside the normal physiological range and locale leads to either a loss of structural responsiveness to normal plasticity-inducing stimuli or overzealous dissolution of the cytoskeleton resulting in disease states (B).

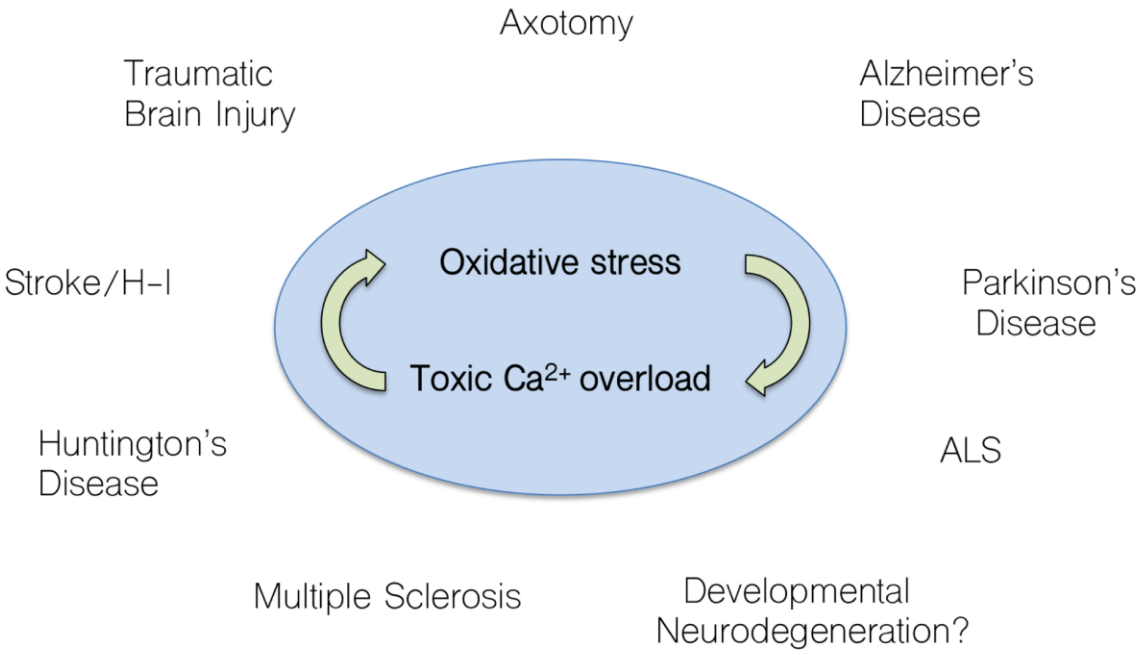

Figure 1.3. Oxidative stress and Ca^{2+} toxicity have emerged as hallmarks of neurodegenerative disease.

Pathological structural changes during diverse neurodegenerative diseases, whether due to chronic and progressive dysregulation (Alzheimer's, Parkinson's and Huntington's diseases, ALS and multiple sclerosis) or acute (stroke and hypoxic-ischemia, traumatic brain injury, axotomy), are accompanied by elevated oxidative and Ca^{2+} stress. Evidence for a role for toxic Ca^{2+} overload has not been reported during developmental degeneration of DRG, an established model system for pathological axon degeneration, and is explored in this thesis.

Chapter 2. A novel method of quantifying axon degeneration

2.1 Abstract

Axons normally degenerate during development of the mammalian nervous system, but dysregulation of the same genetically-encoded destructive cellular machinery can destroy crucial structures during adult neurodegenerative diseases. Nerve growth factor (NGF) withdrawal from dorsal root ganglia (DRG) axons is a well-established *in vitro* experimental model for biochemical and cell biological studies of developmental degeneration. However, definitive methods for measuring axon degeneration have been lacking and here we report a novel method of axon degeneration quantification from bulk cultures of DRG that enables objective and automated measurement of axonal density over the entire field of radial axon outgrowth from the ganglion. As proof of principal, this new method, written as an R script called Axoquant 2.0, was used to examine the role of Ca^{2+} influx in the execution of cytoskeletal disassembly during degeneration of NGF-deprived DRG axons. This method can be easily applied to examine degenerative or neuroprotective effects of gene manipulations and pharmacological interventions.

2.2 Introduction to Chapter 2

In vitro, explanted DRG ganglia extend axons onto the culture substrate in the presence of NGF and these can be induced to degenerate by NGF withdrawal and/or by application of a function-blocking antibody against NGF (Figure 1.1 B) (31). Although the neurotrophic support of DRG neurons (and their degeneration and death following trophic support withdrawal) was discovered by Nobel laureate Rita Levi-Montalcini in 1951, key aspects of the signaling process underlying degeneration remain obscure and mechanistically incomplete (32,33).

Effective use of the DRG & NGF withdrawal system to dissect degenerative signaling *in vitro* relies on objective quantification of axon degeneration. The challenge is heightened by variability in axon length, density and morphology that open the possibility of sampling biases that mask or amplify bona fide biological effects. To address this, we have developed the first automated method for quantifying neurodegeneration from micrographs of whole DRG explants. Unlike currently existing strategies for quantifying degeneration, Axoquant 2.0 reports the degree of axon degeneration over the entire radial growth field from soma to growth cone. It avoids variability introduced by random sampling from within axon fields and circumvents the need to generate dissociated neuron cultures or any manual, subjective quantification based on qualitative criteria that are time consuming and vulnerable to bias. Axoquant 2.0 is written in R, a programming language familiar to computational biologists, bioinformaticians and statisticians, but easily accessible to the first-time user when deployed with the open-ware graphical user interface, R-Studio (http://www.rstudio.com).

As proof-of-principle, we show that Axoquant 2.0 reveals striking preservation of the tubulin cytoskeleton in DRG axons by cation chelator EDTA.

2.3 Materials and methods

2.3.1 Dissection, culturing and NGF deprivation of DRG explants

DRG explants were dissected from pregnant CD1 mice with litters of E13.5 embryos (Charles River). Explants were seeded on 6-well plastic cell culture plates (Greiner) coated in a three-step process with 1 mg/ml poly-D-lysine (Sigma-Aldrich), 10 μg/ml laminin-entactin complex (Corning) and PurCol bovine collagen 0.1 mg/ml (Advanced Biomatrix). Explants were cultured in Neurobasal medium (Invitrogen) supplemented with 2% B-27 serum-free supplement (Invitrogen), 1% L-glutamine (Wisent), 1% penicillin/streptomycin (Wisent), and 10 μM 5-Fluoro-2'-deoxyuridine (FDU, Sigma-Aldrich) with 12.5 ng/ml NGF (Alomone). NGF deprivation was achieved using fresh media as described above but lacking NGF and containing 2.8 μg/ml rabbit anti-NGF antibody for the durations stated in each experiment.

2.3.2 Fixation, cytoskeletal immunostaining and imaging

DRG cultures were fixed in 4% paraformaldehyde in PBS for 15 minutes at room temperature and permeabilized and blocked for immunostaining in TBS-T, 5% skim milk, and 0.3% Triton X-100 for 15 minutes at room temperature. Immunostaining was performed in TBS-T with 5% skim milk and 0.3% Triton X-100 with mouse anti-β-III tubulin (Millipore; 1:10 000) primary antibody and anti-mouse secondary antibody conjugated to Alexa Fluor 488 (ThermoFisher; 1:5000). Cultures were imaged at 5x magnification using a Zeiss Axioscope2 inverted epifluorescence microscope with an automated, motorized stage. Images were stitched automatically with Zen 2 software from Zeiss to produce a master image of all explants on the entire 6-well plate. From this master image, quarter-DRG fields were cropped using NIH ImageJ (FIJI build) to create an image set for quantification.

2.3.3 Axoquant 2.0 workflow

Quarter-field images of DRG explants were cropped and saved (indicated by a dashed-square "✓" in Figure 2.1 A; example regions disqualified for analysis because of interference from neighbouring DRG explants are indicated by a red checkmark "✗"). As many DRG explants as possible per embryo were plated to reduce variability among embryos during analysis, and a minimum of three embryos per treatment were utilized in order to move forward with statistical analyses of effect sizes. Prior to analysis, images of DRG quarter-fields were organized in subfolders (one subfolder per well) named by embryo ID number, treatment name and repetition number within a single parent (experiment) folder (Figure 2.1 B). The R script was directed towards the parent experiment folder by changing the directory path in line 2 of the code designated "experiment.folder," and the code was executed through to the end of the script. As images are processed, the R Studio console displays an ascending image count to indicate progress. When finished with analysis, Axoquant 2.0 automatically exports a *.csv data file to the parent folder that can be opened in spreadsheet and in statistical analysis software (Prism 6, GraphPad).

R can be freely downloaded and installed from the R Project for Statistical Computing (https://www.r-project.org/). Additionally, users will download R Studio, a graphical interface for editing and running R packages freely available for download at https://www.rstudio.com. The Axoquant 2.0 script can be downloaded at https://github.com/BarkerLabUBC/Axoquant2.0 and opened in R Studio.

2.3.4 Ca^{2+} chelation

After 60h of growth in NGF, cultures were either maintained in NGF or were deprived of NGF and exposed to anti-NGF antibody (2.8 µg/ml) in the presence of EDTA 6 mM (Sigma-Aldrich) for either the entire 24-hour duration of NGF withdrawal or for the final 12 hours before fixation with paraformaldehyde 4% in PBS and imaged.

2.4 Results

2.4.1 Axoquant 2.0 automated image processing workflow

The R script automatically detects the location of the neuronal cell bodies in quarter-field images (indicated in Figure 2.1 A; folders are crawled in the organization shown in B) by detecting the most brightly stained corner, and each image is rotated to place the ganglion at the image origin to create a consistently organized image set (Figure 2.2 A with auto-rotated example shown in B). A binary threshold is applied to each image; the default threshold is set at the mean pixel intensity of a given image plus the standard deviation of pixel intensity to create a mask of stained axons (Figure 2.2 C). This threshold value delineates well-stained axons from the substrate, but can be manually changed by users who wish to apply a higher or lower threshold to accommodate suboptimal stains. The density of binary-masked axons is then measured in bins (with a user-adjustable default of 50 pixels per bin) radiating outwards from the ganglia centre (Figure 2.2 D). Axoquant 2.0 automatically creates and saves a master comma separated file (*.csv) for import into spreadsheet software in the parent folder containing the experiment images. This data file contains individual measurements for each DRG, but also the mean of all DRGs within the same well, which is utilized for statistical analysis to compare treatment effects (Figure 2.2 E). The axon density profile can be plotted as a function of distance from the soma in ganglia, and clearly reveals a rapid loss in density with distance, highlighting the imprudence of randomly sampling axons at multiple distances (example individual embryo means shown in Figure 2.2 E, with treatment means and standard error shown in F).

2.4.2 Proof of principal: Ca^{2+} chelation rescues axons from degeneration

To validate Axoquant 2.0 in an experimental setting, DRG cultures were either maintained in NGF (Figure 2.3 A i), deprived of NGF for 24 hours (ii), deprived of NGF in the presence of EDTA for the entire duration of the withdrawal phase (iii), or with EDTA only for the final 12 hours of NGF

withdrawal (iv). NGF deprivation for 24 hours induced robust axonal loss that was partially rescued by incubation with EDTA for the entire deprivation period of 24 hours, but essentially completely protected when EDTA was added for the final 12 hours of the withdrawal period (Figure 2.3 B; axon density curves generated by Axoquant 2.0 shown in Figure 2.3 C). A one factor ANOVA performed on the axon density reported at the bin at 500 μm from soma indicated a significant effect of treatment, $F(3, 32) = 42.13$, $P < 0.0001$, n = 9 embryos from 3 experiments). Tukey's post hoc pairwise contrasts revealed significant reduction in axonal density upon NGF deprivation compared to healthy, NGF-supplied control ($p < 0.0001$), while inclusion of EDTA either for the entire 24 hour NGF deprivation period or for the final 12 hours significantly rescued axon density ($ps < 0.0001$). EDTA added only for the final 12 hours rescued axonal density significantly above the rescue by EDTA applied for 24 hours ($p < 0.01$) indicating that long-term disruption of pro-survival roles of Ca^{2+} by EDTA counteracts protective effects over time. The robust protection by EDTA added only after 12 hours of deprivation indicates that the pro-degenerative role of calcium does not occur during the early hours of NGF deprivation and represents a late-phase event.

2.5 Discussion

In DRG cultures, axonal density decreases as distance from the cell bodies in the ganglia increases and variations in the culture substrate can alter axon density within and between DRG and from experiment to experiment. Objective, automated quantification of neurodegeneration is essential in the DRG system to test the effect of gene knockouts and chemical treatments on axon loss. Axoquant 2.0 accommodates the distinctive radial growth pattern of DRG axons to collect data at all distances from the neuron bodies, providing a global view of axon integrity, and negating the variability introduced by randomly sampling fields over regions that are intrinsically more or less dense as a function of outgrowth distance.

Users image the entire growth surface of 6-well plate, and organize cropped images of quarter-fields of DRG explants by embryo and treatment (Figure 2.1). When directed towards the parent experiment folder, the R script automatically detects the ganglia and re-orients the image if necessary (Figure 2.2 A and B). A binary threshold mask of axons is generated by an automatic threshold value (mean pixel intensity plus one standard deviation is default, Figure 2.2 C). The area occupied by axons is measured in bins with increasing distance from cell bodies, D). Axoquant 2.0 auto-saves a comma separated file (*.csv) containing individual image measurements and embryo mean values, which can be opened by spreadsheet or statistical software (plotted in Figure 2.2 E and F).

Pathological Ca^{2+} stress is emerging as a key factor in diverse neurodegenerative disease states (34,36,37,39,132), but studies from more than 20 years ago examined the role of Ca^{2+} in the death of NGF-dependent neurons and concluded that Ca^{2+} does not play a significant role in degenerative signaling with these cells (45,46,133), prompting us to revisit this issue in DRG. Intriguingly, Figure 1.3 shows that the Ca^{2+} chelator ethylenediaminetetraacetic acid (EDTA) rescues axons from degeneration. DRG cultures were either maintained in NGF (Figure 1.3 A i), deprived of NGF for 24

hours (ii), deprived of NGF in the presence of EDTA for the entire duration of the withdrawal phase (iii), or with EDTA only for the final 12 hours of NGF withdrawal (iv). NGF deprivation for 24 hours induced axonal degeneration that was partially rescued by EDTA during the deprivation period of 24 hours, but more strongly protected when EDTA was added for only the final 12 hours of the withdrawal period (Figure 2.3 B; quantified by Axoquant 2.0 in Figure 2.3 C).

Early studies that failed to report Ca^{2+}-dependent death of trophic factor-deprived sensory neurons utilized cultures maintained for up to 12 days (133,134). However, work published more recently has shown that sensitivity to NGF deprivation is reduced as embryonic cultures age beyond 2-3 days, and established that sensitivity is reduced in DRGs from older embryos (25). Thus, the protective effect of Ca^{2+} chelation that we observed, versus the lack of effect in earlier studies, likely reflects sensitivity of the bioassays employed. Our study has revealed that Ca^{2+} chelation provides clear and robust protection of the tubulin cytoskeleton during the late phase of NGF withdrawal. This provides validation of Axoquant 2.0 as a useful analytical tool and indicates that Ca^{2+} fluxes play a crucial role in developmental degeneration.

2.6 Figures and figure legends

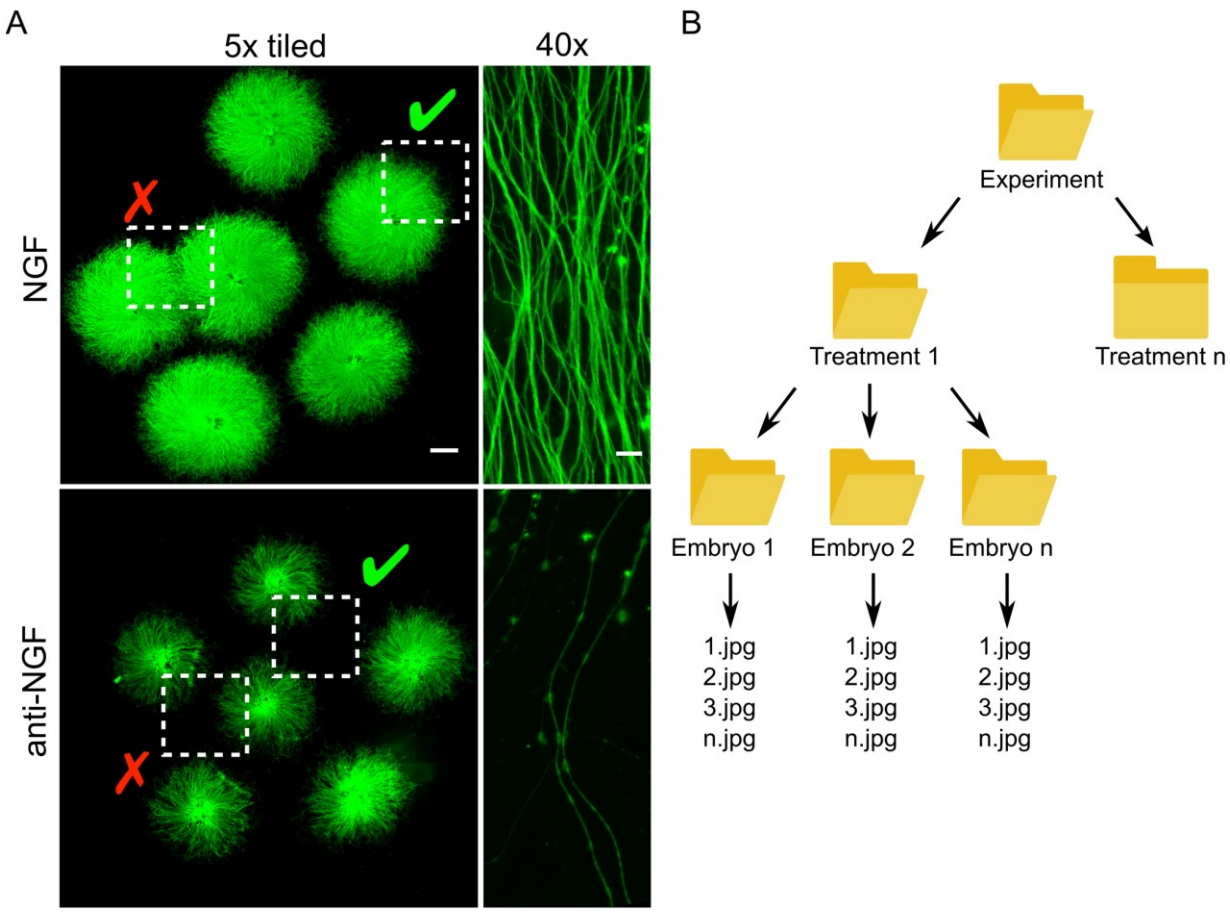

Figure 2.1. Axoquant 2.0 quantifies neurite degeneration from quarter-field images of DRG explants.

To quantify neurodegeneration using Axoquant 2.0, DRG explants are dissected from E13.5 mouse embryos and seeded on 6-well plates (two wells shown in A; NGF (top) & anti-NGF 24h (bottom), scale bar=1 mm for 5x images and 10 µm for 40x images). To quantify the degree of degeneration following a phase of NGF withdrawal and to assess the effect of pharmacological or genetic manipulations on its progression, the entire culture is imaged (after fixation and tubulin cytoskeletal immunostaining) by tile-scanning on a motorized microscope stage and automated stitching, and

quarter-fields are cropped and saved according to embryo and treatment (A; fields containing axons from only a single DRG are chosen, indicated by dotted box and green checkmark). The user directs Axoquant 2.0 to the experimental parent folder, where subfolders organized by treatment and embryo are crawled and quantified automatically (B).

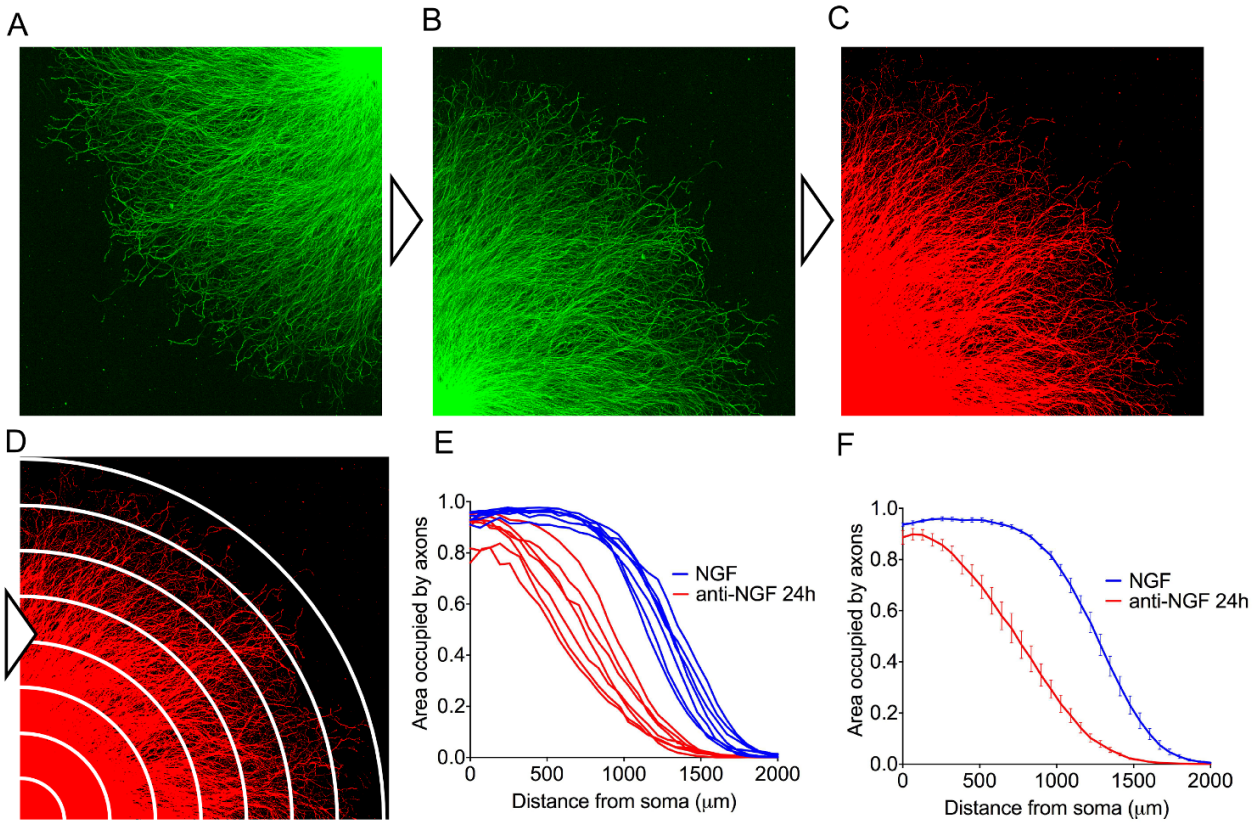

Figure 2.2. Axoquant 2.0 image processing workflow.

The R script automatically crawls folders and opens each quarter-field image (A; scale bar indicates 1 mm) and if necessary, auto-orients the explant centre to the origin (B). Images are converted to binary masks with adaptive thresholding (C), and the area of the substrate occupied by axons is measured in bins radiating from the explant centre (stylized in D). Axoquant 2.0 automatically saves a comma separated file (*.csv) to the experiment parent folder for import into graphing and statistical analysis software. For illustration, example axon density curves are shown as embryo means (E) and treatment means with standard error, n = 8 embryos (F; indicated are mean and SEM).

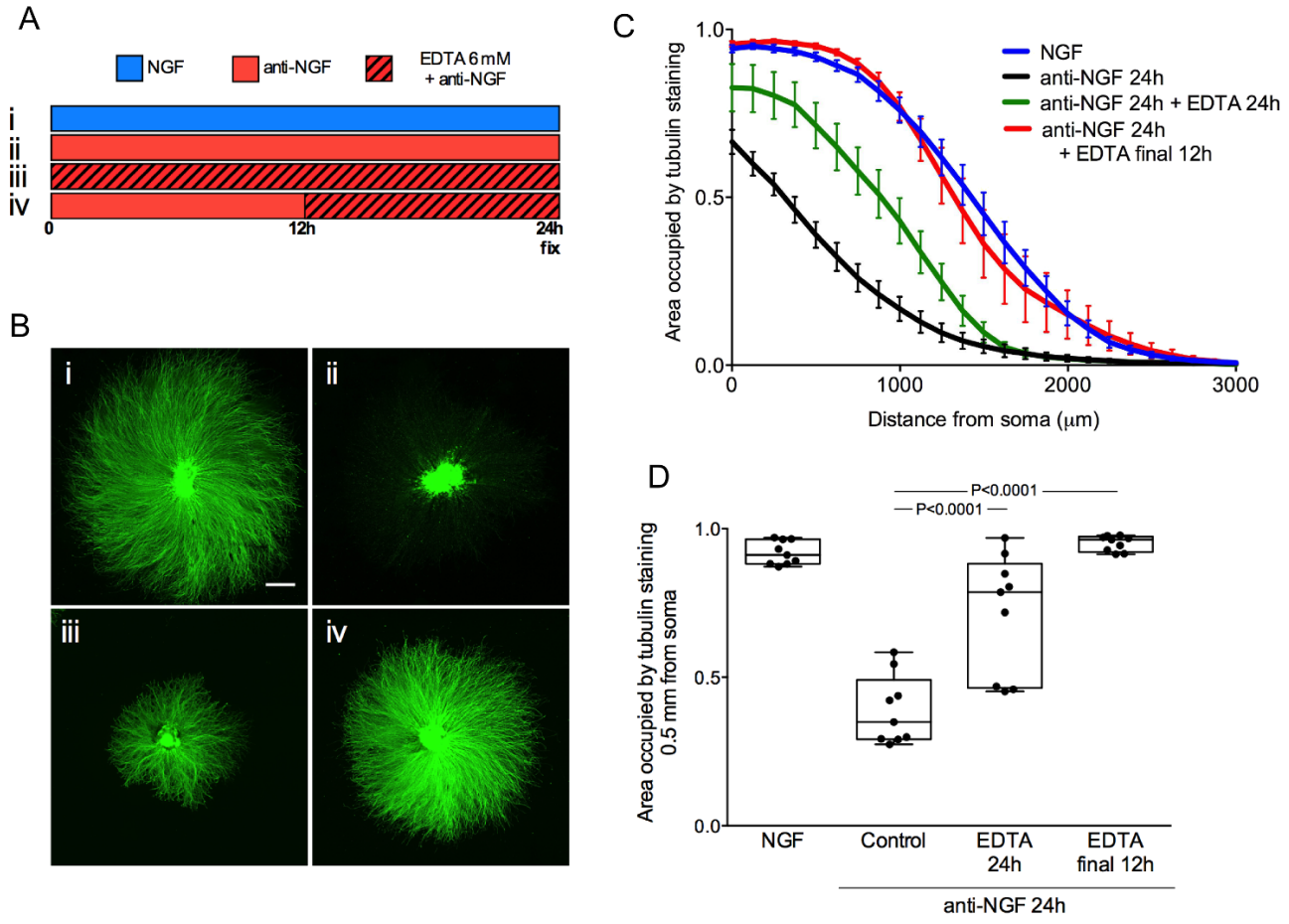

Figure 2.3. Axon degeneration following NGF withdrawal is rescued by calcium chelator EDTA. Experimental design (A); explant ganglia were cultured in NGF and then either maintained in NGF (i), deprived of NGF (ii) or deprived of NGF in the presence of EDTA 6 mM added at time of deprivation (iii) or only for the final 12 hours (iv). Cultures were fixed and immunostained with antibody against β-III tubulin, imaged at 5x and stitched; scale bar indicates 500 μm. EDTA present during the late phase of NGF withdrawal robustly rescued axons from degeneration. Plotted in C are mean embryo values and SEM reflecting the proportion of the culture substrate occupied by tubulin-stained axons as a function of distance from the soma and presented as boxplot are median, 25 & 75 percentile and min & max of all embryos per condition at a single bin including 500 μm from soma in

D. $p<0.0001$, one-way ANOVA with Tukey post-hoc multiple comparison. n=9 embryos per condition pooled from 3 independent litters performed in biological triplicate).

Chapter 3. Developmental neurodegeneration requires axoplasmic Ca^{2+} influx via TrpV1

3.1 Abstract

Ca^{2+} toxicity is associated with progressive neurodegenerative disease states (35,38,41,135) as well as promoting degeneration after acute neuronal injury (43,136), but reports made over 20 years ago concluded that DRG sensory neurons deprived of NGF do not require Ca^{2+} entry for the degeneration program (44,46,134). We revisited this and found that axons exhibit robust Ca^{2+} influx revealed by live and end-point Ca^{2+} imaging with fluo-4 and within GCAMP6f-expressing neurons. Cation chelation by EDTA rescued axons from degeneration, indicating that the observed Ca^{2+} influx was required for degeneration, while axons degenerated normally during Na^{+} channel inhibition. We identified pharmacological TrpV1 inhibitor capsazepine as an inhibitor of cytoskeletal degeneration in a screen of pharmacological Ca^{2+} channel inhibitors, and found capsazepine inhibits Ca^{2+} influx in NGF deprived axons. In cultures of DRG neurons derived from TrpV1-knockout embryos, axonal degeneration is impaired compared to wild-type axons isolated from littermates. Taken together, these results support of a model of TrpV1-dependent Ca^{2+} influx underlying developmental degeneration.

3.2 Introduction to Chapter 3

A series of studies performed more than 20 years ago concluded that Ca^{2+} influx is not a feature of developmental degeneration of sensory neurons, and argued that apoptotic death of these neurons is actually accompanied by a decrease in intracellular Ca^{2+} (46,133,137). However, it has become increasingly clear that elevated Ca^{2+} and resulting activation of destructive proteases and mitochondrial stress is a hallmark of progressive neurodegenerative diseases and in mechanical or hypoxic injury-induced axonal degeneration (38,41–43,132,138–140). This disparity prompted us to revisit the role of Ca^{2+} in developmental degeneration.

Rodent and *in vitro* studies have raised the prospect that Ca^{2+} influx via TrpV1, a cation channel widely expressed in neurons and neuroimmune cells in the CNS and PNS, and in a vast array of cell types in every organ outside the nervous system, underlies the pathogenesis of Alzheimer's and Parkinson's diseases, ALS, stroke and axotomy, as well as in normal physiological maintenance of memory and learning systems (70,97,104,119–121,125,128,141–143). However, results of these studies are difficult to reconcile into a single model for TrpV1 involvement in degeneration and it uncertain whether it plays neuroprotective or neurodegenerative role. For example, TrpV1 genetic knockout rescued RGC sensory axons in an *in vitro* model of glaucoma, but subsequent work from the same group demonstrated that systemic loss of TrpV1 actually accelerates optic nerve degeneration in an *in vivo* rodent model of glaucoma, suggesting a divergence in the role of TrpV1 in neuroprotection via neuron autonomous and non-autonomous mechanisms (124,125). Other studies have utilized experimental approaches using TrpV1 agonist capsaicin and a series of pharmacological TrpV1 antagonists to implicate the channel in physiological and disease states, but interpretation of these results is complicated by the fact that TrpV1 activation leads to desensitization and removal from membrane, so downstream effects may be due either to an increase or a decrease in active TrpV1 in

neurons or other cell types (106,110,116,123). It is clear that TrpV1 activation by exogenous activator capsaicin induces degeneration of sensory nerve endings but whether degeneration is mediated TrpV1 in physiological settings is unknown (108,114,115).

In this chapter, we re-examined the role of Ca^{2+} in developmental neurodegeneration of sensory neurons, and found that axoplasmic free Ca^{2+} rapidly increases prior to degeneration, and this influx is required for cytoskeletal fragmentation. A screen of Ca^{2+} channel inhibitors identified TrpV1 as a candidate mediator of NGF deprivation-induced Ca^{2+} influx, and the physiological important of rescue of axonal cytoskeletal integrity was confirmed by genetic knockout. The placement of TrpV1 within the degenerative signaling pathway downstream of NGF deprivation raises the prospect of TrpV1 as a therapeutic target in neurodegeneration.

3.3 Materials and methods

3.3.1 Dissection, culturing and NGF deprivation of DRG explants

DRG cultures were prepared as described in section **2.3.1**. In cytoskeletal degeneration assays, DRG were seeded on plastic 6-well culture plates (Greiner bio-one). For endpoint and time-course Ca^{2+} imaging, DRG were seeded on 4-well glass-bottom imaging dishes (CellVis).

3.3.2 Fixation, cytoskeletal immunostaining and imaging

Cultures were processed as described in section **2.3.2.**

3.3.3 Pharmacological Ca^{2+} and Na^{+} channel inhibition

All pharmacological channel inhibitors (nifedipine, ZD7288, capsazepine, ruthenium red, suramin, SKF96365 and tetrodotoxin, Tocris) were prepared in DMSO and delivered to cultures at 10 μM with DMSO not exceeding 0.1%. All inhibitors were added at time of NGF deprivation for the full 24 hour withdrawal period.

3.3.4 Generation of mixed-genotype +/-TrpV1 DRG cultures for cytoskeletal degeneration analysis

$TrpV1^{-/-}$ C57BL6 mice carrying the $TrpV1^{tm1Jul}$ (targeted mutation 1, David Julius) knockout allele in homozygosity were obtained from Jackson Laboratories and crossed with wild-type C57BL6 mice to generate $TrpV1^{-/+}$ animals, and these heterozygotes were bred in timed pregnancies to produce mixed-genotype litters of wild-type, TrpV1-/+ and TrpV1-/- E13.5 embryos. Embryos were dissected, cultured and NGF-deprived for 24 hours as described in section **2.3.1** and processed as in **2.3.2**.

3.3.5 End-point Ca^{2+} imaging with Fluo-4

30 minutes prior to imaging, cultures were incubated with 5 μM fluo-4 (Invitrogen) in dimethylsulphoxide (DMSO, Sigma, final concentration in media did not exceed 0.1%) for 15 minutes at 37 C and then allowed to equilibrate in fresh, room-temperature HBSS (Wisent) supplemented with 2 mM $CaCl_2$ for another 15 minutes. Imaging was performed in fresh HBSS with 2 mM $CaCl_2$ with a Leica DMi8 confocal microscope and LAS X software with a 488 nm laser in 0.3 micrometer z-increments with 63x objective to capture at least two fields of axons per ganglia. Background was corrected from images of sum-z-stacks by averaging the mean pixel intensities within four background regions and subtracting this value from each pixel in the image using ImageJ (FIJI build, NIH). The 2D area occupied by axons in each image was then measured using a binary mask of all axons, and the mean pixel intensity value for each image was divided by the area occupied by axons to provide a measure of fluo-4 fluorescence intensity per unit axon area. Field images of DRGs from the same embryo were averaged to produce the embryo mean value. In each experiment, measurements were standardized to the NGF control value of 1.0 and the size of the treatment values expressed as fold-change from NGF control.

3.3.6 Live Ca^{2+} imaging with GCaMP6f

At time of seeding, DRG cultures were infected with HSV-hEF1-GCaMP6f (Massachusetts Institute of Technology Viral Core Facility) followed by 24 hours to allow for neurite growth and GCaMP6f expression. Images of NGF-supplied or deprived axons were acquired at a rate of one every 10 minutes on a Zeiss ObserverZ.1 inverted epifluorescence microscope. Multiple saved field positions were imaged with an automated stage and atmosphere-controlled incubation chamber (Pecon) controlled by ZEN2 software, and 40x objective using a 470 nm Colibri LED light source (Zeiss). Axons were cropped from these movies and background was corrected on each frame using ImageJ (FIJI build,

NIH) by averaging two background regions immediately adjacent to either side of the axon and subtracting this value from each pixel of the uncorrected frame. To standardize fluorescence intensity to the time of morphological degeneration, the frame where axon collapse accompanied by spheroid membrane blebbing was observed was considered time = 0, and time-course values were then standardized to the corrected intensity value of the frame acquired 180 minutes prior and expressed as fold-change from 1.0.

3.4. Results

3.4.1 Axoplasmic Ca^{2+} increases upon NGF deprivation

To determine whether NGF deprivation induces axoplasmic Ca^{2+} influx, DRG neurons were grown in NGF and then either maintained in NGF or deprived of NGF for 15 hours, then loaded with the Ca^{2+} sensor fluo-4 and imaged by confocal microscopy. NGF withdrawal induced a significant increase in fluo-4 signal in axons ($p < 0.0001$, two-tailed t-test, n=16 embryos in each condition pooled from independent experiments, Figure 3.1 B).

To understand the kinetics of the Ca^{2+} increase relative to the timing of membrane blebbing and degeneration, axons were infected with herpes simplex virus (HSV) harbouring the genetically-encoded Ca^{2+} sensor GCaMP6f and live imaged during NGF deprivation to record the timing and rate of Ca^{2+} rise before the catastrophic degenerative event (Figure 3.1 C). Axons in culture degenerate asynchronously beginning ~15 hours of NGF deprivation and degeneration of the culture is essentially complete by 40 hours, so to examine the rate of Ca^{2+} influx, movies were standardized to the frame in which axons were observed to collapse between membrane blebs. Dunnett's post hoc comparison of fluorescence intensity between each time point versus the fluorescence intensity 180 minutes before degeneration indicated significant increase only within the final 40 minutes before degeneration ($p < 0.0001$, Figure 3.1 D), indicating that Ca^{2+} influx occurs proximal to time of gross morphological change (E).

3.4.2 Ca^{2+} chelation by EDTA is only necessary during the late phase of NGF deprivation to rescue axons from degeneration

Since NGF deprivation induced a significant axoplasmic Ca^{2+} influx prior to the time of membrane blebbing (Figure 3.1), we hypothesized that this influx is necessary for the degenerative disassembly of the tubulin cytoskeleton that occurs as a consequence of NGF withdrawal (Figure 3.2). Figure 3.2

A shows representative images of cultures of DRG neurons grown in NGF and then either maintained in NGF (i) deprived of NGF (ii) or deprived of NGF in the presence of EDTA added at the beginning of the deprivation phase (EDTA 24h, (iii)), or only for the final 12 (iv), 9 (v), 6 (vi) or 3 (vii) hours post-deprivation). The experiment was terminated by fixation at 24h post-deprivation and processed for immunofluorescence microscopy with anti-β-III tubulin antibody (A). Axon density vs distance was quantified using Axoquant 2.0 in Figure 3.2 B (two factor ANOVA, $F(525, 4408)=47.79$, $P < 0.0001$). Axons were rescued from degeneration when EDTA was added for the full 24 hours of NGF withdrawal, or added for the final 12, 9 or 6 hours of deprivation (all ps < 0.0001, Tukey's post hoc multiple comparison following one factor ANOVA comparing axonal density at 500 μm from soma, $F (6, 56) = 166.8$, $p < 0.0001$, n= 9 embryos from 3 litters). Axon density was not significantly rescued by EDTA added during the final 3 hours of NGF deprivation, a window during which massive axon degeneration was already underway ($P > 0.05$).

3.4.3 Ca^{2+} channel inhibitors rescue axons from developmental degeneration *in vitro*

Since Ca^{2+} chelation rescued axons from degeneration (Figure 3.2), we asked whether pharmacological inhibition of Ca^{2+} channels prevents loss of cytoskeletal integrity (Figure 3.3). DRG cultures were grown in NGF and then either maintained in NGF, deprived of NGF, or deprived of NGF in the presence of nifedipine (L-type voltage-gated Ca^{2+} channels), ZD7288 (HCN), capsazepine (TrpV1), ruthenium red (broad Trp, broad RyR), suramin (P2X) or SKF96365 (TrpC). After 24 hours of treatment, samples were fixed and processed for tubulin immunofluorescence microscopy using anti-β-III tubulin primary antibody and imaged (Figure 3.3 A, quantified in Figure 3.3 B). One-way ANOVA performed at 500 μm from soma revealed a significant effect of treatment, $F (7, 63) = 19.76$ ($p < 0.0001$, n= 9 embryos). A post hoc Dunnett's analysis comparing each treatment to the anti-NGF control indicated significant protection of axon density by capsazepine, ruthenium red (ps < 0.001),

nifedipine as well as ZD7288 (ps < 0.0001), demonstrating that the pro-degenerative Ca^{2+} influx is channel-dependent. Suramin or SKF96365 did not significantly rescue axons (ps > 0.05).

3.4.4 Developmental degeneration is not activity dependent

To determine whether voltage-gated Na^{+} channels contribute to axonal degeneration following NGF withdrawal, DRG neurons were cultured in NGF and then either maintained in NGF or changed to NGF deprivation media, in the presence or absence of tetrodotoxin (TTX) for 24 hours before fixation and immunostaining for fluorescence microscopy using anti-β-III tubulin primary antibody and quantified (axon density at 500 μm from soma shown in Figure 3.4). A two factor ANOVA revealed no significant interaction between TTX and NGF dose, $F(1, 32) = 0.1363$ ($p=0.7144$, n=9 embryos each condition from 3 experiments), supporting specificity of Ca^{2+} channel activity required for developmental degeneration *in vitro*.

3.4.5 TrpV1 antagonist capsazepine rescues axons from Ca^{2+} influx following NGF deprivation

While several of the Ca^{2+} channel inhibitors conferred neuroprotection (capsazepine, nifedipine, ZD7288 and ruthenium red, Figure 3.3), we chose to delve into the role of TrpV1 and its inhibitor capsazepine due to recent reports implicating TrpV1 in degeneration in other model systems (see section **1.6.4** for review) and the amenability of TrpV1 to genetic experimental approaches not offered by the other positive hits in our screen (L-type Ca^{2+} channels and HCN channels belong to families with overlapping function). We investigated whether NGF deprivation-induced Ca^{2+} entry into axons is blocked by TrpV1 inhibition (A). Following growth in NGF, cultures were either maintained in NGF or deprived of NGF in the presence or absence of capsazepine for 15 hours before loading with Ca^{2+} indicator fluo-4 and imaged (representative images shown in Figure 3.5 B). NGF deprivation induced the formation of membrane spheroids characteristic of degenerating axons (B, top panel). Capsazepine

significantly rescued axons from Ca^{2+} influx compared to axons subjected to NGF deprivation alone (quantified in panel C, $p < 0.001$, Tukey's post-hoc test following two factor ANOVA, $F(1, 24) = 13.52$, $p < 0.01$, n=7 embryos from 4 experiments). NGF-deprived axons treated with capsazepine were not significantly different from healthy axons continuously provided with NGF ($p > 0.05$).

3.4.6 TrpV1 antagonist capsazepine rescues axonal cytoskeletal integrity during developmental degeneration *in vitro*

Cultures of embryonic DRG neurons were grown in NGF and then either maintained in NGF, changed to NGF-deprivation media, or changed to NGF-deprivation media containing the TrpV1 antagonist capsazepine to assess the role of TrpV1 in cytoskeletal degeneration (Figure 3.5). After 24 hours of treatment, cultures were fixed and processed for immunofluorescence microscopy with anti-β-III tubulin primary antibody (representative images are presented in Figure 3.5 D). A post hoc Dunnett's multiple comparison between NGF deprived samples and NGF deprived samples treated with capsazepine indicated a significant rescue of axonal density by TrpV1 inhibition during NGF withdrawal ($p < 0.0001$, Figure 3.5 E; one factor ANOVA, $F(2, 35) = 34.28$, $p < 0.0001$, n=12 embryos from 3 experiments).

3.4.7 Genetic TrpV1 knockout rescues axonal tubulin cytoskeletal integrity during developmental degeneration *in vitro*

To assess the role of TrpV1 in developmental degeneration *in vitro*, DRG neurons were cultured from mixed-genotype litters of wild-type, heterozygous and null TrpV1 embryos and cultured in NGF, and then either maintained in NGF or changed to deprivation media (with anti-NGF antibody) for 24h followed by fixation and cytoskeletal immunostaining with anti-β-III tubulin primary antibody (Figure 3.6 B). Tukey's post hoc pairwise comparison performed on axonal density 500 μm from soma reported a significant difference between wild-type axons grown in NGF and wild-type axons deprived

of NGF ($p < 0.001$), but no significant difference in density between TrpV1-null axons provided with NGF versus deprived null axons ($p > 0.05$). Wild-type, NGF-deprived axons were significantly less dense than TrpV1-null axons deprived of NGF, indicating a pro-degenerative role for TrpV1 during developmental degeneration (Figure 3.6 C; two factor ANOVA, $F(2, 58) = 4.69$, $p < 0.05$, $n = 10$ wild-type, 10 heterozygotes and 12 null embryos pooled from 4 independent litters).

3.5 Discussion

Recent reports have highlighted the essential role of acute Ca^{2+} influx in the axotomy-induced degeneration of DRG axons, and chronically elevated Ca^{2+} has a clearly established role in toxic stress underlying neurodegenerative disease (40,43,46,132,136,137,144–146). However, evidence for a role of Ca^{2+} in developmental degeneration has been contradictory or indirect. An early study reported that there is no increase in intracellular Ca^{2+} in apoptotic DRG neurons deprived of NGF (133). Another study from the same group reported rescue of NGF-deprived DRG neurons *in vitro* by diphenylpiperazine Ca^{2+} channel inhibitors, but the authors explicitly concluded that these compounds rescued by an unknown mechanism other than inhibition of Ca^{2+} entry, since Ca^{2+} imaging performed on the cultures found that neurons committed to die 24 hours after NGF withdrawal exhibited a decline in intracellular Ca^{2+} before apoptotic membrane alterations and degeneration, and the compounds did not alter the profile of intracellular Ca^{2+} flux over time versus NGF deprivation alone (137). Indirect evidence for a role for Ca^{2+} in developmental degeneration was raised by the finding that loss of calpastatin, an endogenous inhibitor of Ca^{2+}-activated proteases, calpains, promotes degeneration (147).

We addressed the lack of clarity by Ca^{2+} imaging in NGF-deprived axons loaded with the dark-to-light Ca^{2+} sensing dye fluo-4 (Figure 3.1). NGF withdrawal from DRG cultures plated on glass imaging dishes for 15 hours displayed spheroid membrane protrusions, or blebs, characteristic of apoptosis-associated decoupling of membrane from underlying cytoskeletal structural support, accompanied by elevated axoplasmic free Ca^{2+} concentration compared to controls continuously provided with NGF (Figure 3.1 A, quantified in B). The influx of axoplasmic Ca^{2+} occurred proximal to the time of frank degeneration axons and appearance of membrane blebs and collapse of the axon (Figure 3.1 C and D), suggesting an acute role for Ca^{2+} in cytoskeletal disassembly following a lag

phase from the initiation of NGF deprivation (Figure 3.1 E). The lag phase prior to rapid Ca^{2+} influx is reminiscent of the kinetics of axotomy-induced degeneration, in which there is a lag of several hours between the injury event and the terminal Ca^{2+} influx; molecular and signaling events that correlate with the lag phase are not yet understood (43).

To test whether this late Ca^{2+} influx event was causative of cytoskeletal fragmentation and axonal degeneration, DRG cultures were deprived of NGF for 24 hours, and free Ca^{2+} was sequestered from biological functions by the addition of EDTA into the culture media (Figure 3.2). EDTA was added either at the time of deprivation, or only for the final 12, 9, 6 or 3 hours of the death stimulus period in order to test the importance of Ca^{2+} during early and late phases of NGF withdrawal. Consistent with a late role for Ca^{2+} influx in degeneration, removal of free Ca^{2+} from the system only for the final 12, 9 or 6 hours significantly rescued axonal density (axon density as a function of distance form soma shown in Figure 3.2 B; axonal density within the bin surrounding 500 μm from soma is presented in C). The axon rescue effect of EDTA was lost when added only for the final 3 hours of the 24-hour NGF deprivation period, before which widespread axonal degeneration has already begun.

Since axonal degeneration was preceded by Ca^{2+} influx (Figure 3.1) and Ca^{2+} influx was found necessary for cytoskeletal degeneration (Figure 3.2), we hypothesized that Ca^{2+} channels are activated in response to NGF deprivation signaling. To test this, we applied a panel of Ca^{2+} channel inhibitors with diverse targets to DRG cultures and compared axonal density following 24 hours of NGF deprivation (Figure 3.3). We found a significant protective effect on the tubulin cytoskeleton by TrpV1 inhibitor capsazepine, L-type Ca^{2+} channel inhibitor nifedipine, hyperpolarization-activated, cyclic nucleotide-gated (HCN) channel inhibitor ZD7288, and broad Trp channel and ryanodine receptor inhibitor ruthenium red (representative images shown in Figure 3.3 A and quantification of axonal density at 500 μm from soma is shown in B). Suramin, a p2x-receptor inhibitor, and TrpC inhibitor

SKF96365 were ineffective (B). Inhibition of Na^+ action potentials by TTX also failed to rescue axons, supporting a specific role for Ca^{2+} influx in promoting degeneration (Figure 3.4). Since nifedipine, ZD7288 and ruthenium red inhibit large families of structurally related proteins, we chose to investigate further the role of capsazepine target TrpV1 because it is amenable to genetic experimental approaches and due to sporadic reports of its role in animal models of neurodegenerative disease (70,118,119,141). Intriguingly, there is evidence elsewhere for interplay between TrpV1 and nifedipine-targeted Ca^{2+} channels, as capsaicin-induced degeneration of cultured cortical neurons was rescued by both capsazepine and nifedipine, suggesting that voltage-gated Ca^{2+} channels are activated downstream of TrpV1-mediated Ca^{2+} influx in these cells (141).

Since TrpV1 inhibitor capsazepine rescued axons from cytoskeletal degeneration (Figure 3.5 D and E), we hypothesized that it does so by blocking Ca^{2+} influx induced by NGF withdrawal (Figure 3.5 B and C). 15 hours of NGF deprivation from DRG explants cultured on glass-bottom imaging dishes showed membrane bleb formation characteristic of degeneration and enriched axoplasmic Ca^{2+} as determined by fluo-4, but inclusion of capsazepine during deprivation significantly blocked Ca^{2+} influx and protected against the appearance of membrane blebbing (Figure 3.5 B; quantified in C). Axonal swellings were observed on some axons in capsazepine-treated samples (B, bottom right panel), suggesting either that TrpV1 activity is required for maintenance of normal axon morphology or that parallel non-TrpV1-mediated pathways are at least partially intact.

We then hypothesized that genetic TrpV1 knockout is neuroprotective during NGF deprivation (Figure 3.6 A). To test this, litters of mixed-genotype TrpV1 embryos were generated by heterozygote parent crosses and DRGs were isolated, cultured and either maintained in NGF or deprived for 24 hours (Figure 3.6 B). While NGF deprivation resulted in significant loss of axonal density in wild-type

axons, TrpV1 knockout axons were significantly more dense after the withdrawal period than were wild-type axons (Figure 3.6 C).

Taken together, these results indicate that NGF-deprivation induced degeneration of embryonic sensory neurons induces a rapid, late Ca^{2+} influx via TrpV1 required for cytoskeletal fragmentation within axons. The molecular signaling and regulatory mechanisms by which NGF deprivation is transduced to activate TrpV1 are explored by experiments in chapter 4.

3.6 Figures and figure legends

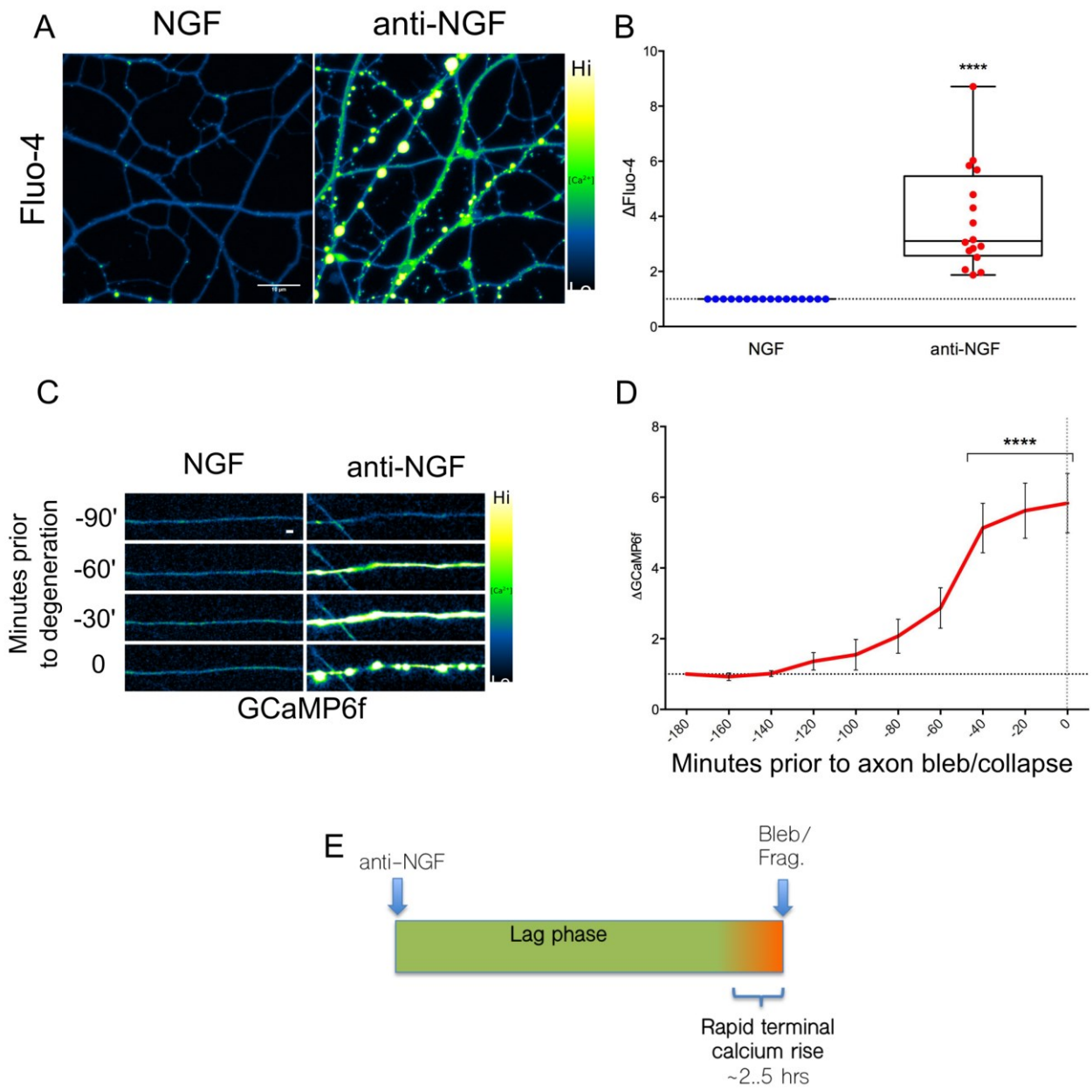

Figure 3.1. NGF deprivation induces an increase in axoplasmic free Ca^{2+}.

DRG neurons were grown in NGF and then either maintained in NGF or deprived of NGF for 15 hours, then loaded with the fluorescent Ca^{2+} sensor dye fluo-4 and imaged by confocal microscopy (A; scale bar indicates 10 μm). NGF withdrawal induced a significant increase in fluo-4 intensity in axons

indicated by a two-tailed t-test versus standardized NGF-provided controls ($p < 0.0001$, n=16 embryos in each condition pooled from independent experiments, B). Ca^{2+} influx occurs proximal to time of membrane blebbing and axon collapse in axons expressing the genetically-encoded Ca^{2+} sensor GCaMP6f (C; scale bar indicates 10 μm). Movies generated by live-imaging were standardized to the frame in which axons were observed to bleb and collapse (a one factor ANOVA found a significant effect of time prior to degeneration on fluo-4 intensity, $F(9, 54) = 13.95$, $P = 0.0001$). Dunnett's post hoc multiple comparisons between fluorescence intensity at each time point and intensity 180 minutes before degeneration indicated significant increase only by the final 40 minutes before degeneration ($p < 0.0001$, D; indicated are mean and SEM). Axons within cultures degenerate asynchronously after a lag phase of between ~15 and 40 hours followed by rapid Ca^{2+} influx (E). Box plots indicate median, 25%, 75% percentile, and min/max.

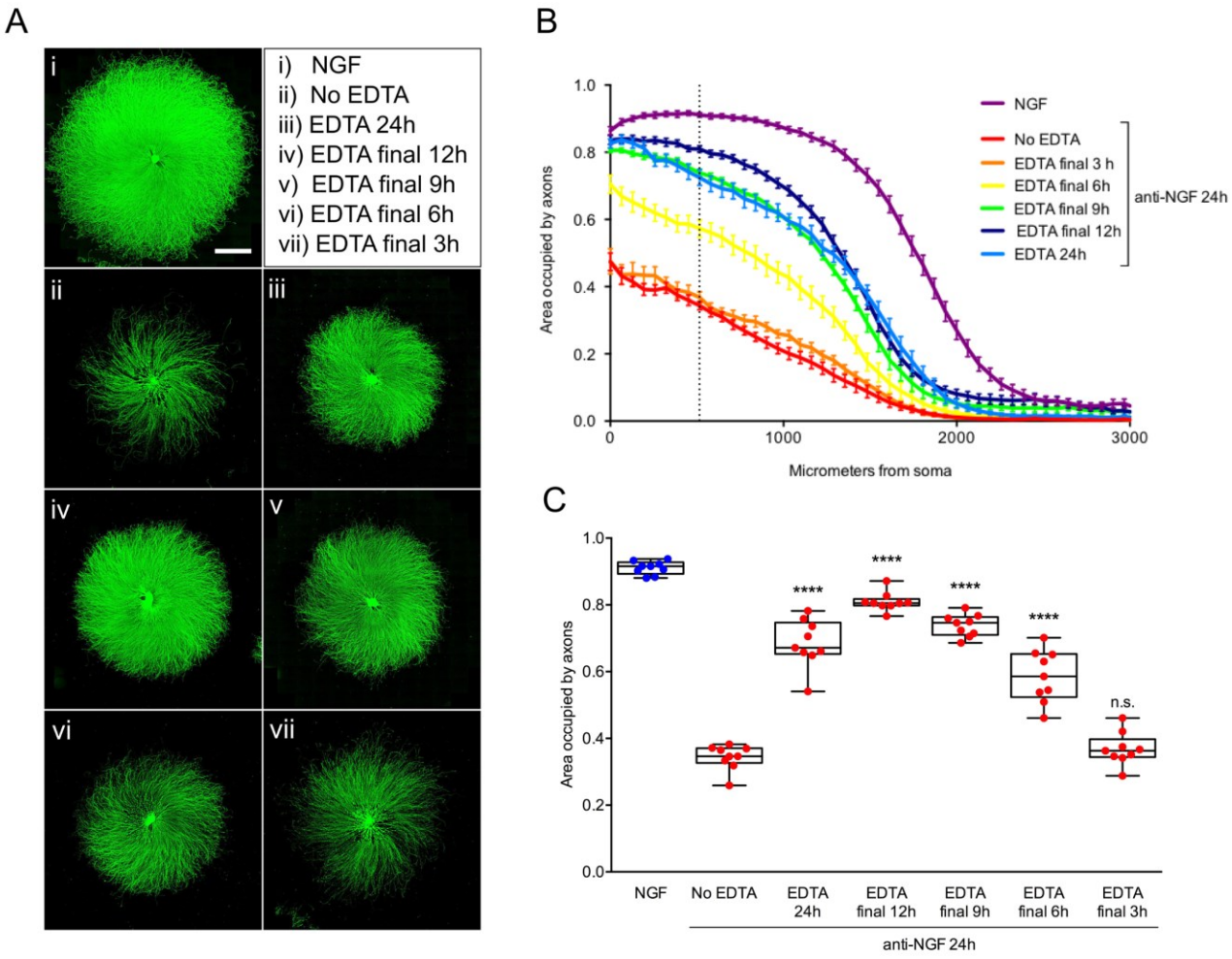

Figure 3.2. Ca^{2+} influx is required for developmental degeneration in vitro but not during the early phase of NGF withdrawal.

Neurons grown in NGF and then either maintained in NGF (i) or deprived of NGF (ii) in the presence of EDTA added at the beginning of the deprivation phase (EDTA 24h, (iii)), or only for the final 12 (iv), 9 (v), 6 (vi) or 3 (vii) hours post-deprivation (A; scale bar indicates 1 mm). Axon density curves reported by Axoquant 2.0 are shown in B. A one factor ANOVA comparing axonal density at 500 µm from soma (indicated as dotted line in B; indicated are mean and SEM) revealed significant treatment effect $F(6, 56) = 166.8$, $p < 0.0001$ (n = 9 embryos from 3 experiments, quantified in Figure 3.2 C).

Tukey's post hoc multiple comparisons indicated a significant rescue of axonal cytoskeleton integrity by EDTA when added at the time of NGF deprivation, or added for the final 12, 9 or 6 hours of deprivation ($p < 0.0001$ at each timepoint), but not when added for the final 3 hours ($p > 0.05$) supporting the hypothesis that Ca^{2+} plays a pro-degenerative role proximal to the timing of degeneration. Boxplots indicate median, 25%, 75% percentile, and min/max.

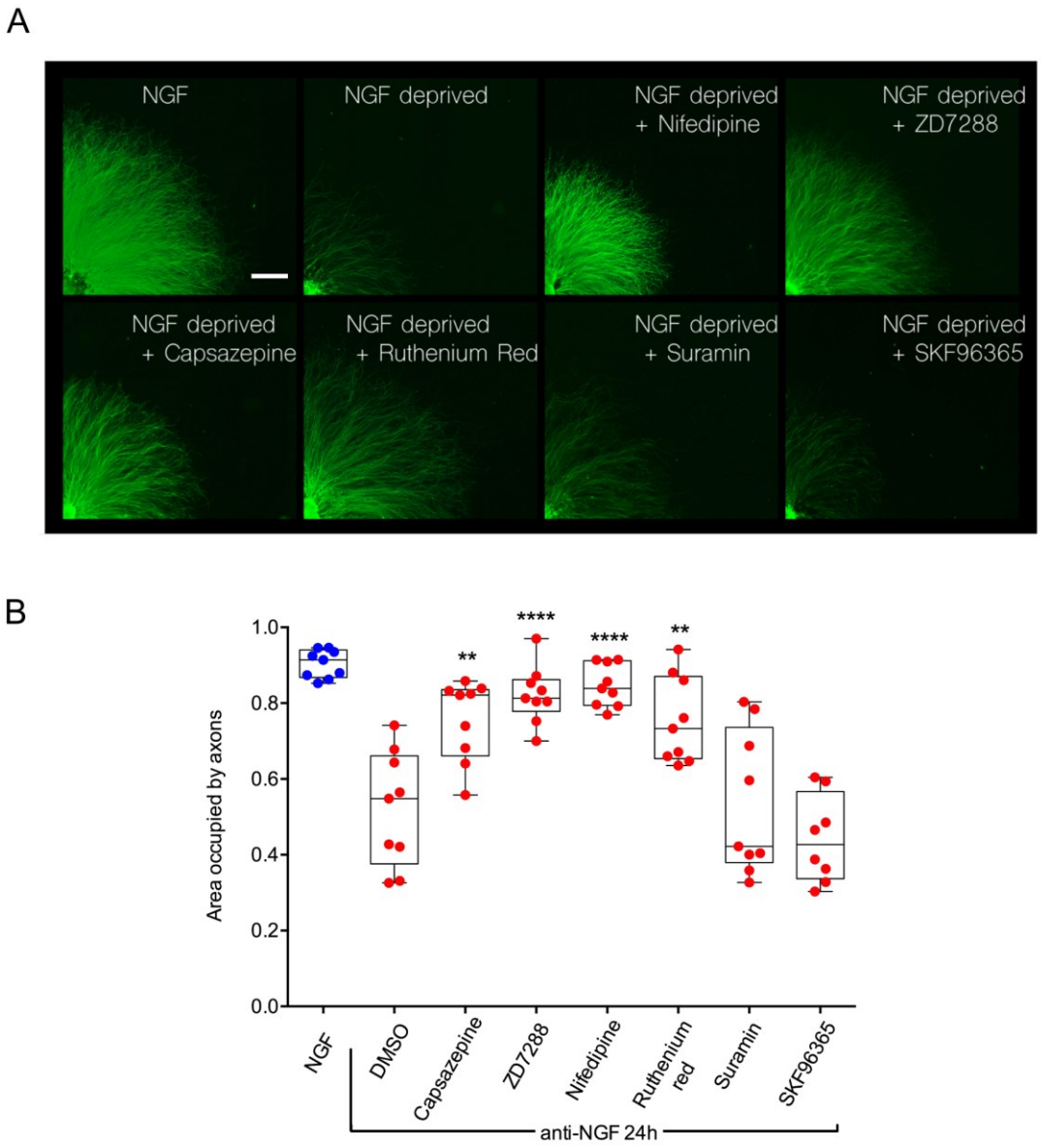

Figure 3.3. Pharmacological inhibition of Ca^{2+} channel proteins rescues axons from degeneration.

DRG cultures grown in NGF and then either maintained in NGF, deprived of NGF, or deprived of NGF in the presence of nifedipine (inhibitor of L-type voltage-gated calcium channels), ZD7288 (HCN), capsazepine (TrpV1), ruthenium red (broad Trp, broad RyR), suramin (P2X) or SKF96365 (TrpC) to examine the role of diverse Ca^{2+} channels in developmental degeneration (scale bar indicates 1 mm). After 24 hours of treatment, samples were fixed and processed for tubulin immunofluorescence

microscopy and imaged (A; quantified in B). One factor ANOVA performed 500 μm from soma revealed a significant treatment effect $F(7, 63) = 19.76$, $p < 0.0001$, n= 9 embryos each treatment from 3 experiments. A post hoc Dunnett's analysis comparing each treatment to the anti-NGF control indicated significant neuroprotection by capsazepine and ruthenium red (ps < 0.001), nifedipine and ZD7288 (ps < 0.0001,) demonstrating that the pro-degenerative Ca^{2+} influx is channel-dependent. Suramin or SKF96365 did not significantly rescue axons (ps > 0.05). Boxplots indicate median, 25%, 75% percentile, and min/max.

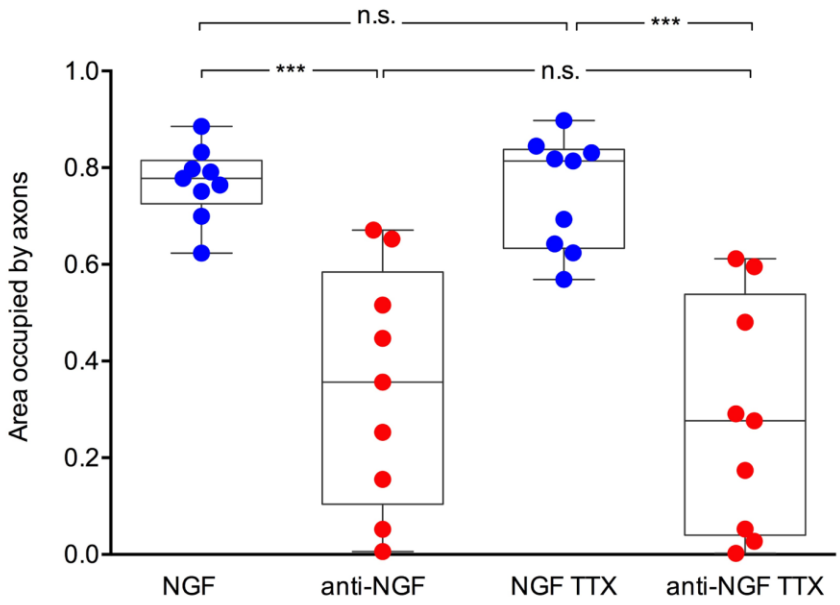

Figure 3.4. Voltage-gated sodium channels are not required for developmental degeneration. DRG neurons were cultured in NGF and then either maintained in NGF or changed to NGF deprivation media in the presence or absence of sodium channel inhibitor tetrodotoxin (TTX) for 24 hours before fixing and immunostaining for fluorescence microscopy. A two factor ANOVA revealed no significant interaction between TTX and NGF-state, $F(1, 32) = 0.1363$, $P = 0.7144$ with $n = 9$ embryos each condition from 3 experiments, indicating that while Ca^{2+} channel activity is required for developmental degeneration *in vitro*, voltage-gated Na^{+} channel activation is dispensable for the effect.

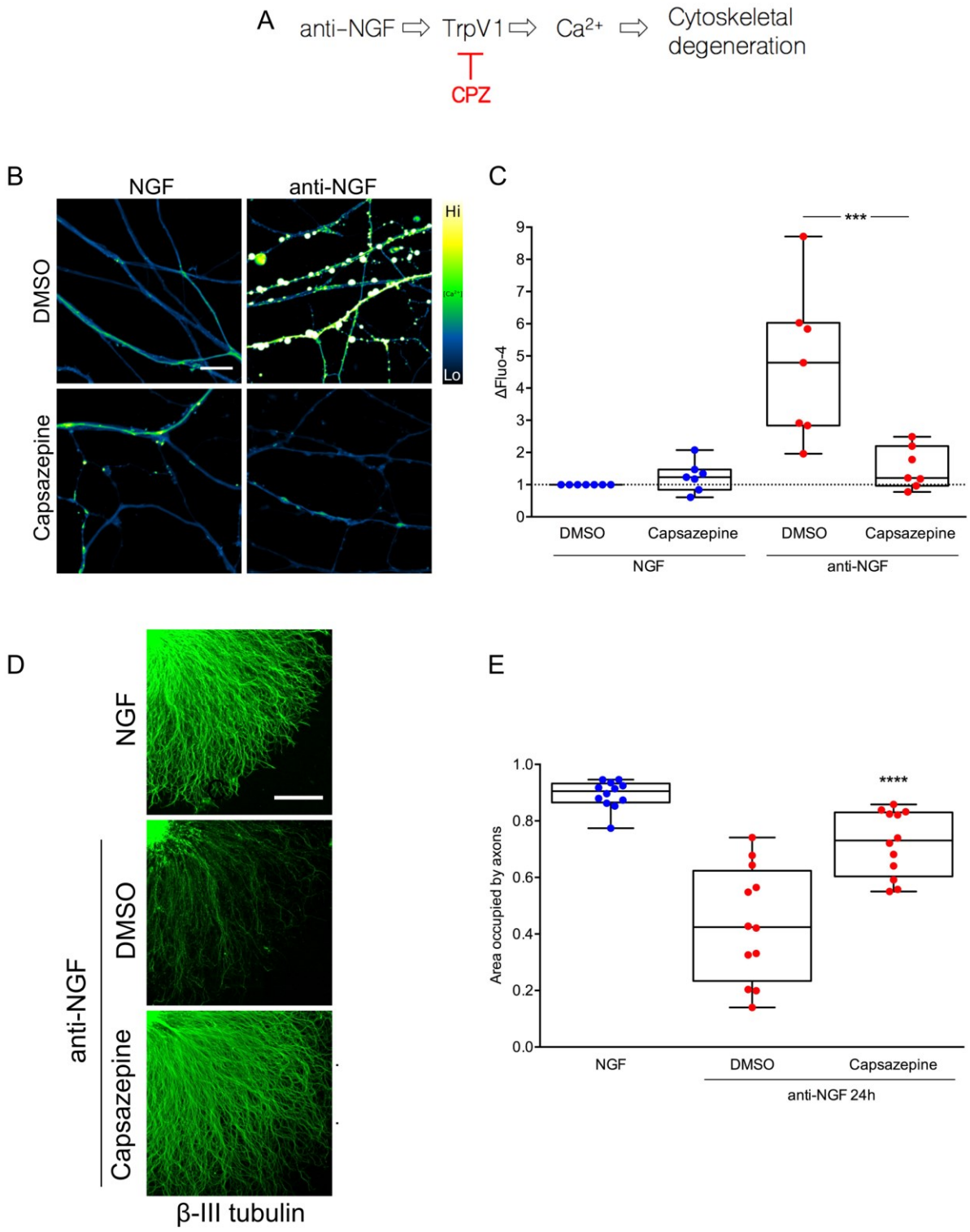

Figure 3.5 Pharmacological TrpV1 inhibition by capsazepine rescues axons from Ca^{2+} influx and cytoskeletal degeneration.

Pharmacological inhibitor capsazepine was used to investigate the role of TrpV1 in degeneration (A). Axons deprived of NGF for 15 hours displayed membrane spheroid formation and significantly elevated free Ca^{2+} determined by imaging with Fluo-4 (representative micrographs shown in B with scale bar indicating 10 μm). Treatment with TrpV1 inhibitor capsazepine during NGF deprivation significantly blocked Ca^{2+} influx versus deprivation alone (panel C; $p < 0.001$, Tukey post-hoc analysis, n=7 embryos). NGF-deprived axons treated with capsazepine were not significantly different from healthy axons continuously provided with NGF ($p > 0.05$). TrpV1 inhibition rescues axons from cytoskeletal disassembly (D and E). Samples were fixed after 24 hours of treatment and processed for immunofluorescence microscopy with anti-β tubulin III primary antibody (representative images are presented in D; scale bar indicates 1 mm). Following a one-factor ANOVA, a post hoc Dunnett's multiple comparison between NGF deprived samples and NGF deprived samples treated with capsazepine indicates a significant rescue of axonal density by TrpV1 inhibition (panel E, $p < 0.0001$, n=12 embryos). Boxplots indicate median, 25%, 75% percentile, and min/max.

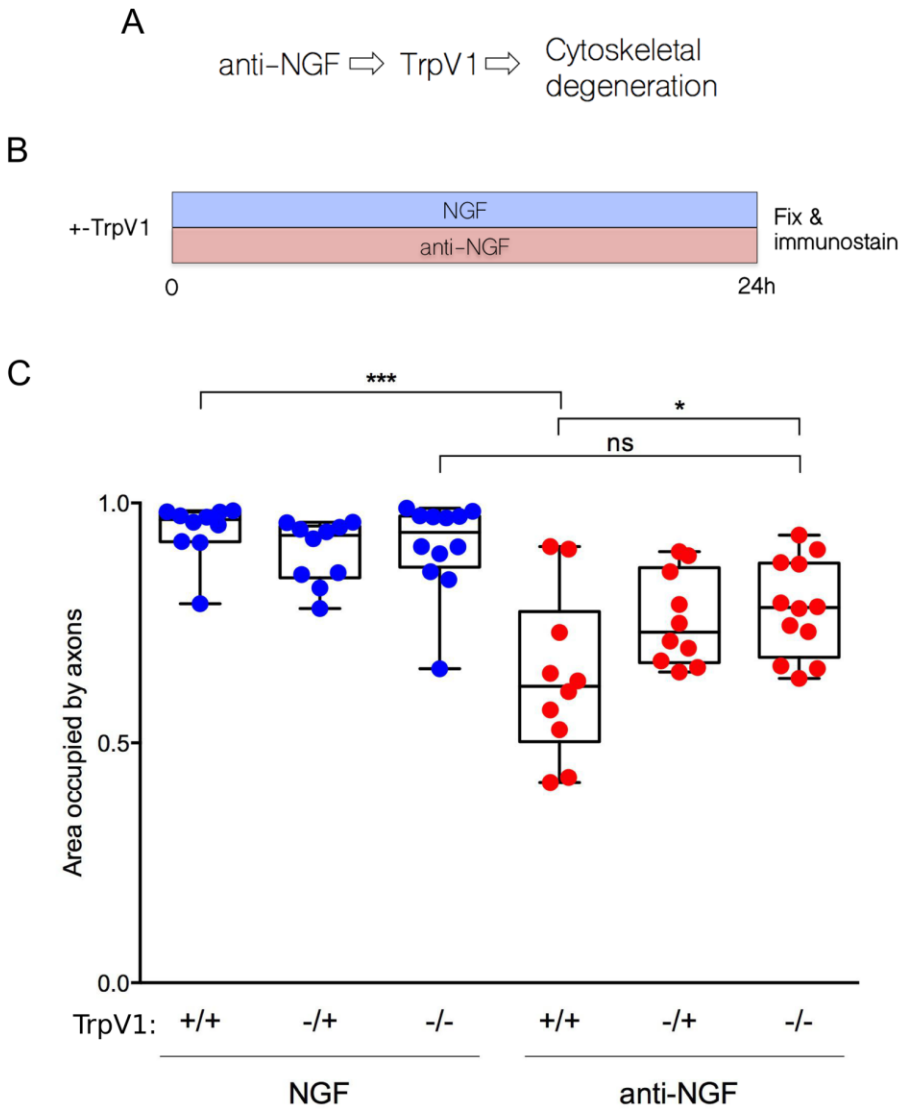

Figure 3.6. TrpV1-null axons are rescued from degeneration.

Mixed-genotype litters of TrpV1 knockout mice were used to assess the role of TrpV1 in degeneration (A). Cultures were either maintained in NGF or changed to deprivation media (containing anti-NGF) for 24h (B) and quantified (axon density reported at 500 μm from soma shown in C). TrpV1-null axons were significantly more dense than wild-type after 24 hours of NGF withdrawal ($p < 0.05$, Tukey post-hoc analysis following two factor ANOVA, $F(2, 58) = 4.69$, $p < 0.05$; n = 10 wild-type, 10

heterozygotes and 12 null embryos pooled from 4 mixed-genotype litters. Boxplots indicate median, 25%, 75% percentile, and min/max).

Chapter 4. Ca^{2+} influx is mediated by a PKC > Nox complex > ROS > TrpV1 axis

4.1 Abstract

Our data indicates a key role for TrpV1-mediated Ca^{2+} influx during developmental axon degeneration. Mutually-enhancing interplay between Ca^{2+} and reactive oxygen species (ROS) is a hallmark of physiological and disease-associated degeneration and is among the earliest measured phenomena in its progression, and TrpV1 is understood to be regulated by redox chemistry (38,41,135,145,148,149). Thus, we hypothesized that during developmental degeneration of DRG sensory neurons deprived of NGF, ROS activate TrpV1-mediate Ca^{2+} influx. Caspase-3 maturation was impaired in the presence of ROS scavenger NAC during NGF withdrawal, and NAC rescued axons from Ca^{2+} influx and cytoskeletal degeneration, while acute oxidative challenge by peroxide robustly activated Ca^{2+} influx. Nox complexes are a major source of enzymatically-generated ROS for intracellular signaling (81,83,86,90,150) and pharmacological Nox inhibition with VAS2870 rescued axons both from Ca^{2+} influx and cytoskeletal degeneration. Assembly and activation of Nox complexes is activated by PKC-mediated phosphorylation of Nox subunits (88,91,151,152), and we find that PKC inhibition rescues axons from Ca^{2+} influx and degeneration, and that acute PKC activation by its direct agonist PMA induces robust Ca^{2+} influx in live-imaged axons. This influx was ROS and Nox complex-dependent, and completely ablated by pharmacological and genetic TrpV1 inhibition. Taken together, our data indicates that a PKC>Nox complex>ROS>TrpV1>Ca^{2+} signaling axis underlies developmental degeneration. We also report the generation of novel imaging tools to examine direct activation of TrpV1 by ROS.

4.2 Introduction to Chapter 4

DRG neurons deprived of NGF undergo Ca^{2+}- mediated axon degeneration contributed to by Ca^{2+} channel TrpV1 (Chapter 3). Although sporadic reports have suggested a role for TrpV1 in diverse neurodegenerative diseases, its context in degenerative signaling pathways is not understood (reviewed in Chapter 1). In other systems, TrpV1 can be regulated by protons, temperatures exceeding ~43 C, exogenous noxious compounds produced by some plants and invertebrates, and endogenous compounds NADA and anandamide, lipids, oxidized protein products and reactive oxygen species (ROS) (51–55,68,73–76,103,149,153). Since elevated intracellular oxidation state is a hallmark of apoptotic-like neurodegenerative signaling (16,42,84,145,154) and TrpV1 contains reactive cysteine residues essential for activation by oxidative modification (68,75,96,149,155), we explored whether NGF deprivation-induced prodegenerative Ca^{2+} influx via TrpV1 is ROS-dependent.

Redox regulation of TrpV1 is supported by several studies employing mutant analysis. Allicin, an oxidizing molecule responsible for the noxious effect of onions and garlic on mucous membranes, activates TrpV1-mediated Ca^{2+} current via a reactive cysteine at amino acid position 157 (63). Mutation of this residue significantly reduced the pool of assembled TrpV1 channels versus monomer, revealing an important role for disulphide linkages in subunit assembly to form the functional pore (68). Injection of H_2O_2 in mouse footpads increased TrpV1-dependent pain sensation, suggesting that oxidation sensitizes TrpV1 (69,70). In HEK293 cells, H_2O_2 has been reported to dose-dependently induce TrpV1-mediated Ca^{2+} influx (71).

A major intracellular source of endogenous ROS for signal transduction from surface receptors are Nox complexes, large proteinaceous membrane-associated oxidases that generate superoxide via electron transfer from NADPH (83,88,157–159). Nox complexes are activated by phosphorylation of the core activator subunit $p47^{phox}$ by members of the PKC family of structurally-related kinases, which

are activated endogenously by diacylglycerol (DAG) generated by phospholipase C, or by pharmacological DAG mimetic PMA (11,77,88,151,153,160). There is evidence from other cell systems that signaling cassettes comprised of PKC > Nox complexes > ROS > TrpV1 > Ca^{2+} transduce changes in the extracellular environment sensed by surface receptors to alterations in intracellular Ca^{2+} concentration (73,77,92,152).

We aimed to place TrpV1 into a signaling context in NGF deprivation-induced, Ca^{2+}-dependent degeneration of DRG neurons. In a series of experiments described in this chapter, we obtained evidence that developmental degeneration depends on ROS *in vitro,* generated by Nox complexes downstream of active PKC. Live Ca^{2+} imaging experiments indicated that PKC stimulation induces Ca^{2+} influx that is sensitive to antioxidant and Nox complex inhibition, and that PKC-induced Ca^{2+} influx is sensitive to pharmacological and genetic TrpV1 loss-of-function. Finally, we developed a set of tools for investigating the direct role of ROS in TrpV1-mediated Ca^{2+} influx.

4.3 Materials and methods

4.3.1 Dissection and culturing of DRG explants

DRG cultures were prepared as described in section **2.3.1**.

4.3.2 Fixation, cytoskeletal immunostaining and imaging

Cultures were processed for cytoskeletal immunostaining as described in section **2.3.2**.

4.3.3 Pharmacological PKC and Nox complex inhibitors

PKC inhibitors Gö6976 and Gö6983 and Nox complex inhibitors apocynin and VAS2870 (all obtained from Tocris) were prepared in DMSO and delivered to cultures at 10 μM with the exception of apocynin which was delivered at 100 μM. DMSO did not exceed 0.1% in final culture in any case.

4.3.4 End-point Ca^{2+} imaging with Fluo-4

End-point Ca^{2+} imaging with Fluo-4 was performed as described in section **4.3.3**.

4.3.5 Live Ca^{2+} imaging with Fluo-4 in wild-type CD1 axons

30 minutes prior to imaging, cultures were incubated with 5 μM Fluo-4 (Invitrogen) in dimethylsulphoxide (DMSO, Sigma, final concentration in media did not exceed 0.1%) for 15 minutes at 37 C and then allowed to equilibrate in room-temperature, fresh HBSS (Wisent) supplemented with 2 mM $CaCl_2$ for another 15 minutes. Fields of >100 axons each were acquired at 40x at a rate of one frame every 5 seconds on a Zeiss ObserverZ.1 inverted epifluorescence microscope controlled by ZEN2 software with an atmosphere-controlled incubation chamber (Pecon) and 470 nm Colibri LED light source (Zeiss). Before injection of stimulus (capsaicin 100 nM, PMA 100 nM or H_2O_2 800 μM) baseline fluorescence was recorded for 1 minute (12 frames). Background was corrected from each frame individually in each movie by averaging the pixel intensity value of 4 background regions and

subtracting this value from the mean pixel intensity of the uncorrected frame (NIH ImageJ, FIJI build). Fluo-4 responses were standardized for each run as fold-change from the initial frame (set to 1.0).

4.3.6 Generation of mixed-genotype +/-TrpV1 DRG cultures and live Ca^{2+} imaging with Fluo-4

Wild-type and null TrpV1 E13.5 embryos were generated as described in section **3.4.7** and cultured as in section **2.3.1**. Imaging was performed as in section **4.3.5** with one frame captured every 6 seconds, and PMA 100 nM was injected after capturing baseline (5 frames). Background correction and standardization was performed as described in section **4.3.5**.

4.3.7 Ca^{2+} imaging with TrpV1-GECO fusion proteins

HEK293T cells were cultured on 4-well glass-bottom imaging dishes (CelVis) and infected with HSV harbouring either wild-type TrpV1-R-GECO, C157A-R-GECO or Δp-loop-G-GECO followed by a 24 hour expression period. Prior to imaging, cells were switched to fresh HBSS supplemented with 2 mM $CaCl_2$. Cells were imaged as described in **4.3.5** at 3-second intervals and H_2O_2 800 μM was injected after 1 minute of baseline collection (15 frames). Background correction was performed by obtaining the mean pixel intensity of 4 background regions this value was subtracted from the mean intensity of each cell region of interest on a frame-by-frame basis (NIH ImageJ, FIJI build). GECO responses were standardized as fold-change from GECO intensity at frame 1 (set to 1.0).

4.4 Results

4.4.1 ROS promote maturation of prodegenerative protease caspase-3 during NGF deprivation

The major executioner caspase-3 is initially produced as a precursor that undergoes cleavage to become mature in response to NGF deprivation (Figure 4.1 A). To investigate whether caspase-3 activation is dependent on ROS generated during NGF withdrawal, the effect of antioxidant NAC on caspase-3 maturation in NGF-deprived DRG neurons was assessed by Western blot (representative experiment shown in Figure 4.1 B and quantified in C). Tukey's post hoc multiple comparison indicated a significant induction of mature caspase-3 by 15 hours of NGF withdrawal versus control axons continuously provided with NGF ($p < 0.0001$). However, NGF-deprived axons treated with antioxidant NAC during NGF deprivation (Figure 4.1 C) displayed significantly less caspase-3 maturation ($p < 0.001$), indicating caspase-3 maturation is ROS-dependent (two factor ANOVA, $F(1, 32) = 10.30$, $P = 0.003$; n=9 embryos from 3 experiments).

4.4.2 Axonal Ca^{2+} influx is activated by acute oxidative stress

We hypothesized that acute oxidative stress is an activator of axoplasmic Ca^{2+} influx, since blockade of ROS using antioxidant NAC prevented the maturation of caspase-3 in NGF-deprived axons (Figure 4.1). To test this, H_2O_2 or buffer control was added to fluo-4-loaded axons during live-imaging and the fluorescence response was compared (representative frames shown in Figure 4.2 A). The quantified time-course of fluo-4 response shown in B with significant indicated during the final 1.5 minutes of recording, $p < 0.05$, Sidak's post hoc, two factor ANOVA, $F(120, 720) = 5.363$, $P < 0.0001$ (n=4 embryos). A two-tailed unpaired t-test comparing maximum fluo-4 responses indicated significant calcium entry into axoplasm ($p < 0.05$) upon oxidative challenge by peroxide (Figure 4.2 C).

4.4.3 ROS derived from NADPH-oxidase (Nox) complexes activate Ca^{2+} influx after NGF deprivation

Since axoplasmic Ca^{2+} influx can be activated by acute oxidative stress induced by peroxide (Figure 4.2), we asked whether the physiological Ca^{2+} influx during NGF deprivation is stimulated by ROS generated by the NADPH oxidase (Nox) complex. As shown schematically in Figure 4.3A-B, Nox complexes activated by phosphorylation produce highly-reactive superoxide from O_2 upon enzymatic electron transfer from NADPH. In Figure 4C, healthy axons or axons deprived of NGF for 15 hours in the presence or absence of antioxidant NAC or Nox complex inhibitor VAS2870 were loaded with fluo-4 and imaged. A one factor ANOVA revealed significant interaction between NGF-state and compound treatment, $F(3, 8) = 13.43$, $P = 0.0017$ (n=3 embryos each treatment). Tukey's post hoc pairwise comparisons indicated a significant blockade of Ca^{2+} influx by the antioxidant ($p < 0.01$) and by Nox complex inhibition ($p < 0.05$). Treatment by either compound restored fluo-4 intensity to a level not significantly different from healthy, NGF-provided axons (all p values > 0.05).

4.4.4 Axonal tubulin cytoskeleton is rescued from degeneration by pharmacological Nox complex inhibition or antioxidant NAC

Consistent with our finding that Nox complex inhibition or inclusion of an antioxidant rescues axons from NGF deprivation-induced Ca^{2+} influx, an axonal degeneration assay performed on tubulin-immunostained axons (Figure 4.3 E) revealed that Nox complex inhibitors had a significant effect on NGF withdrawal-induced axonal density loss (one factor ANOVA, $F(5, 12) = 10.29$, $P = 0.0005$, n=3). Tukey's post hoc multiple comparison indicated that inhibition of the Nox complex with VAS2870 or inclusion of the antioxidant NAC in NGF-deprived axons restored axonal density to a degree not significantly different from the healthy control, regardless of whether the compounds were added at the time of deprivation, or 12 hours into the 24-hour deprivation period, indicating a late-phase role for Nox complex signaling after NGF deprivation consistent with the timing of Ca^{2+} influx (Figure

3.2) (all ps > 0.05). NGF deprivation alone induced degeneration significantly greater than that observed when axons are deprived but treated with NAC or VAS2870 (all ps < 0.01).

4.4.5 PKC activation induces axonal Ca^{2+} influx

Nox complexes are stimulated to produce ROS upon phosphorylation by PKC in diverse neuronal and other cell models, and thus we hypothesized that the pro-degenerative, Nox-derived ROS that activate calcium influx during NGF deprivation (Figure 4.3) are activated by PKC. First, we tested whether stimulation of PKC with diacylglycerol-mimetic phorbol 12-myristate 13-acetate (PMA) is capable of inducing calcium influx into axons (Figure 4.4 A). Live-imaged fluo-4-loaded axons were treated either with fresh HBSS or PMA (representative frames shown in Figure 4.4 B, quantified in C). Significant effect of PMA on Ca^{2+} influx was indicated by two-way ANOVA, $F(178, 4654) = 3.073$, $P < 0.0001$ (n=14 embryos). A comparison of maximum fluo-4 fluorescence intensity responses between PMA- and HBSS-treated axons (D) with a two-tailed unpaired t-test indicated significant calcium influx upon PKC activation by PMA ($p < 0.0001$).

4.4.6 PKC inhibitors rescue axons from Ca^{2+} influx following NGF deprivation

Since PKC stimulation is capable of activating Ca^{2+} influx (Figure 4.4), we hypothesized that antagonizing PKC during NGF deprivation can rescue axons from Ca^{2+} influx (Figure 4.5 A). PKC promotes assembly of Nox complex subunits via direct phosphorylation, activating ROS production (B). DRG cultures were either supplied with NGF or deprived for 15 hours in the presence or absence of pharmacological inhibitors of PKC Gö6976 and Gö6983, then loaded with Ca^{2+} sensor fluo-4 and imaged (Figure 4.5 C). Tukey's post hoc pairwise test indicated that NGF deprivation induced a significantly increased axoplasmic concentration of free Ca^{2+} as reported by fluo-4 ($p < 0.0001$, D). Axons deprived of NGF but provided with PKC inhibitors Gö6976 and Gö6983 showed no significant

fluo-4 intensity above the NGF-supplied healthy control axons, indicating blockade by PKC inhibition (both ps > 0.05). NGF deprived axons showed significantly greater fluo-4 intensity than deprived axons subjected to PKC inhibition (ps < 0.0001, one factor ANOVA, $F(3, 20) = 19.74$, $P < 0.0001$ with n=6 embryos from 4 experiments).

4.4.7 PKC inhibition prevents disassembly of the tubulin cytoskeleton in NGF-deprived axons

Since pharmacological PKC inhibitors rescued axons from Ca^{2+} influx, we asked whether the tubulin cytoskeleton is rescued from disassembly by PKC inhibition by Gö6976 (representative images are shown in Figure 4.5 E and quantified at 1 mm from soma in F). A two factor ANOVA indicated a significant interaction between NGF-state and presence/absence of the drug, $F (1, 24) = 47.81$, $P < 0.0001$ with n=6 embryos from 3 experiments, on axonal density as reported by anti-tubulin immunostaining. Axons provided with Gö6976 are significantly more dense following a 24-hour phase of NGF deprivation versus axons deprived in the absence of inhibitor, indicating a pro-degenerative role for PKC in this setting ($p < 0.0001$, Tukey's post hoc contrast). NGF deprived axons treated with Gö6976 were not significantly different from healthy NGF controls ($p > 0.05$).

4.4.8 Ca^{2+} influx activated by PKC depends on ROS via Nox complex

Since oxidative stress activates Ca^{2+} influx (Figure 4.2), promotes pro-degenerative caspase-3 activation (Figure 4.1), and PKC inhibition rescues axons degeneration and inhibits Ca^{2+} influx during NGF deprivation (Figure 4.5), we investigated whether the Ca^{2+} influx activated by PKC described in Figure 4.4 is dependent on Nox-derived ROS (Figure 4.7). To assess the role of ROS in PKC-induced Ca^{2+} influx, axons were loaded with fluo-4 and live-imaged during stimulation of PKC by PMA in the presence or absence of antioxidant NAC (hypothesis and approach summarized by Figure 4.7 A). The time-course of fluo-4 response is shown in B over a 15-minute recording period, and the increased fluorescence intensity induced by PMA stimulation is negated in the presence of NAC (two factor

ANOVA, F (537, 3580) = 3.644, P < 0.0001, n=6 experiments, B). Tukey's post hoc comparison of maximum fluo-4 responses (C) between PMA-stimulated axons and axons treated with HBSS buffer alone indicated a significant calcium influx upon PKC activation ($p < 0.05$), but PMA in the presence of antioxidant NAC did not significantly increase fluo-4 intensity compared to buffer only control ($p > 0.05$), arguing that the Ca^{2+} concentration increase observed upon PMA application is ROS-dependent (two factor ANOVA, F (1, 20) = 5.123, P = 0.0349).

Nox complexes have emerged as key intracellular sources of signaling ROS downstream of PKC in diverse models, and we thus hypothesized that the ROS generated in response to PKC activator PMA (Figure 4.7 B & C) is derived from activated Nox complexes (D). Fluo-4-loaded axons were live-imaged during PKC stimulation by PMA in the presence or absence of the Nox complex inhibitor apocynin (E; two factor ANOVA F (537, 2864) = 1.989, P < 0.0001). Maximum fluo-4 responses from the experiment (F) were compared with Tukey's post hoc method, and indicated a significant Ca^{2+} influx by PKC stimulation versus buffer-only control ($p < 0.01$), while axons stimulated with PMA but in the presence of apocynin displayed no greater Ca^{2+} influx than unstimulated axons ($p > 0.05$, two factor ANOVA between PMA dose (0, 100 nM) and apocynin dose (0, 100 μM), F (1, 16) = 4.963, P = 0.0406), indicating PMA-induced ROS produced by Nox complexes are sufficient to activate significant Ca^{2+} influx.

4.4.9 TrpV1 mediates Ca^{2+} influx downstream of PKC activation

We hypothesized that the Ca^{2+} influx observed downstream of PKC activation occurs via opening of the TrpV1 channel. Chemical and genetic loss-of-function approaches were used to test whether PMA-induced Ca^{2+} influx is impaired by TrpV1 deficiency (Figures 4.8 & 4.9). First, a pharmacological approach to TrpV1 inhibition was taken (Figure 4.8 A); axons loaded with fluo-4 were treated either with PMA or HBSS buffer (supplemented with 2mM Ca^{2+}), in the presence or absence of the TrpV1

inhibitor capsazepine during live imaging (representative frames before and after PMA application are shown in Figure 4.8 B, and quantified in C). A pairwise multiple comparison of maximum fluo-4 responses (D) using Tukey's post hoc method indicated a significant increase in fluo-4 fluorescence intensity in response to PMA ($p < 0.01$) that is abolished in the presence of capsazepine as compared to buffer-only control, indicating a key role for TrpV1 in transducing Ca^{2+} influx downstream of PKC ($p > 0.05$, Tukey's post-hoc two factor ANOVA, $F(1, 20) = 6.418$, $P = 0.0198$, n=7 embryos from 4 experiments)

We next took a genetic approach to investigate the role of TrpV1 in transducing PKC activation into Ca^{2+} influx (Figure 4.9 A). Cultures of wild-type and TrpV1-null axons were generated from mixed-genotype littermate embryos; TrpV1-null axons were confirmed to be insensitive to its specific and potent agonist capsaicin (Figure 4.9 B; representative trace shown in C). Next, the contribution of TrpV1 to PKC-induced Ca^{2+} influx was examined by live-imaging of fluo-4-loaded axons stimulated with PMA (Figure 4.9 D; n=6 pooled embryos of each genotype). Sidak's pairwise multiple comparison indicated significantly greater Ca^{2+} influx in wild-type versus TrpV1-null axons following PMA addition between 5 and 15 seconds after application ($p < 0.0001$; two factor ANOVA, $F(25, 260) = 5.044$, $P < 0.0001$, D). A two-tailed t-test performed on the maximum fluo-4 responses of each genotype indicated a significant ablation of the Ca^{2+} response to PKC activation via TrpV1 knockout ($p < 0.0001$, E).

4.4.10 Development of reagents for TrpV1 mutant analysis to investigate activation by ROS

Since our data indicate that ROS generated by Nox complexes downstream of PKC activates Ca^{2+} influx via TrpV1, we hypothesize that TrpV1 is directly activated by ROS during NGF withdrawal. To investigate whether reactive cysteine modification mediates TrpV1 activation, we developed a set of recombinant imaging tools for delivery by viral vector comprised of a **g**enetically-**e**ncoded **c**alcium

indicator for **o**ptical imaging (GECO) fused to wild-type TrpV1 (Figure 4.10 A), or a TrpV1 mutant lacking reactive cysteine 157 (C157A-R-GECO), along with a negative control lacking the pore domain (Δp-loop-G-GECO). TrpV1-GECO reports activation by capsaicin (a representative experiment and trace is shown in Figure 4.10 B & C). To validate whether TrpV1 C157A mediates ROS-dependent calcium influx under idealized conditions (Figure 4.10 D), HEK293T were infected with modified herpes simplex virus (HSV) harbouring wild-type TrpV1 or mutant C157 and pore-defective (p-loop) GECO fusions, and challenged with H_2O_2 (800 μM) during live-imaging (two factor ANOVA performed on mean responses from 3 pooled independent experiments indicated significant interaction between time and construct, $F(292, 876) = 8.610$, $P < 0.0001$). A comparison of maximum GECO responses with Tukey's pairwise method (one factor ANOVA, $F(2, 6) = 32.36$, $P = 0.006$) indicated that wild-type TrpV1 stimulated by peroxide induces significantly greater Ca^{2+} influx than TrpV1 lacking the pore domain ($p < 0.001$) or lacking cysteine residue 157 ($p < 0.01$), validating a key role for oxidation in TrpV1 activation, and justifying its use for future experiments in TrpV1-null axons to assess the importance of C157A and ROS in NGF-deprivation induced neurodegeneration (E).

4.5 Discussion

Oxidative intracellular status and elevated Ca^{2+} tone are causatively associated in physiological, regulatory settings and in disease states (40,41,132,140,145,146,161,162). Evidence supports the existence of a signaling cassette comprised of ROS-generating Nox complexes in association with redox-regulated Trp Ca^{2+} channels to achieve Ca^{2+} flux in other models (73,77,92,123,163). Since our data indicates TrpV1 mediates Ca^{2+} influx required for developmental degeneration (Figures 3.5 and 3.6), we hypothesized that ROS generated by Nox complexes activate TrpV1 in this context.

Cleavage of pro-caspase-3 into a mature, proteolytically-active form is required to cleave peptide targets resulting in fragmentation of the axonal cytoskeleton during developmental degeneration *in vivo* and *in vitro* (25,164–166). Caspase-3 activation has been reported to depend on upstream ROS generation during NGF withdrawal in cultured sympathetic neurons and PC12 cells, both of which depend on NGF for survival like DRG neurons (167–169). We thus utilized caspase-3 maturation as a downstream marker of pro-degenerative signaling to test our hypothesis that ROS mediate developmental degeneration of sensory neurons (Figure 4.1 A). NGF deprivation induced robust generation of the ~17 kDa subunit of active caspase-3 after 15 hours of NGF deprivation (a representative Western blot from one of three pooled experiments is shown in Figure 4.1 B and quantified in C). Application of antioxidant and reducing agent NAC to cultures significantly reduced the pool of cleaved, mature caspase-3 induced by NGF deprivation, indicating a key role for ROS in transduction of TrkA/TNFR-mediated degenerative signing to downstream disintegration of the axonal cytoskeleton.

Since Ca^{2+} (Figures 3.1 and 3.2) and ROS (Figure 4.1) were both required for degenerative signaling after NGF withdrawal, we hypothesized that ROS are upstream activators of Ca^{2+} influx in these axons. Fluo-4-loaded axons were live-imaged during oxidative challenge by hydrogen peroxide,

which induced a significant increase in axoplasmic free Ca^{2+} compared to axons mock-stimulated with HBSS buffer alone (Figure 4.2). More importantly, NAC also inhibited the Ca^{2+} influx observed in axons after 15 hours of NGF deprivation (Figure 4.3 C). We tested our hypothesis that the physiological sources of ROS generated during developmental degeneration are Nox complexes (Figure 4.3 A and B). To test this hypothesis, axons were incubated with triazolo-pyrimidine VAS2870, a Nox complex inhibitor without intrinsic antioxidant properties, nor inhibitory effects on xanthine oxidase or nitric oxide synthase, two other major catalysts of reactive species generated for cell signaling (Figure 4.3 A) (170–172). Nox complex inhibition by VAS2870 during 15 hours of NGF deprivation significantly inhibited axoplasmic Ca^{2+} influx (representative image shown in Figure 4.3 C, quantified in D). Both NAC and VAS2870 rescued axons from cytoskeletal degeneration when present in NGF-deprived cultures for the full 24-hour deprivation period, or only for the final 12 hours of deprivation (Figure 4.3 E), indicating that Nox complex activity is not required during the early phase of withdrawal for its protective effect on the axonal tubulin cytoskeleton, as we also observed by Ca^{2+} chelation (Figure 3.2). Elsewhere, an siRNA approach to identifying specific Nox complexes was reportedly successful in identifying Nox2,3,4 and DUOX2 as having a role in axotomy-induced axon degenerationwhile DUOX1 knockdown was ineffective; a similar genetic approach may bolster the pharmacological approach taken here (173).

Nox complexes are activated by PKC-dependent phosphorylation of the core regulator Nox subunit $p47^{phox}$ (83,159,174), and thus we hypothesized that direct PKC activation by PMA is sufficient to induce axoplasmic Ca^{2+} influx (Figure 4.4 A). PMA injection into cultures during live imaging resulted in significantly enriched axoplasmic free Ca^{2+} compared to injection of HBSS buffer alone (representative images before and after injection are shown in Figure 4.4 B and the time course of activation and maximum Fluo-4 responses are shown in C and D, respectively). PMA-stimulated axons

displayed a distinctive immediate Ca^{2+} "spike" that recovers partially before a steady increase, ultimately resulting in Ca^{2+}-rich axons with membrane spheroid formation (Figure 4.4 C). Since acute PKC stimulation by its pharmacological activator PMA induced Ca^{2+} influx, we hypothesized that a PKC activates Ca^{2+} influx during NGF deprivation and tested this by inhibiting PKC with potent and specific bisindolylmaleimides Gö6976 and Gö6983 during NGF withdrawal (Figure 4.5 A and B). Both PKC inhibitors significantly blocked Ca^{2+} influx and membrane blebbing induced by 15 hours of NGF deprivation (representative images shown in Figure 4.5 C and quantified in D). PKC inhibition was also highly effective in rescuing the axonal cytoskeleton from degeneration in cultures deprived of NGF for 24 hours (representative images shown in Figure 4.5 E and axon density is quantified at 1 mm from soma in F). Since PKC is a large superfamily of structurally-related proteins, a genetic approach to identifying the specific isoform(s) responsible for pro-degenerative signaling downstream of NGF withdrawal using siRNA knockdown should be taken in future experiments to

Since our data indicated that PKC, Nox complexes, ROS and TrpV1 all lie upstream of Ca^{2+} influx and axonal degeneration during developmental degeneration, we sought to identify whether these events occur in sequence to comprise a signaling axis (Figure 4.6). In other cell models, PKC-dependent stimulation of ROS via Nox complexes and TrpV1 activation by ROS has been reported (66,67,73,91,153). Thus, we hypothesized that a PKC > Nox complex > ROS > TrpV1 signaling axis achieves axonal Ca^{2+} influx in these axons. To test this logic, PKC was stimulated acutely by exogenous PMA during Ca^{2+} imaging, and we utilized a suite of pharmacological inhibitors to test the requirement of downstream components for Ca^{2+} influx (Figure 4.6 A; schematic of the cassette shown in B). First, we tested the hypothesis that PKC-induced Ca^{2+} influx is ROS-dependent (Figure 4.7 A). PMA application induced a significant increase in axoplasmic free Ca^{2+} but the response was completely blocked by ROS scavenging by antioxidant NAC (time course presented in Figure 4.7 B,

and maximum Fluo-4 responses are shown in C). Since ROS blockade prevented the PKC-induced Ca^{2+} influx, we tested whether these ROS originate from activated Nox complexes with the Nox complex inhibitor apocynin (Figure 4.7 D). PMA-induced PKC stimulation induced a significant increase in Fluo-4 fluorescence intensity, but pre-incubation and co-application of apocynin restored the response to a level not significantly different from buffer-only control (time courses presented in E and maximum Fluo-4 responses compared in F). Apocynin, an inhibitor of Nox complex core activator assembly and activation, was used in this assay due to an apparent photosensitizing effect of VAS2870 on axons that precluded live-imaging under these conditions. siRNA knockdown of Nox complexes may provide another venue to identify the specific isoforms responsible for mediating the effect.

Next we hypothesized that TrpV1 mediates PKC-induced Ca^{2+} influx and tested this by stimulating PKC with PMA in the presence or absence of capsazepine (Figure 4.8 A), which we found earlier to block Ca^{2+} influx and cytoskeletal degeneration during NGF deprivation (Figure 3.5). The activation of Ca^{2+} influx typical of PKC stimulation was essentially entirely blocked by TrpV1 inhibition (representative images before and after PMA injection are shown in Figure 4.8 B, and time courses and maximum Fluo-4 responses are presented in C and D, respectively). This pharmacological result was then confirmed genetically in TrpV1-null axons generated from mixed-genotype litters of embryos (Figure 4.9). Axons lacking the TrpV1 gene were completely unresponsive to the specific TrpV1 activator capsaicin (Figure 4.9 A; representative images taken before and after capsaicin injection on wild-type and $TrpV1^{-/-}$ axons are shown in B and a representative trace of the Fluo-4 response to free Ca^{2+} is presented in C). PMA stimulation induced the characteristic immediate Ca^{2+} spike in wild-type axons but was entirely absent in axons lacking TrpV1 (time course of Fluo-4 responses after injection of PMA are shown in Figure 4.9 D and maximum responses are presented in

E). Taken together, these experiments demonstrate that PKC-dependent axonal Ca^{2+} influx requires ROS generation via Nox complexes, and subsequent opening of the TrpV1 Ca^{2+} channel.

We developed a suite of novel imaging tools to explore direct activation of TrpV1 by ROS (Figure 4.10). Wild-type TrpV1 was recombinantly fused at its C-terminus to R-GECO, a genetically-encoded calcium sensor (Figure 4.10 A) (175). The resulting TrpV1-R-GECO protein responded to capsaicin application when expressed via HSV viral vector (GECO fluorescence response shown in Figure 4.10 B, and a TrpV1-R-GECO-expressing DRG neuron is shown in C before and after capsaicin stimulation of TrpV1-mediated Ca^{2+} influx). To create an imaging tool for investigating ROS-dependence of TrpV1 activation, the cysteine residue at position 157 in wild-type TrpV1, reported elsewhere to be a key redox-sensitive residue for TrpV1 subunit assembly and activation, was mutated to alanine (68,149). A third construct was generated for use as a negative control, and lacks the pore-loop domain essential for functional cation pore formation (designated Δp-loop-G-GECO) (176). To compare the activation profiles of these 3 recombinant TrpV1-based Ca^{2+} sensors in response to oxidative conditions, each was expressed in HEK293T cells and challenged with hydrogen peroxide during live imaging (time courses of GECO activation are presented in Figure 4.10 D). We chose to validate these constructs in HEK293T cells because this line does not express TrpV1 (177), or show Ca^{2+} influx response to challenge by H_2O_2 (178). Wild-type TrpV1 mediated an increase in free cytoplasmic Ca^{2+} that was significantly higher than cells expressing either the negative control (Δp-loop-G-GECO) or TrpV1 lacking cysteine 157 (Figure 4.10 E). These constructs are amenable to expression in primary neurons via viral vectors and future experiments will utilize them to investigate whether TrpV1-mediated Ca^{2+} influx is impaired by mutation of regulatory cysteine C157 during NGF deprivation. They will also be used to test whether the C157A mutation results in a dominant-negative TrpV1 mutant that can rescue axons from degeneration during NGF deprivation in future experiments.

Taken together, our data support a model of TrpV1-mediated Ca^{2+} influx downstream of PKC-dependent Nox complex activation and ROS generation in DRG axons during developmental degeneration.

4.6 Figures and figure legends

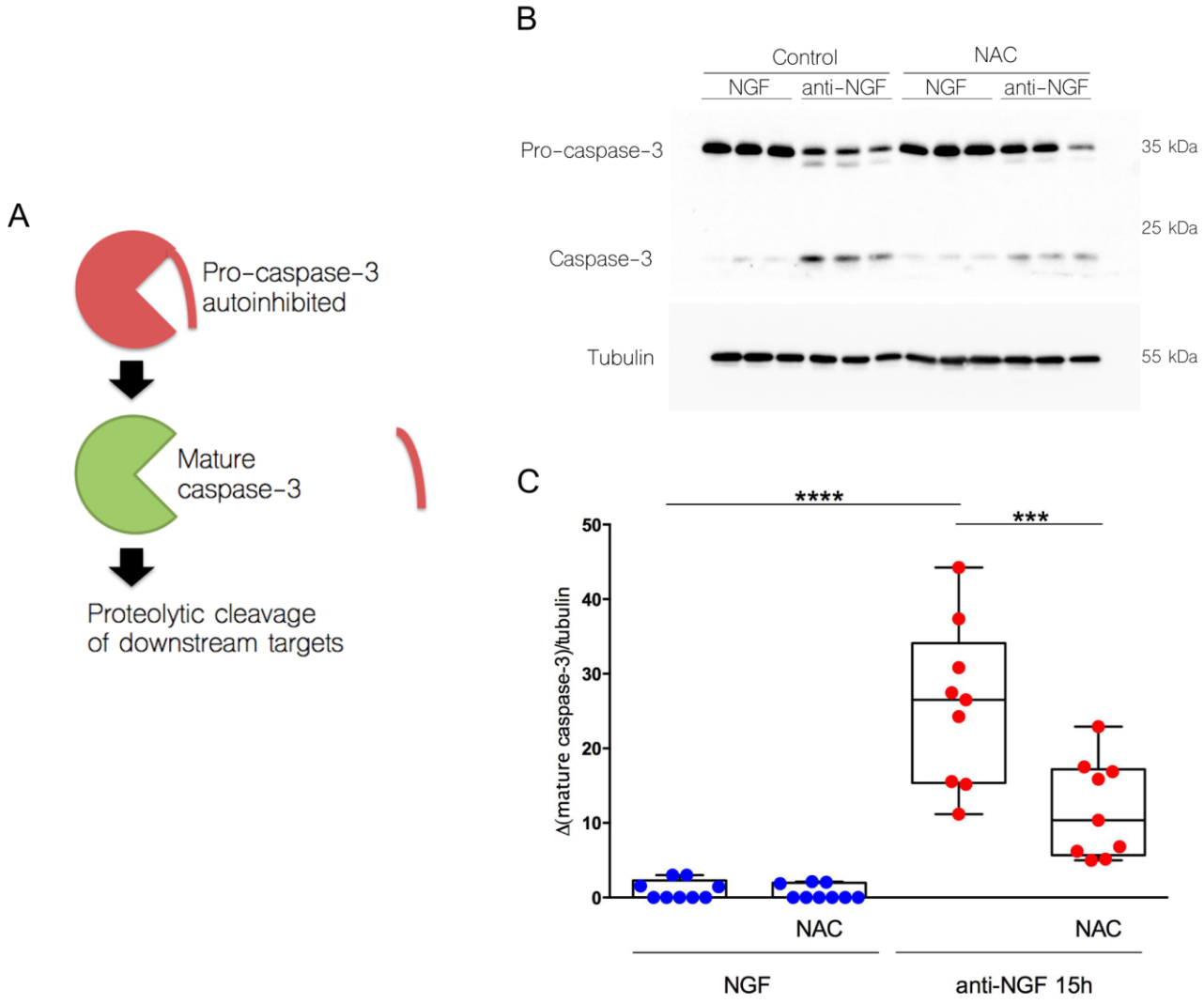

Figure 4.1. Maturation of the pro-degenerative protease caspase-3 is ROS dependent in developmental degeneration in vitro.

The major executioner caspase-3 is initially produced as a precursor that undergoes cleavage to become mature in response to NGF deprivation (A). To investigate whether caspase-3 activation is dependent on ROS generated during NGF withdrawal, the effect of antioxidant NAC on caspase-3 maturation in NGF-deprived DRG neurons was assessed by Western blot (B). A two factor ANOVA performed on the data revealed a significant interaction between NGF-state and NAC dose (0 and 20 mM), F (1, 32)

= 10.30, P = 0.003 (n=9 embryos from 3 experiments, Figure 4.1 C). Tukey's post hoc multiple comparison indicated a significant induction of mature caspase-3 by NGF withdrawal ($p < 0.0001$), and a significant reduction in capase-3 maturation in deprived axons treated with antioxidant NAC versus axons deprived of NGF without antioxidant ($p < 0.001$). Boxplots indicate median, 25%, 75% percentile, and min/max.

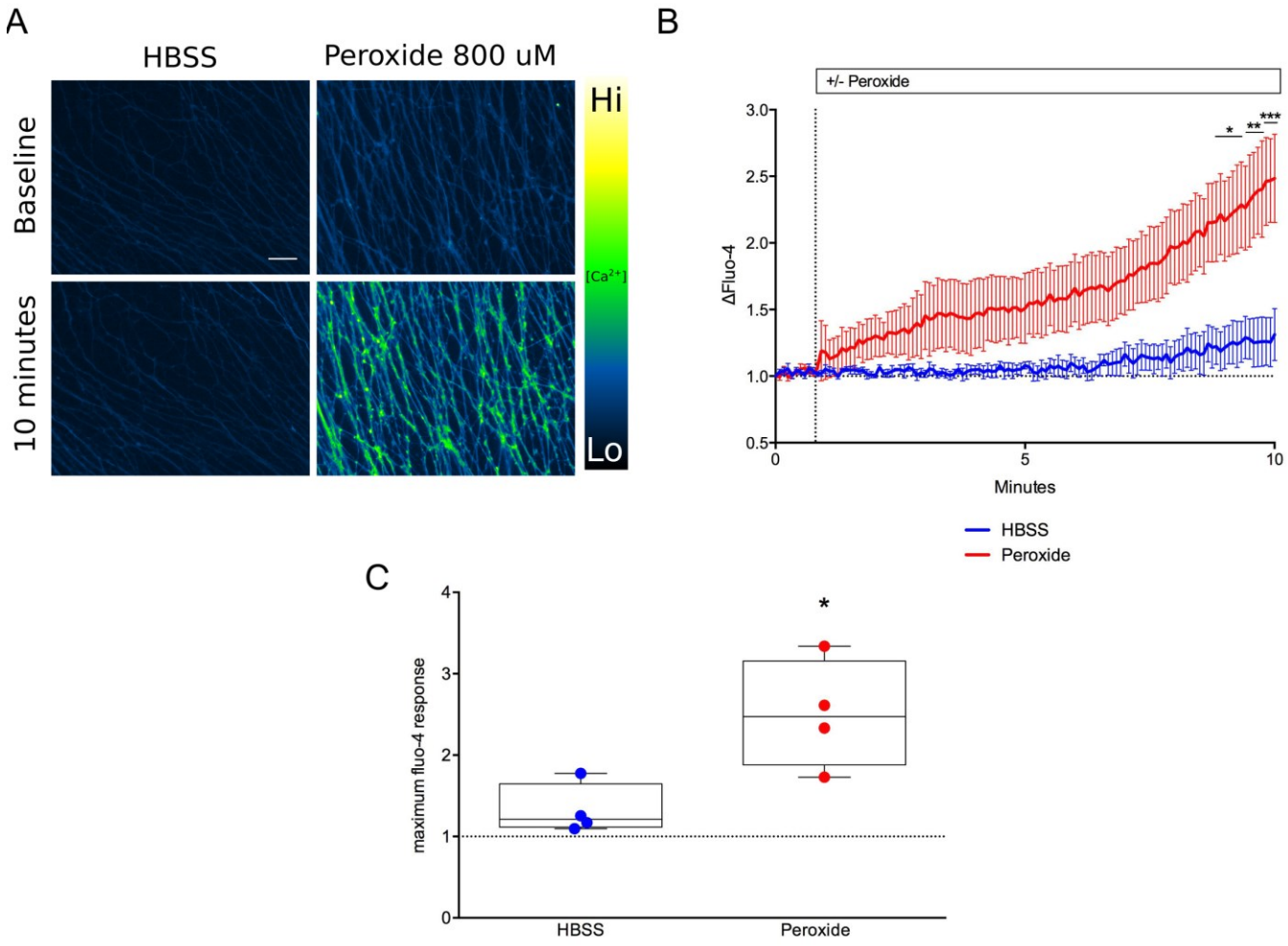

Figure 4.2. Oxidative stress induces Ca^{2+} influx.

Oxidative stress was induced by application of H_2O_2 800 µM onto fluo-4-loaded axons during live-imaging and the fluorescence intensity response was compared to a buffer-only control (representative images before and after injection shown in A, scale bar = 10 µm). A two factor ANOVA revealed a significant interaction between time and peroxide dose (0 and 800 µM) on fluo-4 response, F (120, 720) = 5.363, P < 0.0001 (time course of fluo-4 response is shown in B, n=4 embryos each condition, mean and SEM *p<0.05, **p<0.01, ***p0.001). A two-tailed unpaired t-test comparing maximum

fluo-4 responses indicated significant Ca^{2+} entry into axoplasm ($p < 0.05$) upon oxidative challenge by peroxide (C). Boxplots indicate median, 25%, 75% percentile, and min/max.

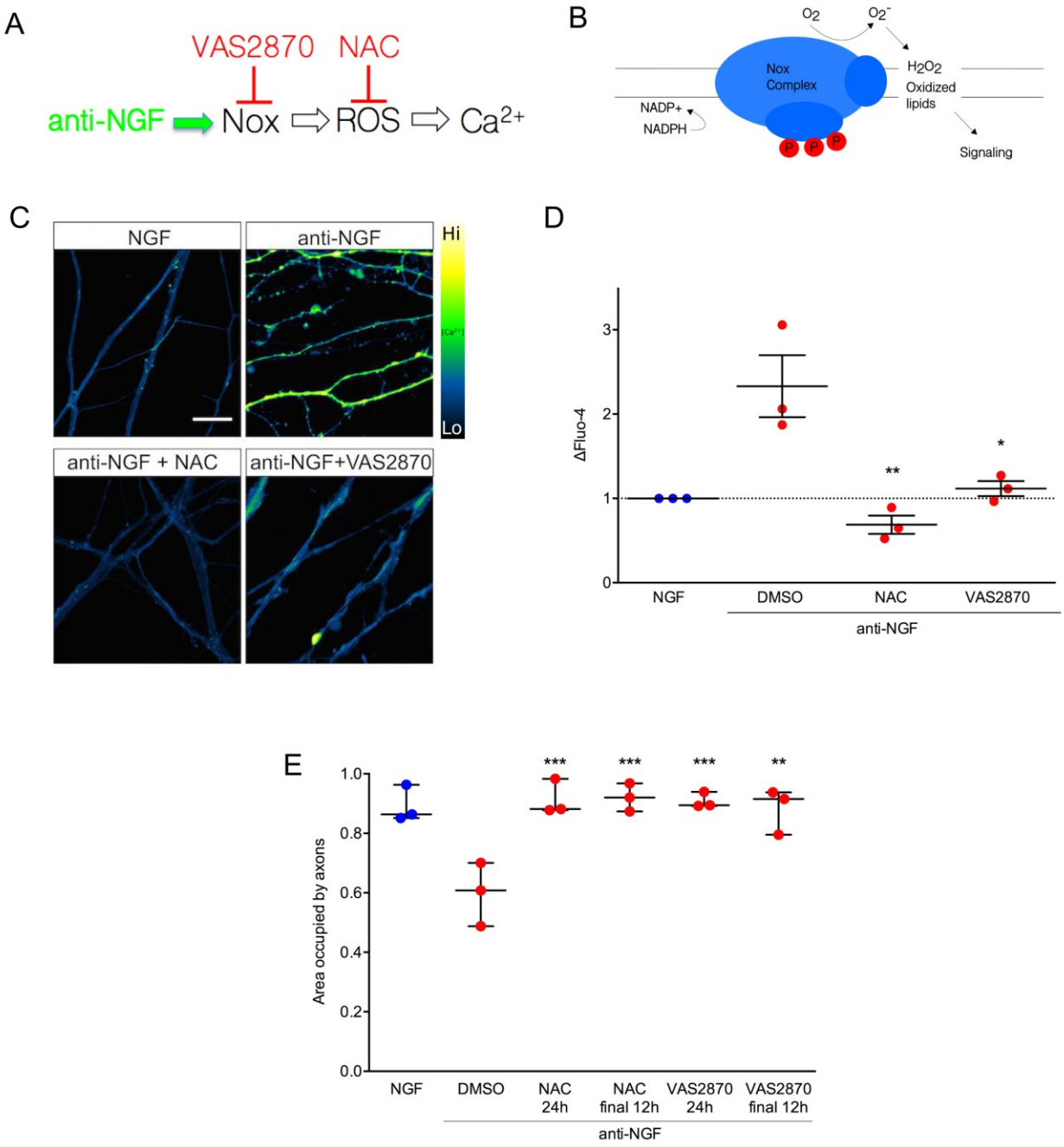

Figure 4.3. ROS derived from the Nox complex promote Ca^{2+} influx and axon degeneration.

Anti-oxidant NAC and Nox complex inhibitor VAS2870 were used to investigate whether ROS generated by Nox complex activation contributes to Ca^{2+} influx and axon degeneration

(pharmacological approach illustrated in A; Nox complexes generate reactive superoxide by catalyzing electron transfer from NADPH, B). Healthy, NGF-supplied axons or axons deprived of NGF for 15 hours in the presence or absence of antioxidant NAC or Nox complex inhibitor VAS2870 were loaded with fluo-4 to compare axoplasmic calcium levels (representative images shown in Figure 4.3 C). Tukey's post hoc pairwise comparisons indicated a significant blockade of Ca^{2+} influx by the antioxidant NAC ($p < 0.01$) and by Nox complex inhibition ($p < 0.05$, D). Treatment by either compound restored fluo-4 intensity to a level not significantly different from that observed in healthy, NGF-provided axons (ps > 0.05, one factor ANOVA, $F(3, 8) = 13.43$, $P = 0.0017$, n= 3 embryos each treatment). A cytoskeletal degeneration assay with Axoquant 2.0 and analyzed at 500 μm from soma (E) revealed a significant interaction between NGF-state and compounds on axonal density (one factor ANOVA, $F(5, 12) = 10.29$, $P = 0.0005$ n = 3 embryos each condition). Tukey's post hoc multiple comparison indicated that inhibition of the Nox complex with VAS2870 or inclusion of the antioxidant NAC in NGF-deprived axons restored axonal density to a degree not significantly different from the healthy control, regardless of whether the compounds were added at the time of deprivation, or 12 hours into the 24-hour deprivation period, indicating a late-phase role for Nox complex signaling after NGF deprivation consistent with the timing of calcium influx explored in Figures 3.1 and 3.2, all ps > 0.05). NGF deprivation alone induced degeneration significantly greater than that observed when axons are deprived but treated with NAC or VAS2870 (all ps < 0.01). Indicated are mean and SEM.

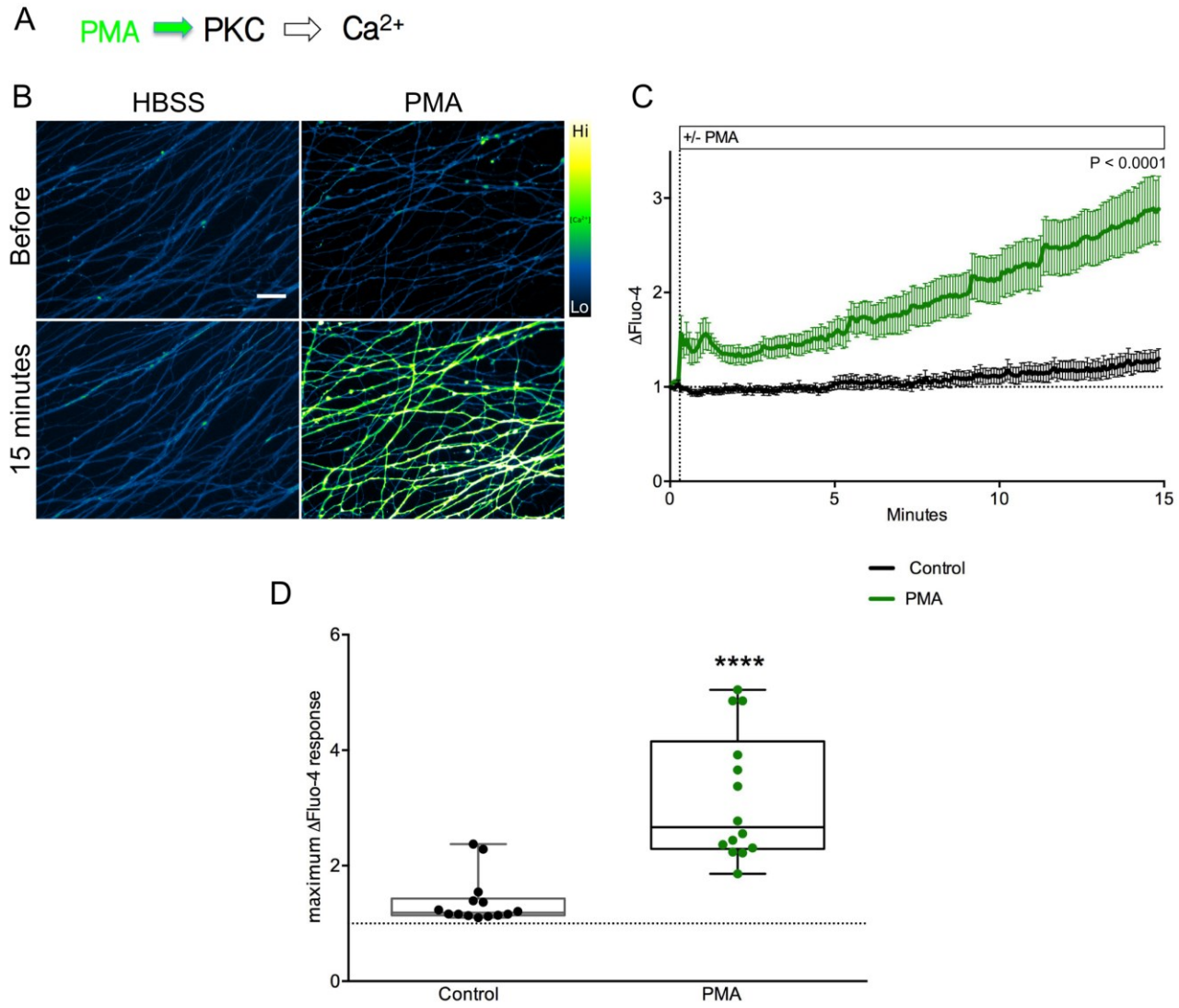

Figure 4.4. PKC activation induces Ca^{2+} influx.

PKC is directly activated by diacylglycerol-mimetic phorbol 12-myristate 13-acetate (PMA), and is capable of inducing Ca^{2+} influx into axons (A). Live-imaged, fluo-4-loaded axons were treated with PMA or HBSS buffer (B, quantified in C, mean and SEM) and a two-way ANOVA revealed a significant interaction between the PMA dose (0 or 100 nM) and time, $F(178, 4654) = 3.073$, $P < 0.0001$ (n=14 embryos, Figure 4.4 C). PMA induced a significantly greater fluo-4 intensity response than HBSS alone as revealed by a two-tailed unpaired t-test performed on maximum responses over

the 15 minute recording period, indicating significant Ca^{2+} influx upon PKC activation ($p < 0.0001$, D). Boxplots indicate median, 25%, 75% percentile, and min/max.

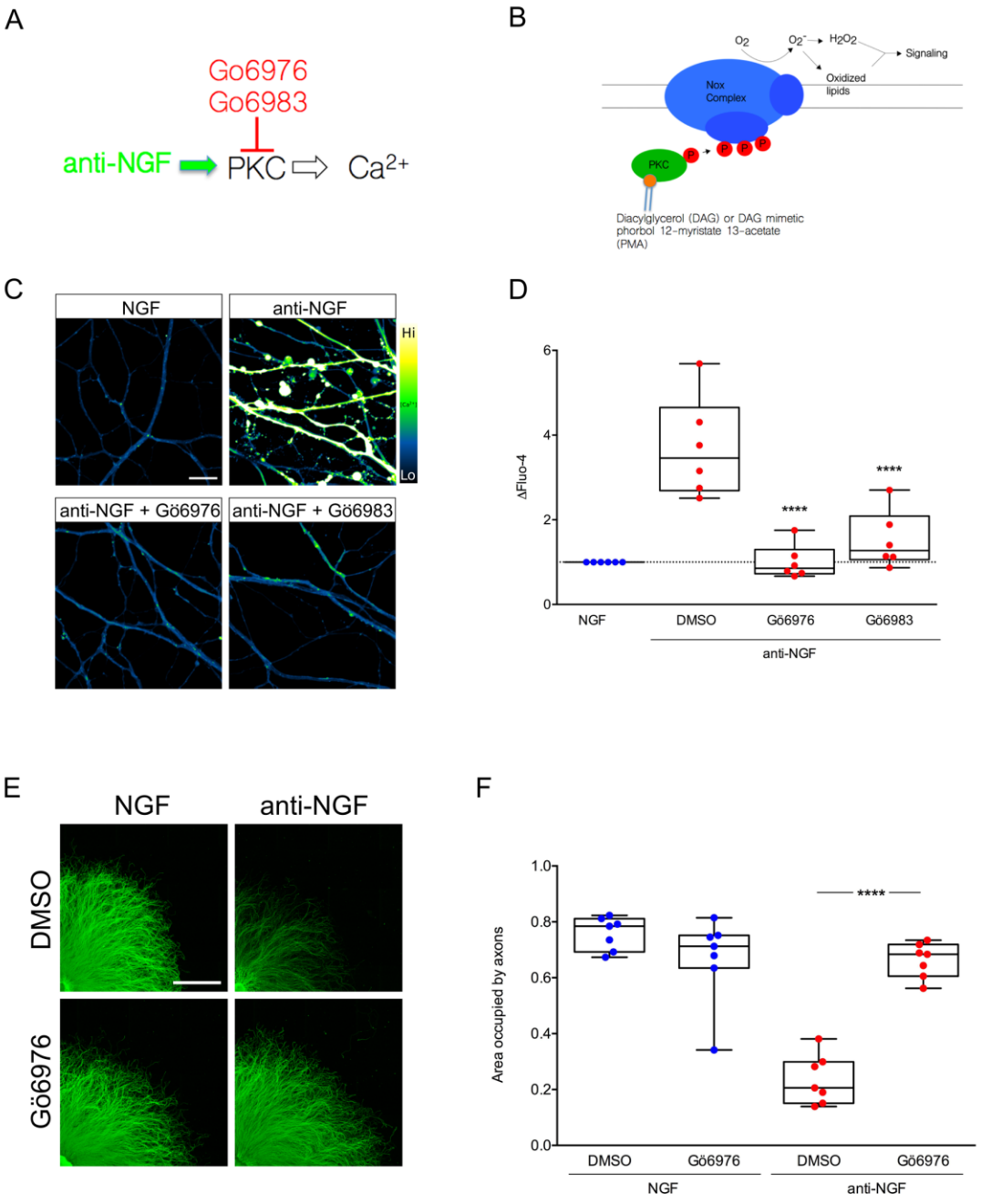

Figure 4.5. PKC inhibition rescues axons from cytoskeletal Ca^{2+} influx and degeneration.

Pharmacological PKC inhibitors were used to test the hypothesis that Ca^{2+} influx and the resulting cytoskeletal degeneration induced by NGF deprivation is PKC-dependent (A), since active PKC promotes assembly of ROS-producing Nox complexes via phosphorylation (B). Ca^{2+} influx was blocked by PKC inhibitors Gö6976 and Gö6983 15 hours after NGF withdrawal (representative images shown in C). NGF deprivation induced a significantly increased axoplasmic concentration of free Ca^{2+} as reported by fluo-4 ($p < 0.0001$, Tukey's post-hoc comparison, D), but axons deprived of NGF and provided with PKC inhibitors Gö6976 and Gö6983 showed no significant fluo-4 intensity above the NGF-supplied healthy control axons, indicating blockade by PKC inhibition (both $ps > 0.05$, one factor ANOVA, $F(3, 20) = 19.74$, $P < 0.0001$ with $n = 6$ embryos). Axons provided with Gö6976 are significantly more dense following a 24-hour phase of NGF deprivation versus axons deprived in the absence of PKC inhibitor (representative images shown in E with scale bar indicating 1 mm; quantified in F), indicating a pro-degenerative role for PKC ($p < 0.0001$). NGF deprived axons treated with were not significantly less dense than healthy NGF controls ($p > 0.05$, two factor ANOVA, $F (1, 24) = 47.81$, $P < 0.0001$ ($n = 7$ embryos each condition; boxplots indicate median, 25%, 75% percentile, and min/max.).

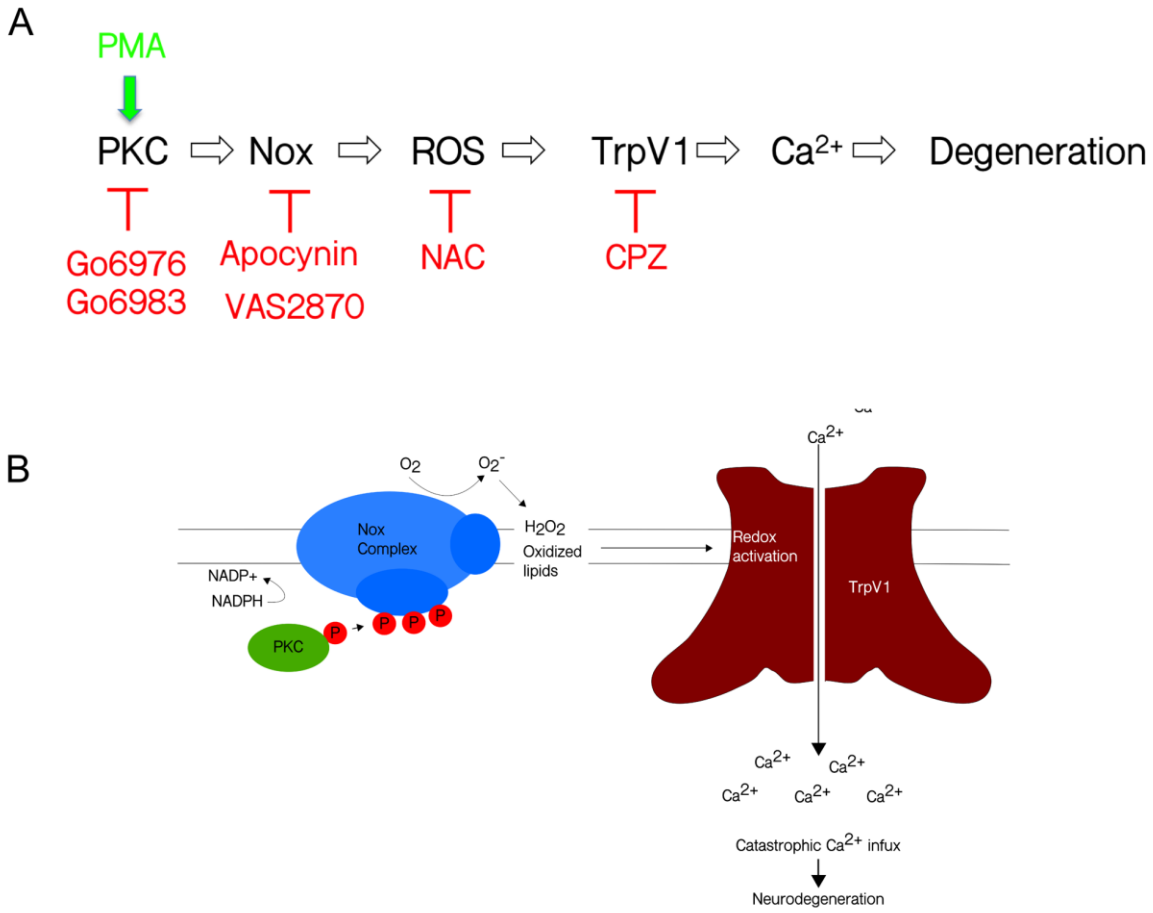

Figure 4.6. Pharmacological approach to investigating a PKC > Nox > ROS > TrpV1 axis regulating Ca^{2+} influx in axons of DRG neurons.

A suite of pharmacological inhibitors were deployed to investigate the sequence of molecular events leading to Ca^{2+} influx by TrpV1 downstream of PKC in PMA-stimulated axons (A). Based on data from neuronal and other model systems, we tested the hypothesis that TrpV1 channel activation lies downstream of ROS generated by Nox complexes stimulated by active PKC (B).

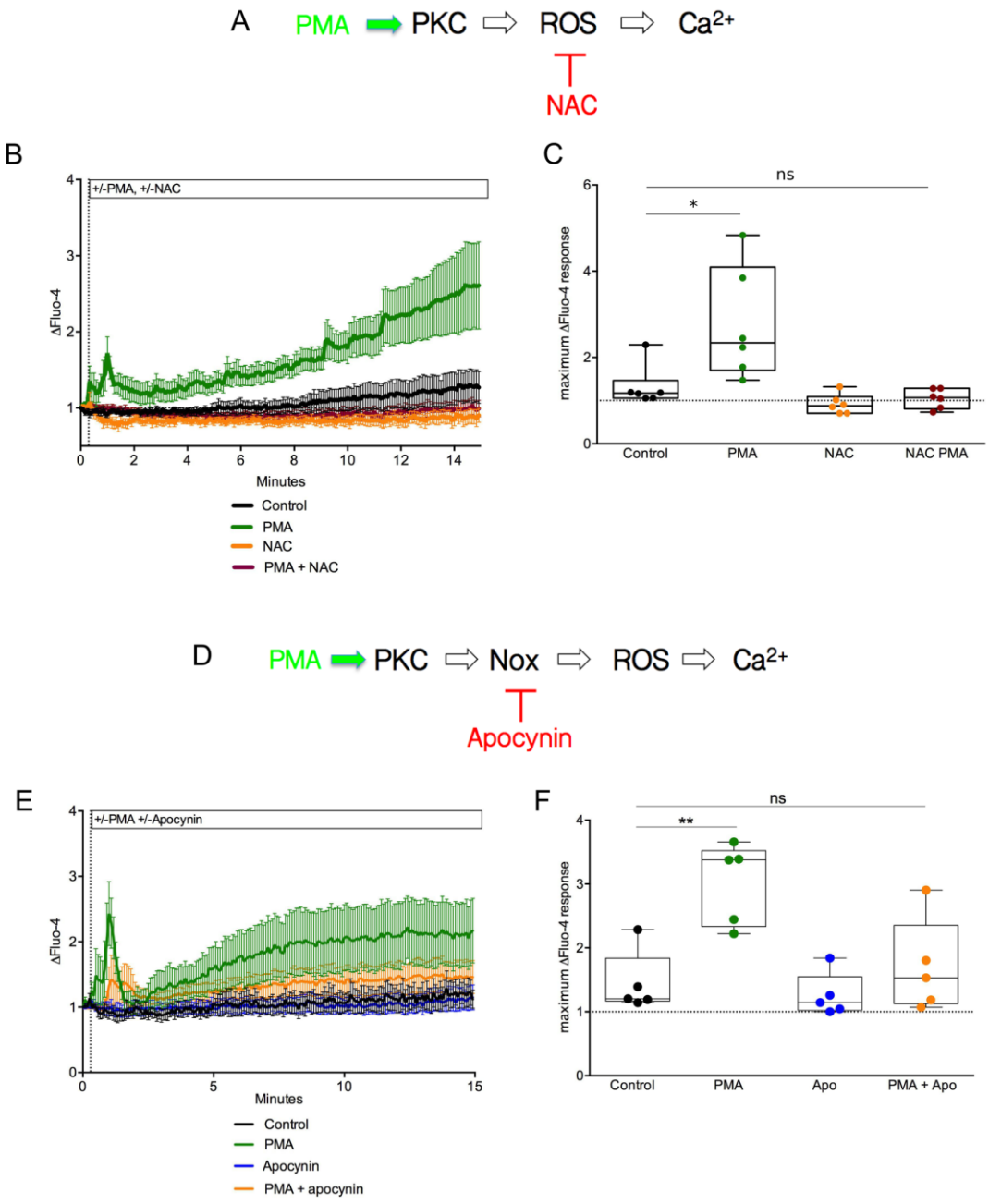

Figure 4.7. Ca^{2+} influx is activated by Nox complex-derived ROS downstream of PKC.

The ROS-dependence of the Ca^{2+} influx activated by PKC stimulation was tested by Ca^{2+} imaging in the presence of antioxidant NAC (A). Live-imaged, Fluo-4-loaded axons were stimulated with PMA

100 nM in the presence or absence of NAC 20 mM (mean responses and SEM from n=6 experiments are shown in B; two factor ANOVA, $F(537, 3580) = 3.644$, $P < 0.0001$). Tukey's post hoc comparison performed on maximum fluo-4 responses indicated that PMA induced a significant Ca^{2+} influx versus buffer control ($p < 0.05$), but NAC co-incubation negated the effect of PMA to a level not different from control (C, $p>0.05$; one factor ANOVA, $F(1,20)=5.123$, $P=0.0349$). Nox complexes were hypothesized to be the source of ROS activating Ca^{2+} influx (D). Fluo-4-loaded axons were live-imaged during PKC stimulation by PMA in the presence or absence of the Nox complex inhibitor apocynin 100 μM (E; two factor ANOVA, $F(537, 2864) = 1.989$, $P < 0.0001$, n=5 embryos, indicated are mean and SEM). A comparison of maximum fluo-4 responses (F) were analyzed via two factor ANOVA and revealed a significant interaction between PMA dose (0, 100 nM) and apocynin dose (0, 100 μM), $F(1, 16) = 4.963$, $P = 0.0406$). Tukey's post hoc multiple comparison vs buffer control indicated that the significant effect of PMA on fluo-4 intensity ($p < 0.01$) is lost in the presence of apocynin when compared to buffer only control ($p > 0.05$) indicating PMA-induced ROS produced by Nox complexes are sufficient to activate axonal Ca^{2+} influx. Boxplots indicate median, 25%, 75% percentile, and min/max.

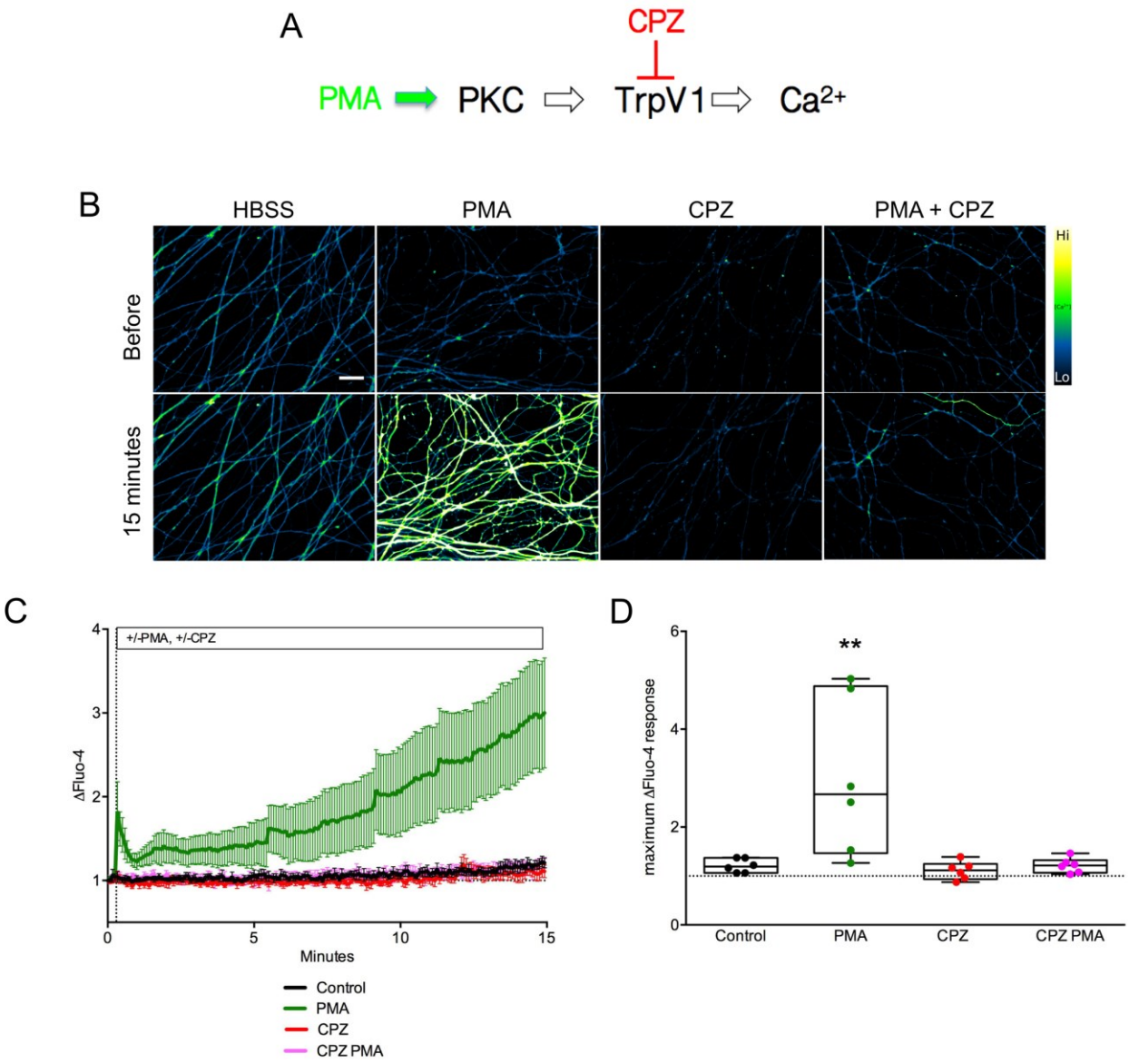

Figure 4.8. PKC-mediated Ca^{2+} influx is impaired by pharmacological TrpV1 inhibition.

Capsazepine was used to test the hypothesis that TrpV1 mediates Ca^{2+} influx induced by PKC stimulation (A). Fluo-4-loaded axons were stimulated with PMA during live imaging in the presence or absence of capsazepine (B, time course of activation quantified in C, indicated are mean and SEM). PMA application significantly increased fluo-4 intensity versus buffer control (D; $p < 0.01$, Tukey

post-hoc analysis), an effect that was abolished in the presence of capsazepine as compared to buffer only control, indicating a key role for TrpV1 in transducing Ca^{2+} influx downstream of PKC ($p > 0.05$; two factor ANOVA, $F(1, 20) = 6.418$, $P = 0.0198$, $n = 6$ embryos from 4 experiments). Boxplots indicate median, 25%, 75% percentile, and min/max.

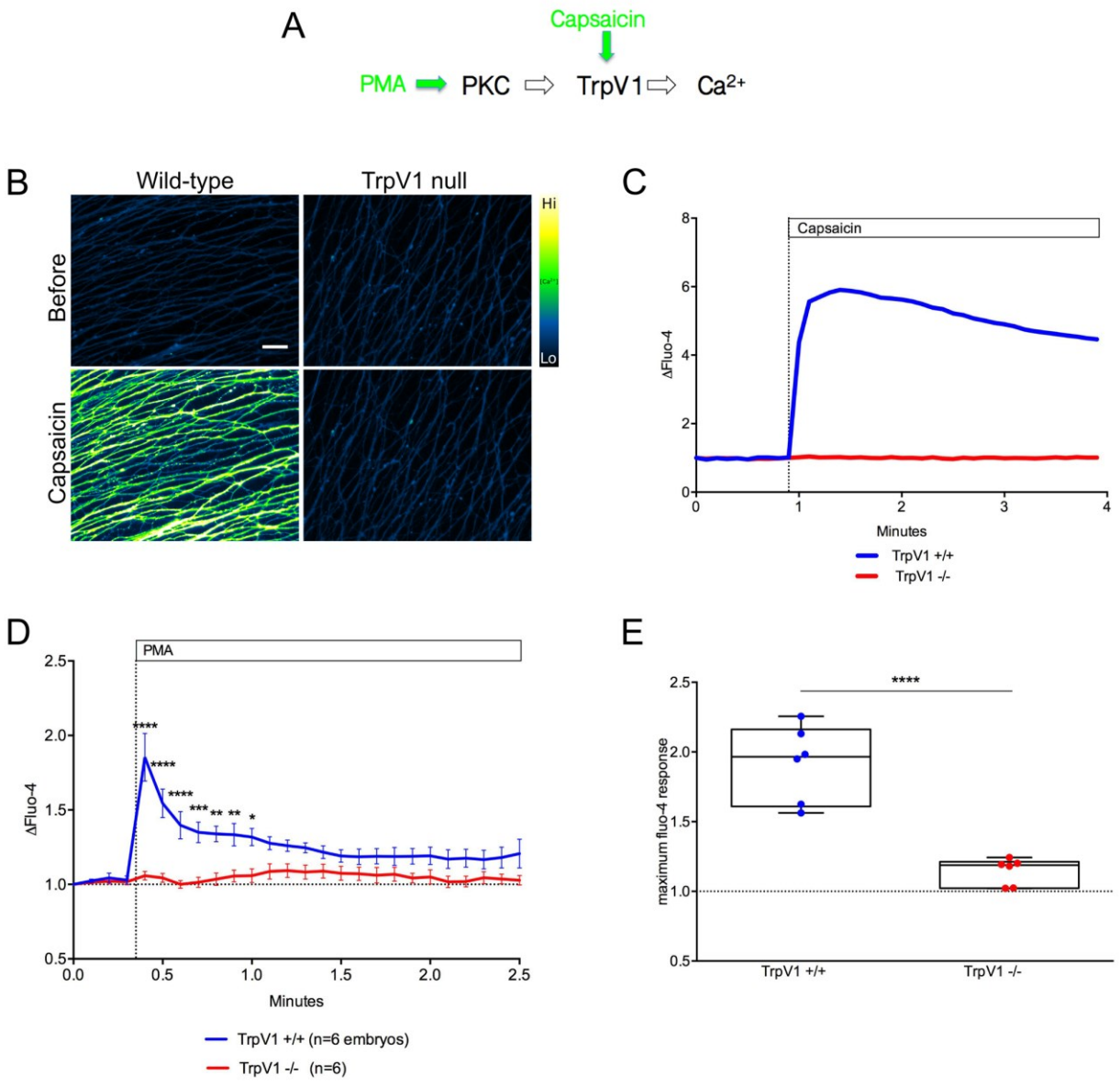

Figure 4.9. PKC-mediated Ca^{2+} influx is TrpV1-dependent.

PKC-dependent Ca^{2+} influx response was lost in DRG axons derived from TrpV1-null embryos (A). Axons were confirmed to be TrpV1-null by capsaicin application, which induced a robust fluo-4 response in wild-type axons (B, representative experiment shown in C). Mixed-genotype TrpV1 cultures were generated and axons were stimulated with PMA during live imaging with fluo-4 (D, mean and SEM, n=6). Significantly greater Ca^{2+} influx was observed in wild-type versus TrpV1-null

axons following PMA addition ($p < 0.0001$, Sidak's post-hoc comparison, two factor ANOVA, $F(25, 260) = 5.044$, $P < 0.0001$. A two-tailed t-test performed on the maximum fluo-4 responses of each genotype indicated a significant ablation of the Ca^{2+} response to PKC activation via TrpV1 knockout ($p < 0.0001$). Boxplots indicate median, 25%, 75% percentile, and min/max.

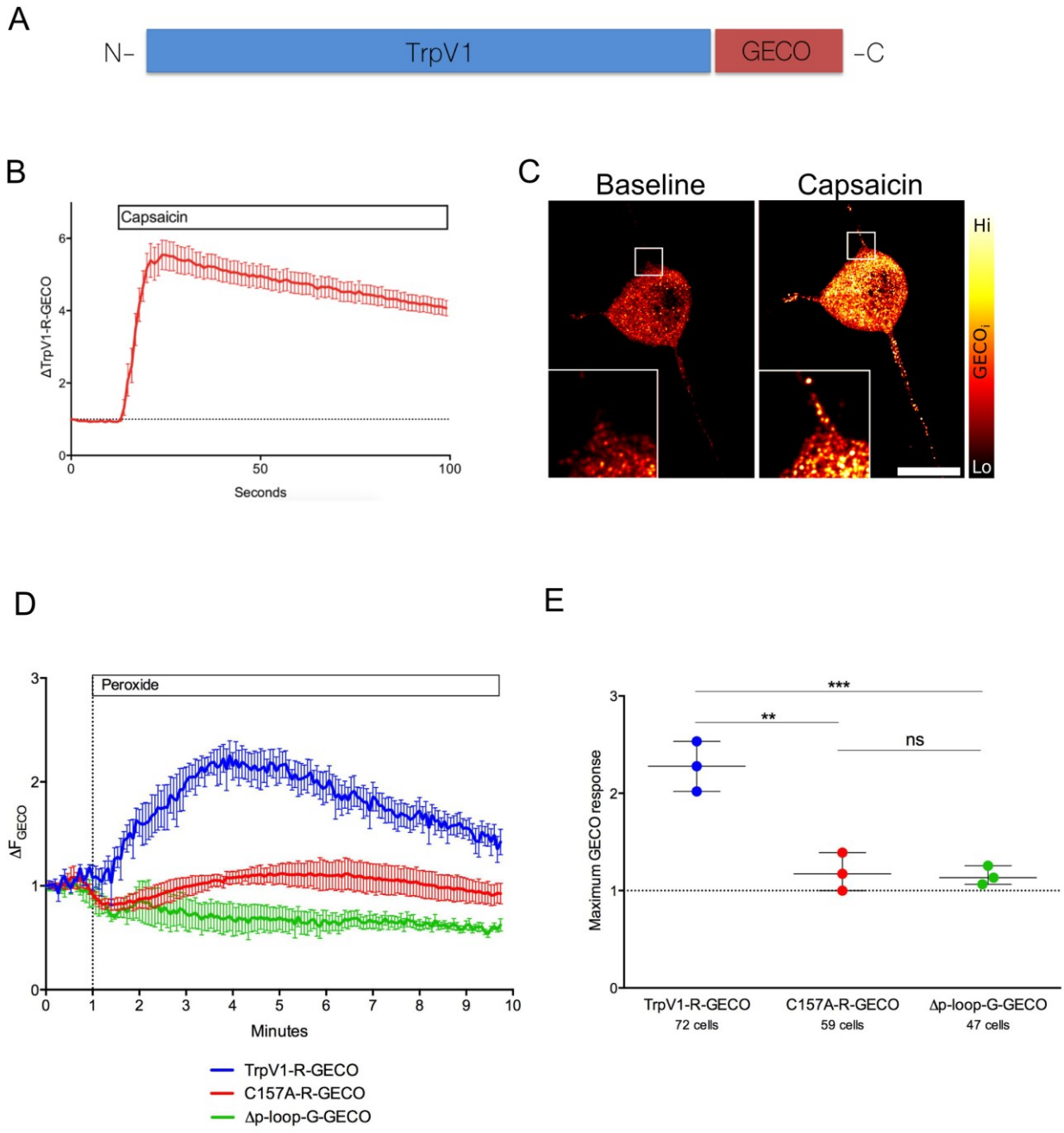

Figure 4.10. Development of novel imaging tools to investigate TrpV1 activation by oxidative cysteine modification.

TrpV1-R-GECO is a novel genetic fusion of the TrpV1 Ca^{2+} channel and red fluorescent genetically-encoded calcium indicator for optical imaging (R-GECO) to study Ca^{2+} influx via TrpV1 and the relationship between cellular oxidative status and its activity (A). Wild-type axons infected with HSV

harbouring TrpV1-R-GECO reports activation by capsaicin (representative experiment shown in B and C; scale bar indicates 10 μm). Compared to wild-type, the TrpV1-R-GECO redox mutant lacking reactive cysteine 157 (C157A-R-GECO) responded less upon stimulation with H_2O_2 800 μM during live-imaging of infected HEK293T cells along with an inactive negative control lacking the pore domain (Δp-loop-G-GECO; time-course of activation shown in D). Wild-type TrpV1 activated by oxidation induces significantly greater Ca^{2+} influx than TrpV1 lacking the pore domain ($p < 0.001$) or lacking cysteine residue 157 ($p < 0.01$; Tukey's post-hoc comparison following one factor ANOVA $F(2, 6) = 32.36$, $P = 0.006$, E.) Indicated are mean and SEM (D) or median and min/max (E). n=3 experiments, 72 wild-type TrpV1-R-GECO expressing cells, 59 C157A-R-GECO and 47 Δp-loop-G-GECO.

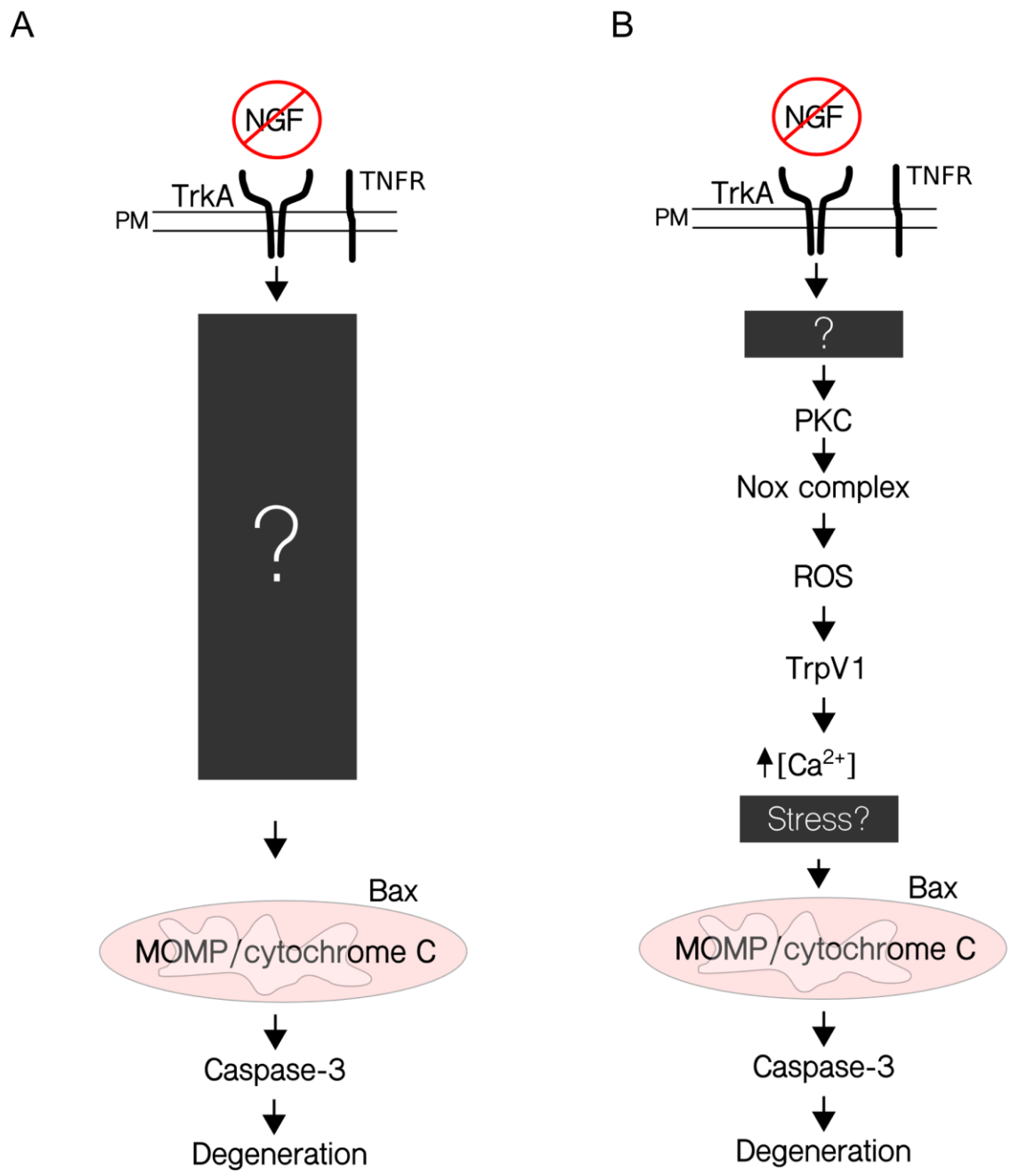

Figure 4.11. An updated model of NGF deprivation signaling integrating evidence from this thesis.

Apical and late signaling events transducing NGF deprivation to catastrophic mitochondrial outer membrane permeabilization (MOMP) and caspase activation have been identified over decades of

study, but the molecular mechanism transducing the unliganded TrkA signal to degenerative execution events remains one of the key gaps in our understanding (A). Evidence from this thesis work supports a model of NGF deprivation signaling whereby active PKC downstream of TrkA promotes subunit assembly and activation of Nox complexes by phosphorylation, resulting in ROS generation and activation of Ca^{2+} channel TrpV1. Toxic stress resulting from Ca^{2+} influx induces MOMP, caspase activation and degeneration of axonal cytoskeletal integrity (B).

Chapter 5. General Discussion and Conclusions

Plasticity of neural structures, over orders of organization from synapses to neurites to entire neurons and networks, depends on tightly regulated equilibrium between cytoskeleton polymerization and depolymerisation mediated by caspase activity (Figure 1.1) (27,28,166,179). The emerging conservation of signaling pathways raises the prospect that understanding of apoptotic-like pathways can be leveraged to guide hypotheses exploring non-lethal sub-neuronal plasticity events in both the normal physiological functioning of the nervous system, and also in the earliest changes during neurodegenerative disease to halt their progression (28).

Neurons possess the genetic means to degenerate and subpopulations normally do so during embryonic development to establish the mature nervous system (Figure 1.2) (19,180,181). Using a novel method for objective quantification of developmental axon degeneration in cultures of primary DRG sensory neurons (Figures 2.1 and 2.2), we investigated the role of Ca^{2+} influx in developmental degeneration. This quantification method assesses the entire area of axonal growth to avoid variability that can be introduced by sampling only small regions within the axonal fields. This contribution improves the sensitivity and reliability of cytoskeletal degeneration assays using the DRG system. Our data indicates that NGF-deprived DRG axons become Ca^{2+}-rich prior to membrane blebbing and degeneration, and cation chelation rescued these axons from degeneration (Figures 3.1 and 3.2). Capsazepine, an inhibitor of Ca^{2+} channel TrpV1, rescued axons from degeneration, while inhibition of Na^{+} currents had no effect, indicating specificity of Ca^{2+} influx in this process (Figures 3.3, 3.4 and 3.5). TrpV1 inhibition also blocked Ca^{2+} influx induced by 15 hours of NGF deprivation (Figure 3.5) and axons generated from TrpV1 knockout embryos show impaired cytoskeletal fragmentation after 24 hours without NGF (Figure 3.6).

We next explored how TrpV1 is activated in order to place it in signaling context. We hypothesized that reactive oxygen species (ROS) mediate the activation of TrpV1 in this setting and consistent with this, ROS scavenging inhibited caspase-3 maturation in NGF-deprived cultures (Figure 4.1), and acute oxidative challenge by peroxide induced robust Ca^{2+} influx (Figure 4.2). ROS scavenging and Nox complex inhibition rescued axons from Ca^{2+} influx and degeneration (Figures 4.3). Nox complexes are typically activated by PKC and we show that PKC inhibitors block Ca^{2+} influx and degeneration (Figure 4.5) whereas PMA, a PKC activator, induces potent NOX-and ROS-dependent activation (Figures 4.4 and 4.6) of TrpV1-dependent Ca^{2+} currents in DRG axons (Figure 4.7). We conclude that a PKC>Nox>ROS>TrpV1 axis induces toxic Ca^{2+} overload to drive developmental axon degeneration. Since PKC isoforms belong to large superfamilies of structurally related kinases, a genetic approach should be taken to identify those isoforms that are activated by NGF deprivation upstream of TrpV1 activation. Future experiments using novel imaging tools generated by genetic fusion of GECO fluorescent Ca^{2+} sensor with TrpV1 and a TrpV1 mutant lacking key redox-regulated residue C157 will be used to test whether NGF deprivation-induced Ca^{2+} influx is impaired when this ROS-sensitive site is absent.

How the loss of NGF from its receptor TrkA leads to activation of prodegenerative PKC upstream of Nox complexes and TrpV1 remains unknown. While NGF-bound TrkA activates survival pathways, degeneration after NGF withdrawal is not due simply to a lack of survival signaling, but appears to require activation of a pro-degenerative signal by TrkA (15). In experimental settings that investigated TrkA-TrpV1 interaction in survival and in nociception contexts, a clear linker appears to be the enzyme phospholipase C (PLC), which generates lipid products as second messengers in signaling downstream of receptor activation (11,182). There are several indicators that PLC may link NGF deprivation signaling from TrkA to the downstream PKC > Nox complex > ROS > TrpV1

cassette described in this thesis. Active PLC consumes PIP2 to generate 1,4,5-triphosphate (IP_3) and diacylglycerol (DAG) (183). DAG is a potent and direct activator of PKC, like its mimetic PMA, and stimulates ROS production by Nox complexes as a consequence (91,152). Though published studies disagree whether PIP2 is a TrpV1 activator or inhibitor, its action may depend on context (184); if PIP2 is indeed a TrpV1 inhibitor, as argued by a group led by David Julius, a scenario can be imagined whereby TrkA-mediated PLC activation has a two-pronged effect mediated i) by the consumption of PIP2 (removing TrpV1 inhibition), and ii) generation of DAG and subsequent PKC activation upstream of Nox complexes and TrpV1 (184,185). However, others have shown that PIP2 can directly activate TrpV1; TrpV1-mediated currents induced by exogenous PIP2 were almost entirely blocked by capsazepine in inside-out patches from HEK293T cells, and PIP2 depletion impaired TrpV1, arguing for an activating role for PIP2 (182). TrkA also signals via phosphoinositide 3-kinase (PI3K), which has been shown to directly interact with TrpV1 to mediate NGF-stimulated TrpV1 trafficking to the membrane (182). It will be particularly enlightening to dernd whether NGF deprivation of DRG neurons stimulates PIP2 production, or whether PIP2 is depleted during NGF deprivation, and fluorescent sensors (eg PH-GFP) exist to directly monitor intracellular PIP2 level. Similarly, whether exogenous PIP2 accelerates or delays axon degeneration in our experimental context will shed light on whether a TrkA-PLC-PKC axis links NGF withdrawal to TrpV1 activation.

Acute activation of TrpV1 in DRG neurons by capsaicin induced degeneration induced by mitochondrial Ca^{2+} stress, loss of potential, and fission, and it is likely that preventing the TrpV1-mediated Ca^{2+} influx may rescue mitochondria from toxic Ca^{2+} overload and loss of potential (114,115). It is well established that ROS generated by dysfunction of the electron transport chain in mitochondria are a major contributor to apoptotic cell death (39,42,115,148,186). However, since Nox complex inhibition rescued axons from Ca^{2+} influx and degeneration, our data indicate that ROS

initially activating TrpV1 are derived from Nox complexes. It remains possible, and even likely, that mitochondrial-derived ROS are activated downstream of TrpV1-mediated Ca^{2+} influx to comprise a feedback loop between ROS and Ca^{2+} following mitochondrial Ca^{2+} stress via PKC > Nox > ROS > TrpV1 > Ca^{2+}. Mechanistically linking the PKC > Nox > ROS >TrpV1 signaling cassette within the context of NGF deprivation signaling by TrkA, perhaps via PLC, and downstream events including mitochondrial dysfunction are next steps in understanding the continuous signaling pathway mediating NGF-withdrawal induced neurodegeneration and plasticity in the developing nervous system.

References

1. Saxena S, Caroni P. Mechanisms of axon degeneration: from development to disease. Prog Neurobiol [Internet]. 2007 Oct [cited 2014 Nov 6];83(3):174–91. Available from: http://www.ncbi.nlm.nih.gov/pubmed/17822833
2. Fischer LR, Glass JD. Axonal degeneration in motor neuron disease. Neurodegener Dis [Internet]. 2007 Jan [cited 2014 Oct 29];4(6):431–42. Available from: http://www.ncbi.nlm.nih.gov/pubmed/17934327
3. Kanaan NM, Pigino GF, Brady ST, Lazarov O, Binder LI, Morfini GA. Axonal degeneration in Alzheimer's disease: when signaling abnormalities meet the axonal transport system. Exp Neurol [Internet]. 2013 Aug [cited 2014 Oct 27];246:44–53. Available from: http://www.pubmedcentral.nih.gov/articlerender.fcgi?artid=3465504&tool=pmcentrez&rendertype=abstract
4. Vickers JC, King AE, Woodhouse A, Kirkcaldie MT, Staal JA, McCormack GH, et al. Axonopathy and cytoskeletal disruption in degenerative diseases of the central nervous system. Brain Res Bull [Internet]. 2009 Oct 28 [cited 2014 Oct 31];80(4–5):217–23. Available from: http://www.ncbi.nlm.nih.gov/pubmed/19683034
5. Barde YA. Trophic factors and neuronal survival. Neuron [Internet]. 1989 Jun [cited 2018 Mar 14];2(6):1525–34. Available from: http://www.ncbi.nlm.nih.gov/pubmed/2697237
6. Kaplan DR, Miller FD. Neurotrophin signal transduction in the nervous system. Curr Opin Neurobiol [Internet]. 2000 Jun [cited 2018 Apr 5];10(3):381–91. Available from: http://www.ncbi.nlm.nih.gov/pubmed/10851172
7. Bothwell M. NGF, BDNF, NT3, and NT4. In Springer, Berlin, Heidelberg; 2014 [cited 2018 Jun 27]. p. 3–15. Available from: http://link.springer.com/10.1007/978-3-642-45106-5_1
8. Delcroix J-D, Valletta JS, Wu C, Hunt SJ, Kowal AS, Mobley WC. NGF signaling in sensory neurons: evidence that early endosomes carry NGF retrograde signals. Neuron [Internet]. 2003 Jul 3 [cited 2014 Nov 9];39(1):69–84. Available from: http://www.ncbi.nlm.nih.gov/pubmed/12848933
9. Barker PA, Shooter EM. Disruption of NGF binding to the low affinity neurotrophin receptor p75LNTR reduces NGF binding to TrkA on PC12 cells. Neuron [Internet]. 1994 Jul 1 [cited 2018 Mar 14];13(1):203–15. Available from: http://www.ncbi.nlm.nih.gov/pubmed/7519025
10. Barker PA, Hussain NK, McPherson PS. Retrograde signaling by the neurotrophins follows a well-worn trk. Trends Neurosci [Internet]. 2002 Aug 1 [cited 2018 Jun 27];25(8):379–81. Available from: https://www.sciencedirect.com/science/article/pii/S0166223602021999?via%3Dihub
11. Grimes ML, Zhou J, Beattie EC, Yuen EC, Hall DE, Valletta JS, et al. Endocytosis of activated TrkA: evidence that nerve growth factor induces formation of signaling endosomes. J Neurosci [Internet]. 1996 Dec 15 [cited 2014 Nov 9];16(24):7950–64. Available from: http://www.ncbi.nlm.nih.gov/pubmed/8987823
12. Beattie EC, Zhou J, Grimes ML, Bunnett NW, Howe CL, Mobley WC. A signaling endosome hypothesis to explain NGF actions: potential implications for neurodegeneration. Cold Spring Harb Symp Quant Biol [Internet]. 1996 Jan [cited 2014 Nov 9];61:389–406. Available from: http://www.ncbi.nlm.nih.gov/pubmed/9246468

13. Hempstead BL, Martin-Zanca D, Kaplan DR, Parada LF, Chao M V. High-affinity NGF binding requires coexpression of the trk proto-oncogene and the low-affinity NGF receptor. Nature [Internet]. 1991 Apr 25 [cited 2018 Mar 14];350(6320):678–83. Available from: http://www.nature.com/doifinder/10.1038/350678a0
14. Neukomm LJ, Freeman MR. Diverse cellular and molecular modes of axon degeneration. Trends Cell Biol [Internet]. 2014 Sep [cited 2014 Oct 15];24(9):515–23. Available from: http://www.ncbi.nlm.nih.gov/pubmed/24780172
15. Nikoletopoulou V, Lickert H, Frade JM, Rencurel C, Giallonardo P, Zhang L, et al. Neurotrophin receptors TrkA and TrkC cause neuronal death whereas TrkB does not. Nature [Internet]. 2010 Sep 2 [cited 2014 Oct 19];467(7311):59–63. Available from: http://dx.doi.org/10.1038/nature09336
16. Kirkland RA, Franklin JL. Bax, reactive oxygen, and cytochrome c release in neuronal apoptosis. Antioxid Redox Signal [Internet]. 2003 Oct 5 [cited 2014 Nov 5];5(5):589–96. Available from: http://online.liebertpub.com/doi/abs/10.1089/152308603770310257
17. Papadakis ES, Finegan KG, Wang X, Robinson AC, Guo C, Kayahara M, et al. The regulation of Bax by c-Jun N-terminal protein kinase (JNK) is a prerequisite to the mitochondrial-induced apoptotic pathway. FEBS Lett [Internet]. 2006 Feb 20 [cited 2014 Oct 28];580(5):1320–6. Available from: http://www.febsletters.org/article/S0014579306001062/fulltext
18. Kirkland RA, Windelborn JA, Kasprzak JM, Franklin JL. A Bax-induced pro-oxidant state is critical for cytochrome c release during programmed neuronal death. J Neurosci [Internet]. 2002 Aug 1 [cited 2014 Nov 9];22(15):6480–90. Available from: http://www.ncbi.nlm.nih.gov/pubmed/12151527
19. Patel TD, Jackman A, Rice FL, Kucera J, Snider WD. Development of sensory neurons in the absence of NGF/TrkA signaling in vivo. Neuron [Internet]. 2000 Feb [cited 2014 Nov 9];25(2):345–57. Available from: http://www.ncbi.nlm.nih.gov/pubmed/10719890
20. Liu J, Lin A. Role of JNK activation in apoptosis: a double-edged sword. Cell Res [Internet]. 2005 Jan [cited 2014 Nov 9];15(1):36–42. Available from: http://dx.doi.org/10.1038/sj.cr.7290262
21. Simon DJ, Weimer RM, McLaughlin T, Kallop D, Stanger K, Yang J, et al. A caspase cascade regulating developmental axon degeneration. J Neurosci [Internet]. 2012 Dec 5 [cited 2014 Jul 11];32(49):17540–53. Available from: http://www.jneurosci.org/content/32/49/17540
22. Liu MC, Akle V, Zheng W, Dave JR, Tortella FC, Hayes RL, et al. Comparing calpain- and caspase-3-mediated degradation patterns in traumatic brain injury by differential proteome analysis. Biochem J [Internet]. 2006 Mar 15 [cited 2015 Nov 19];394(Pt 3):715–25. Available from: http://www.pubmedcentral.nih.gov/articlerender.fcgi?artid=1383722&tool=pmcentrez&rendertype=abstract
23. Pinan-Lucarre B, Gabel C V, Reina CP, Hulme SE, Shevkoplyas SS, Slone RD, et al. The core apoptotic executioner proteins CED-3 and CED-4 promote initiation of neuronal regeneration in Caenorhabditis elegans. PLoS Biol [Internet]. 2012 Jan [cited 2015 Nov 4];10(5):e1001331. Available from: http://www.pubmedcentral.nih.gov/articlerender.fcgi?artid=3358320&tool=pmcentrez&rendertype=abstract
24. Finn JT, Weil M, Archer F, Siman R, Srinivasan A, Raff MC. Evidence that Wallerian

degeneration and localized axon degeneration induced by local neurotrophin deprivation do not involve caspases. J Neurosci [Internet]. 2000 Feb 15 [cited 2014 Nov 10];20(4):1333–41. Available from: http://www.ncbi.nlm.nih.gov/pubmed/10662823
25. Unsain N, Higgins JM, Parker KN, Johnstone AD, Barker PA. XIAP regulates caspase activity in degenerating axons. Cell Rep [Internet]. 2013 Aug 29 [cited 2014 Oct 20];4(4):751–63. Available from: http://www.ncbi.nlm.nih.gov/pubmed/23954782
26. White K, Arama E, Hardwick JM. Controlling caspase activity in life and death. PLoS Genet [Internet]. 2017 [cited 2018 Mar 14];13(2):e1006545. Available from: http://www.ncbi.nlm.nih.gov/pubmed/28207784
27. Aram L, Yacobi-Sharon K, Arama E. CDPs: caspase-dependent non-lethal cellular processes. Cell Death Differ [Internet]. 2017 Aug 10 [cited 2018 Mar 14];24(8):1307–10. Available from: http://www.nature.com/doifinder/10.1038/cdd.2017.111
28. Unsain N, Barker PA. New Views on the Misconstrued: Executioner Caspases and Their Diverse Non-apoptotic Roles. Neuron [Internet]. 2015 Nov 4 [cited 2015 Nov 5];88(3):461–74. Available from: http://www.cell.com/article/S0896627315007230/fulltext
29. Huesmann GR, Clayton DF. Dynamic role of postsynaptic caspase-3 and BIRC4 in zebra finch song-response habituation. Neuron [Internet]. 2006 Dec 21 [cited 2015 Nov 24];52(6):1061–72. Available from: http://www.sciencedirect.com/science/article/pii/S0896627306008695
30. Li Z, Jo J, Jia J-M, Lo S-C, Whitcomb DJ, Jiao S, et al. Caspase-3 activation via mitochondria is required for long-term depression and AMPA receptor internalization. Cell [Internet]. 2010 May 28 [cited 2015 Aug 8];141(5):859–71. Available from: http://www.sciencedirect.com/science/article/pii/S0092867410003727
31. Levi-Montalcini R, Booker B. Destruction of the sympathetic ganglia in mammals by an antiserum to a nerve-growth protein. Proc Natl Acad Sci [Internet]. 1960 Mar 1 [cited 2014 Nov 12];46(3):384–91. Available from: http://www.pnas.org/content/46/3/384.full?ijkey=087c79d81ac182f1a4600220a3c8eabee6520e13&keytype2=tf_ipsecsha
32. Levi-Montalcini R, Hamburger V. Selective growth stimulating effects of mouse sarcoma on the sensory and sympathetic nervous system of the chick embryo. J Exp Zool [Internet]. 1951 Mar [cited 2014 Nov 12];116(2):321–61. Available from: http://doi.wiley.com/10.1002/jez.1401160206
33. Levi-Montalcini R, Hamburger V. A diffusible agent of mouse sarcoma, producing hyperplasia of sympathetic ganglia and hyperneurotization of viscera in the chick embryo. J Exp Zool [Internet]. 1953 Jul [cited 2014 Nov 12];123(2):233–87. Available from: http://doi.wiley.com/10.1002/jez.1401230203
34. Sanabria-Castro A, Alvarado-Echeverría I, Monge-Bonilla C. Molecular Pathogenesis of Alzheimer's Disease: An Update. Ann Neurosci [Internet]. 2017 May [cited 2017 Nov 29];24(1):46–54. Available from: http://www.ncbi.nlm.nih.gov/pubmed/28588356
35. Schampel A, Kuerten S. Danger: High Voltage—The Role of Voltage-Gated Calcium Channels in Central Nervous System Pathology. Cells [Internet]. 2017 Nov 15 [cited 2018 Mar 5];6(4):43. Available from: http://www.ncbi.nlm.nih.gov/pubmed/29140302
36. Surmeier DJ, Halliday GM, Simuni T. Calcium, mitochondrial dysfunction and slowing the progression of Parkinson's disease. Exp Neurol [Internet]. 2017 Dec [cited 2017 Nov 29];298(Pt B):202–9. Available from: http://www.ncbi.nlm.nih.gov/pubmed/28780195

37. Pchitskaya E, Popugaeva E, Bezprozvanny I. Calcium signaling and molecular mechanisms underlying neurodegenerative diseases. Cell Calcium [Internet]. 2017 Jun 30 [cited 2017 Nov 29]; Available from: http://www.ncbi.nlm.nih.gov/pubmed/28728834
38. Mattson MP. Calcium and neurodegeneration. Aging Cell [Internet]. 2007 Jun [cited 2018 Mar 5];6(3):337–50. Available from: http://www.ncbi.nlm.nih.gov/pubmed/17328689
39. Prudent J, Zunino R, Sugiura A, Mattie S, Shore GC, McBride HM. MAPL SUMOylation of Drp1 Stabilizes an ER/Mitochondrial Platform Required for Cell Death. Mol Cell [Internet]. 2015 Sep 17 [cited 2016 Feb 15];59(6):941–55. Available from: http://www.ncbi.nlm.nih.gov/pubmed/26384664
40. Bezprozvanny I. Calcium signaling and neurodegenerative diseases. Trends Mol Med [Internet]. 2009 Mar [cited 2018 Mar 16];15(3):89–100. Available from: http://www.ncbi.nlm.nih.gov/pubmed/19230774
41. Marambaud P, Dreses-Werringloer U, Vingtdeux V. Calcium signaling in neurodegeneration. Mol Neurodegener [Internet]. 2009 May 6 [cited 2018 Mar 16];4:20. Available from: http://www.ncbi.nlm.nih.gov/pubmed/19419557
42. Celsi F, Pizzo P, Brini M, Leo S, Fotino C, Pinton P, et al. Mitochondria, calcium and cell death: A deadly triad in neurodegeneration. Biochim Biophys Acta - Bioenerg [Internet]. 2009 May 1 [cited 2018 Mar 16];1787(5):335–44. Available from: https://www.sciencedirect.com/science/article/pii/S0005272809000826
43. Vargas ME, Yamagishi Y, Tessier-Lavigne M, Sagasti A. Live Imaging of Calcium Dynamics during Axon Degeneration Reveals Two Functionally Distinct Phases of Calcium Influx. J Neurosci [Internet]. 2015 Nov 11 [cited 2018 Mar 29];35(45):15026–38. Available from: http://www.ncbi.nlm.nih.gov/pubmed/26558774
44. Eichler ME, Dubinsky JM, Rich KM. Relationship of intracellular calcium to dependence on nerve growth factor in dorsal root ganglion neurons in cell culture. J Neurochem [Internet]. 1992 Jan [cited 2018 Mar 29];58(1):263–9. Available from: http://www.ncbi.nlm.nih.gov/pubmed/1727434
45. Eichler ME, Dubinsky JM, Tong J, Rich KM. The Ability of Diphenylpiperazines to Prevent Neuronal Death in Dorsal Root Ganglion Neurons In Vitro After Nerve Growth Factor Deprivation and In Vivo After Axotomy. J Nettrochernislry Raven Press [Internet]. [cited 2017 Nov 29]; Available from: https://s3.amazonaws.com/objects.readcube.com/articles/downloaded/wiley/1dab3fa5dc12f0d5c11fdbb7860e436cc6042c7e902f09b8888bbae346e6cf94.pdf?X-Amz-Algorithm=AWS4-HMAC-SHA256&X-Amz-Credential=AKIAIS5LBPCM5JPOCDGQ%2F20171129%2Fus-east-1%2Fs3%2Faws4_request&X-Amz-Date=20171129T213642Z&X-Amz-Expires=94997&X-Amz-SignedHeaders=host&X-Amz-Signature=2ba8bc344698cef8d31804c5d4a01265a5cad27596a67986c22048d19592aa4e
46. Tong JX, Eichler ME, Rich KM. Intracellular Calcium Levels Influence Apoptosis in Mature Sensory Neurons after Trophic Factor Deprivation. Exp Neurol [Internet]. 1996 Mar [cited 2017 Nov 29];138(1):45–52. Available from: http://www.ncbi.nlm.nih.gov/pubmed/8593895
47. Cosens DJ, Manning A. Abnormal electroretinogram from a Drosophila mutant. Nature [Internet]. 1969 Oct 18 [cited 2018 Mar 14];224(5216):285–7. Available from:

http://www.ncbi.nlm.nih.gov/pubmed/5344615
48. Minke B, Wu C, Pak WL. Induction of photoreceptor voltage noise in the dark in Drosophila mutant. Nature [Internet]. 1975 Nov 6 [cited 2018 Mar 14];258(5530):84–7. Available from: http://www.ncbi.nlm.nih.gov/pubmed/810728
49. Venkatachalam K, Montell C. TRP channels. Annu Rev Biochem [Internet]. 2007 [cited 2018 Mar 14];76:387–417. Available from: http://www.ncbi.nlm.nih.gov/pubmed/17579562
50. Julius D, Caterina MJ, Schumacher MA, Tominaga M, Rosen TA, Levine JD. The capsaicin receptor: a heat-activated ion channel in the pain pathway. Nature [Internet]. 1997 Oct 23 [cited 2018 Mar 14];389(6653):816–24. Available from: http://www.ncbi.nlm.nih.gov/pubmed/9349813
51. Hakim M, Jiang W, Luo L, Li B, Yang S, Song Y, et al. Scorpion Toxin, BmP01, Induces Pain by Targeting TRPV1 Channel. Toxins (Basel) [Internet]. 2015 Sep 14 [cited 2018 Mar 14];7(12):3671–87. Available from: http://www.ncbi.nlm.nih.gov/pubmed/26389953
52. Geron M, Hazan A, Priel A. Animal Toxins Providing Insights into TRPV1 Activation Mechanism. Toxins (Basel) [Internet]. 2017 Oct 16 [cited 2018 Mar 14];9(12):326. Available from: http://www.ncbi.nlm.nih.gov/pubmed/29035314
53. Fenwick AJ, Fowler DK, Wu S-W, Shaffer FJ, Lindberg JEM, Kinch DC, et al. Direct Anandamide Activation of TRPV1 Produces Divergent Calcium and Current Responses. Front Mol Neurosci [Internet]. 2017 Jun 21 [cited 2018 Mar 14];10:200. Available from: http://www.ncbi.nlm.nih.gov/pubmed/28680392
54. Grabiec U, Dehghani F. *N* -Arachidonoyl Dopamine: A Novel Endocannabinoid and Endovanilloid with Widespread Physiological and Pharmacological Activities. Cannabis Cannabinoid Res [Internet]. 2017 Jul [cited 2018 Mar 14];2(1):183–96. Available from: http://www.ncbi.nlm.nih.gov/pubmed/29082315
55. Winter Z, Buhala A, Ötvös F, Jósvay K, Vizler C, Dombi G, et al. Functionally important amino acid residues in the transient receptor potential vanilloid 1 (TRPV1) ion channel--an overview of the current mutational data. Mol Pain [Internet]. 2013 Jun 22 [cited 2018 Mar 16];9:30. Available from: http://www.ncbi.nlm.nih.gov/pubmed/23800232
56. Wang S, Chuang H-H. C-terminal Dimerization Activates the Nociceptive Transduction Channel Transient Receptor Potential Vanilloid 1 *. Publ JBC Pap Press [Internet]. 2011 [cited 2017 Jul 5]; Available from: http://pubmedcentralcanada.ca/pmcc/articles/PMC3220497/pdf/zbc40601.pdf
57. Dhaka A, Uzzell V, Dubin AE, Mathur J, Petrus M, Bandell M, et al. TRPV1 is activated by both acidic and basic pH. J Neurosci [Internet]. 2009 Jan 7 [cited 2018 Mar 16];29(1):153–8. Available from: http://www.ncbi.nlm.nih.gov/pubmed/19129393
58. Liao M, Cao E, Julius D, Cheng Y. Structure of the TRPV1 ion channel determined by electron cryo-microscopy. Nature [Internet]. 2013 Dec 5 [cited 2018 Mar 14];504(7478):107–12. Available from: http://www.ncbi.nlm.nih.gov/pubmed/24305160
59. Sadofsky L, Sreekrishna K, Lin Y, Schinaman R, Gorka K, Mantri Y, et al. Unique Responses are Observed in Transient Receptor Potential Ankyrin 1 and Vanilloid 1 (TRPA1 and TRPV1) Co-Expressing Cells. Cells [Internet]. 2014 Jun 11 [cited 2018 Mar 14];3(4):616–26. Available from: http://www.ncbi.nlm.nih.gov/pubmed/24921186
60. Hellwig N, Albrecht N, Harteneck C, Schultz G, Schaefer M. Homo- and heteromeric assembly of TRPV channel subunits. J Cell Sci [Internet]. 2005 Mar 1 [cited 2018 Mar

14];118(Pt 5):917–28. Available from: http://www.ncbi.nlm.nih.gov/pubmed/15713749
61. Cao E, Liao M, Cheng Y, Julius D. TRPV1 structures in distinct conformations reveal activation mechanisms. Nature [Internet]. 2013 Dec 5 [cited 2018 Mar 15];504(7478):113–8. Available from: http://www.ncbi.nlm.nih.gov/pubmed/24305161
62. Liao M, Cao E, Julius D, Cheng Y. Structure of the TRPV1 ion channel determined by electron cryo-microscopy. Nature [Internet]. 2013 Dec 5 [cited 2018 Mar 15];504(7478):107–12. Available from: http://www.ncbi.nlm.nih.gov/pubmed/24305160
63. Gao Y, Cao E, Julius D, Cheng Y. TRPV1 structures in nanodiscs reveal mechanisms of ligand and lipid action. Nature [Internet]. 2016 May 18 [cited 2018 Mar 15];534(7607):347–51. Available from: http://www.ncbi.nlm.nih.gov/pubmed/27281200
64. Melnick C, Kaviany M. Thermal actuation in TRPV1: Role of embedded lipids and intracellular domains. J Theor Biol [Internet]. 2018 May 7 [cited 2018 Mar 15];444:38–49. Available from: http://www.ncbi.nlm.nih.gov/pubmed/29425725
65. Lundbaek JA, Birn P, Tape SE, Toombes GES, Søgaard R, Koeppe RE, et al. Capsaicin regulates voltage-dependent sodium channels by altering lipid bilayer elasticity. Mol Pharmacol [Internet]. 2005 Sep 1 [cited 2016 Feb 4];68(3):680–9. Available from: http://molpharm.aspetjournals.org/content/68/3/680.full
66. Salazar H, Llorente I, Jara-Oseguera A, García-Villegas R, Munari M, Gordon SE, et al. A single N-terminal cysteine in TRPV1 determines activation by pungent compounds from onion and garlic. Nat Neurosci [Internet]. 2008 Mar 24 [cited 2017 Jul 5];11(3):255–61. Available from: http://www.nature.com/doifinder/10.1038/nn2056
67. Salazar H, Jara-Oseguera A, Hernández-García E, Llorente I, Arias-Olguín II, Soriano-García M, et al. Structural determinants of gating in the TRPV1 channel. Nat Struct Mol Biol [Internet]. 2009 Jul 28 [cited 2018 Mar 16];16(7):704–10. Available from: http://www.nature.com/articles/nsmb.1633
68. Ogawa N, Kurokawa T, Fujiwara K, Polat OK, Badr H, Takahashi N, et al. Functional and Structural Divergence in Human TRPV1 Channel Subunits by Oxidative Cysteine Modification. J Biol Chem [Internet]. 2016 Feb 19 [cited 2018 Mar 16];291(8):4197–210. Available from: http://www.ncbi.nlm.nih.gov/pubmed/26702055
69. Keeble JE, Bodkin JV, Liang L, Wodarski R, Davies M, Fernandes ES, et al. Hydrogen peroxide is a novel mediator of inflammatory hyperalgesia, acting via transient receptor potential vanilloid 1-dependent and independent mechanisms. Pain [Internet]. 2009 Jan [cited 2018 Mar 16];141(1):135–42. Available from: http://content.wkhealth.com/linkback/openurl?sid=WKPTLP:landingpage&an=00006396-200901000-00022
70. Fernandes ES, Fernandes MA, Keeble JE. The functions of TRPA1 and TRPV1: moving away from sensory nerves. Br J Pharmacol [Internet]. 2012 May [cited 2018 Mar 12];166(2):510–21. Available from: http://www.ncbi.nlm.nih.gov/pubmed/22233379
71. Chuang H, Lin S. Oxidative challenges sensitize the capsaicin receptor by covalent cysteine modification. Proc Natl Acad Sci U S A [Internet]. 2009 Nov 24 [cited 2018 Mar 15];106(47):20097–102. Available from: http://www.ncbi.nlm.nih.gov/pubmed/19897733

72. Hargreaves KM, Ruparel S. Role of Oxidized Lipids and TRP Channels in Orofacial Pain and Inflammation. J Dent Res [Internet]. 2016 Sep 20 [cited 2018 Mar 16];95(10):1117–23. Available from: http://www.ncbi.nlm.nih.gov/pubmed/27307050
73. Ding R, Jiang H, Sun B, Wu X, Li W, Zhu S, et al. Advanced oxidation protein products sensitized the transient receptor potential vanilloid 1 via NADPH oxidase 1 and 4 to cause mechanical hyperalgesia. Redox Biol [Internet]. 2016 Dec [cited 2018 Mar 16];10:1–11. Available from: http://www.ncbi.nlm.nih.gov/pubmed/27665186
74. Poblete H, Oyarzún I, Olivero P, Comer J, Zuñiga M, Sepulveda R V., et al. Molecular Determinants of Phosphatidylinositol 4,5-Bisphosphate (PI(4,5)P $_2$) Binding to Transient Receptor Potential V1 (TRPV1) Channels. J Biol Chem [Internet]. 2015 Jan 23 [cited 2018 Mar 16];290(4):2086–98. Available from: http://www.ncbi.nlm.nih.gov/pubmed/25425643
75. Morales-Lázaro SL, Llorente I, Sierra-Ramírez F, López-Romero AE, Ortíz-Rentería M, Serrano-Flores B, et al. Inhibition of TRPV1 channels by a naturally occurring omega-9 fatty acid reduces pain and itch. Nat Commun [Internet]. 2016 Oct 10 [cited 2018 Mar 16];7:13092. Available from: http://www.ncbi.nlm.nih.gov/pubmed/27721373
76. Morales-Lázaro SL, Rosenbaum T. A painful link between the TRPV1 channel and lysophosphatidic acid. Life Sci [Internet]. 2015 Mar 15 [cited 2018 Mar 16];125:15–24. Available from: http://www.ncbi.nlm.nih.gov/pubmed/25445434
77. Ibi M, Matsuno K, Shiba D, Katsuyama M, Iwata K, Kakehi T, et al. Reactive oxygen species derived from NOX1/NADPH oxidase enhance inflammatory pain. J Neurosci [Internet]. 2008 Sep 17 [cited 2018 Mar 15];28(38):9486–94. Available from: http://www.ncbi.nlm.nih.gov/pubmed/18799680
78. Li Q, Spencer NY, Oakley FD, Buettner GR, Engelhardt JF. Endosomal Nox2 facilitates redox-dependent induction of NF-kappaB by TNF-alpha. Antioxid Redox Signal [Internet]. 2009 Jun [cited 2014 Nov 10];11(6):1249–63. Available from: http://www.pubmedcentral.nih.gov/articlerender.fcgi?artid=2842115&tool=pmcentrez&rendertype=abstract
79. Bedard K, Krause K-H. The NOX family of ROS-generating NADPH oxidases: physiology and pathophysiology. Physiol Rev [Internet]. 2007 Jan [cited 2014 Sep 20];87(1):245–313. Available from: http://www.ncbi.nlm.nih.gov/pubmed/17237347
80. Li Q, Harraz MM, Zhou W, Zhang LN, Ding W, Zhang Y, et al. Nox2 and Rac1 regulate H2O2-dependent recruitment of TRAF6 to endosomal interleukin-1 receptor complexes. Mol Cell Biol [Internet]. 2006 Jan 1 [cited 2014 Oct 22];26(1):140–54. Available from: http://mcb.asm.org/content/26/1/140.long
81. Pal R, Basu Thakur P, Li S, Minard C, Rodney GG. Real-time imaging of NADPH oxidase activity in living cells using a novel fluorescent protein reporter. PLoS One [Internet]. 2013 Jan [cited 2014 Nov 7];8(5):e63989. Available from: http://www.pubmedcentral.nih.gov/articlerender.fcgi?artid=3660327&tool=pmcentrez&rendertype=abstract
82. Spencer NY, Engelhardt JF. The basic biology of redoxosomes in cytokine-mediated signal transduction and implications for disease-specific therapies. Biochemistry [Internet]. 2014 Mar 18 [cited 2018 Jun 27];53(10):1551–64. Available from: http://www.ncbi.nlm.nih.gov/pubmed/24555469
83. Petry A, Weitnauer M, Görlach A. Receptor activation of NADPH oxidases. Antioxid Redox Signal [Internet]. 2010 Aug 15 [cited 2014 Nov 10];13(4):467–87. Available from:

http://www.ncbi.nlm.nih.gov/pubmed/20001746
84. Reczek CR, Chandel NS. ROS-dependent signal transduction. Curr Opin Cell Biol [Internet]. 2014 Oct 8 [cited 2014 Oct 12];33C:8–13. Available from: http://www.ncbi.nlm.nih.gov/pubmed/25305438
85. Maher P, Schubert D. Signaling by reactive oxygen species in the nervous system. Cell Mol Life Sci [Internet]. 2000 Aug [cited 2014 Nov 10];57(8–9):1287–305. Available from: http://www.ncbi.nlm.nih.gov/pubmed/11028919
86. Oakley FD, Abbott D, Li Q, Engelhardt JF. Signaling components of redox active endosomes: the redoxosomes. Antioxid Redox Signal [Internet]. 2009 Jun [cited 2014 Nov 10];11(6):1313–33. Available from: http://www.pubmedcentral.nih.gov/articlerender.fcgi?artid=2842130&tool=pmcentrez&rendertype=abstract
87. Deshpande SS, Angkeow P, Huang J, Ozaki M, Irani K. Rac1 inhibits TNF-alpha-induced endothelial cell apoptosis: dual regulation by reactive oxygen species. FASEB J [Internet]. 2000 Sep [cited 2014 Nov 7];14(12):1705–14. Available from: http://www.ncbi.nlm.nih.gov/pubmed/10973919
88. Frey RS, Rahman A, Kefer JC, Minshall RD, Malik AB. PKCzeta regulates TNF-alpha-induced activation of NADPH oxidase in endothelial cells. Circ Res [Internet]. 2002 May 17 [cited 2014 Nov 10];90(9):1012–9. Available from: http://www.ncbi.nlm.nih.gov/pubmed/12016268
89. Jefferies C, Bowie A, Brady G, Cooke EL, Li X, O'Neill LA. Transactivation by the p65 subunit of NF-kappaB in response to interleukin-1 (IL-1) involves MyD88, IL-1 receptor-associated kinase 1, TRAF-6, and Rac1. Mol Cell Biol [Internet]. 2001 Jul [cited 2014 Nov 10];21(14):4544–52. Available from: http://www.pubmedcentral.nih.gov/articlerender.fcgi?artid=87113&tool=pmcentrez&rendertype=abstract
90. Tammariello SP, Quinn MT, Estus S. NADPH oxidase contributes directly to oxidative stress and apoptosis in nerve growth factor-deprived sympathetic neurons. J Neurosci [Internet]. 2000 Jan 1 [cited 2014 Oct 20];20(1):RC53. Available from: http://www.ncbi.nlm.nih.gov/pubmed/10627630
91. Cox JA, Jeng AY, Sharkey NA, Blumberg PM, Tauber AI. Activation of the human neutrophil nicotinamide adenine dinucleotide phosphate (NADPH)-oxidase by protein kinase C. J Clin Invest [Internet]. 1985 Nov [cited 2018 Mar 16];76(5):1932–8. Available from: http://www.ncbi.nlm.nih.gov/pubmed/2997297
92. Lin C-S, Lee S-H, Huang H-S, Chen Y-S, Ma M-C. H 2 O 2 generated by NADPH oxidase 4 contributes to transient receptor potential vanilloid 1 channel-mediated mechanosensation in the rat kidney. [cited 2018 Mar 16]; Available from: https://pdfs.semanticscholar.org/14fd/d5a7cc35aaf2c922b2b69e53c87e42d039a9.pdf
93. Brenner R, Baskaran P, Thyagarajan B. Regulation of TRPV1 Expression in Non-Neuronal Tissues by BDNF, Sp1, and Sp4. Biophys J [Internet]. 2018 Feb 2 [cited 2018 Mar 12];114(3):483a. Available from: https://www.sciencedirect.com/science/article/pii/S0006349517338869
94. Watanabe N, Horie S, Michael GJ, Spina D, Page CP, Priestley J V. Immunohistochemical localization of vanilloid receptor subtype 1 (TRPV1) in the guinea pig respiratory system. Pulm Pharmacol Ther [Internet]. 2005 Jun [cited 2018 Mar 12];18(3):187–97. Available from: http://www.ncbi.nlm.nih.gov/pubmed/15707853

95. Uchida K, Dezaki K, Yoneshiro T, Watanabe T, Yamazaki J, Saito M, et al. Involvement of thermosensitive TRP channels in energy metabolism. J Physiol Sci [Internet]. 2017 Sep 27 [cited 2018 Mar 11];67(5):549–60. Available from: http://www.ncbi.nlm.nih.gov/pubmed/28656459
96. Miyake T, Shirakawa H, Nakagawa T, Kaneko S. Activation of mitochondrial transient receptor potential vanilloid 1 channel contributes to microglial migration. Glia [Internet]. 2015 Oct [cited 2016 Feb 8];63(10):1870–82. Available from: http://www.ncbi.nlm.nih.gov/pubmed/26010461
97. Bennion D, Jensen T, Walther C, Hamblin J, Wallmann A, Couch J, et al. Transient receptor potential vanilloid 1 agonists modulate hippocampal CA1 LTP via the GABAergic system. Neuropharmacology [Internet]. 2011 Sep [cited 2018 Mar 12];61(4):730–8. Available from: http://www.ncbi.nlm.nih.gov/pubmed/21645527
98. Cavanaugh DJ, Chesler AT, Bráz JM, Shah NM, Julius D, Basbaum AI. Restriction of transient receptor potential vanilloid-1 to the peptidergic subset of primary afferent neurons follows its developmental downregulation in nonpeptidergic neurons. J Neurosci [Internet]. 2011 Jul 13 [cited 2018 Mar 12];31(28):10119–27. Available from: http://www.ncbi.nlm.nih.gov/pubmed/21752988
99. Hjerling-Leffler J, AlQatari M, Ernfors P, Koltzenburg M. Emergence of Functional Sensory Subtypes as Defined by Transient Receptor Potential Channel Expression. J Neurosci [Internet]. 2007 Mar 7 [cited 2018 Mar 12];27(10):2435–43. Available from: http://www.ncbi.nlm.nih.gov/pubmed/17344381
100. Ramírez-Barrantes R, Cordova C, Poblete H, Muñoz P, Marchant I, Wianny F, et al. Perspectives of TRPV1 Function on the Neurogenesis and Neural Plasticity.
101. Marsch R, Foeller E, Rammes G, Bunck M, Kössl M, Holsboer F, et al. Reduced anxiety, conditioned fear, and hippocampal long-term potentiation in transient receptor potential vanilloid type 1 receptor-deficient mice. J Neurosci [Internet]. 2007 Jan 24 [cited 2018 Mar 12];27(4):832–9. Available from: http://www.ncbi.nlm.nih.gov/pubmed/17251423
102. Cristino L, de Petrocellis L, Pryce G, Baker D, Guglielmotti V, Di Marzo V. Immunohistochemical localization of cannabinoid type 1 and vanilloid transient receptor potential vanilloid type 1 receptors in the mouse brain. Neuroscience [Internet]. 2006 Jan 1 [cited 2018 Mar 12];139(4):1405–15. Available from: https://www.sciencedirect.com/science/article/pii/S0306452206002405
103. Tóth A, Boczán J, Kedei N, Lizanecz E, Bagi Z, Papp Z, et al. Expression and distribution of vanilloid receptor 1 (TRPV1) in the adult rat brain. Mol Brain Res [Internet]. 2005 Apr 27 [cited 2018 Mar 12];135(1–2):162–8. Available from: https://www.sciencedirect.com/science/article/pii/S0169328X04006242
104. Li H-B, Mao R-R, Zhang J-C, Yang Y, Cao J, Xu L. Antistress Effect of TRPV1 Channel on Synaptic Plasticity and Spatial Memory. Biol Psychiatry [Internet]. 2008 Aug 15 [cited 2018 Mar 12];64(4):286–92. Available from: http://www.ncbi.nlm.nih.gov/pubmed/18405883
105. Brown TE, Chirila AM, Schrank BR, Kauer JA. Loss of interneuron LTD and attenuated pyramidal cell LTP in *Trpv1* and *Trpv3* KO mice. Hippocampus [Internet]. 2013 Aug [cited 2018 Mar 12];23(8):662–71. Available from: http://www.ncbi.nlm.nih.gov/pubmed/23536486
106. Gebhardt C, Albrecht D. Glutamate receptor GluA1 subunit is implicated in capsaicin induced modulation of amygdala LTP but not LTD. Learn Mem [Internet]. 2018 Jan 15

[cited 2018 Mar 12];25(1):1–7. Available from: http://www.ncbi.nlm.nih.gov/pubmed/29246976
107. Medvedeva Y V., Kim M-S, Usachev YM. Mechanisms of Prolonged Presynaptic Ca2+ Signaling and Glutamate Release Induced by TRPV1 Activation in Rat Sensory Neurons. J Neurosci [Internet]. 2008 May 14 [cited 2018 Mar 12];28(20):5295–311. Available from: http://www.jneurosci.org/cgi/doi/10.1523/JNEUROSCI.4810-07.2008
108. Gibbons CH, Wang N, Freeman R. Capsaicin induces degeneration of cutaneous autonomic nerve fibers. Ann Neurol [Internet]. 2010 Dec [cited 2018 Mar 16];68(6):888–98. Available from: http://www.ncbi.nlm.nih.gov/pubmed/21061393
109. Sann H, Jancsó G, Ambrus A, Pierau F-K. Capsaicin treatment induces selective sensory degeneration and increased sympathetic innervation in the rat ureter. Neuroscience [Internet]. 1995 Aug 1 [cited 2018 Mar 16];67(4):953–66. Available from: https://www.sciencedirect.com/science/article/pii/030645229500102O
110. Jancso G, Király E, Joó F, Such G, Nagy A. Selective degeneration by capsaicin of a subpopulation of primary sensory neurons in the adult rat. Neurosci Lett [Internet]. 1985 Aug 30 [cited 2018 Mar 16];59(2):209–14. Available from: https://www.sciencedirect.com/science/article/pii/0304394085902010
111. Wang DH, Wu W, Lookingland KJ. Degeneration of Capsaicin-Sensitive Sensory Nerves Leads to Increased Salt Sensitivity Through Enhancement of Sympathoexcitatory Response. [cited 2018 Mar 16]; Available from: http://hyper.ahajournals.org/content/hypertensionaha/37/2/440.full.pdf
112. Chiang H, Chang K-C, Kan H-W, Wu S-W, Tseng M-T, Hsueh H-W, et al. Physiological and pathological characterization of capsaicin-induced reversible nerve degeneration and hyperalgesia. Eur J Pain [Internet]. 2018 Feb 2 [cited 2018 Mar 16]; Available from: http://www.ncbi.nlm.nih.gov/pubmed/29392825
113. Şavk E. Neurologic Itch Management. In: Current problems in dermatology [Internet]. 2016 [cited 2018 Mar 16]. p. 116–23. Available from: http://www.ncbi.nlm.nih.gov/pubmed/27578080
114. Wang S, Wang S, Asgar J, Joseph J, Ro JY, Wei F, et al. Ca $^{2+}$ and calpain mediate capsaicin-induced ablation of axonal terminals expressing transient receptor potential vanilloid 1. J Biol Chem [Internet]. 2017 May 19 [cited 2018 Mar 16];292(20):8291–303. Available from: http://www.ncbi.nlm.nih.gov/pubmed/28360106
115. Chiang H, Ohno N, Hsieh Y-L, Mahad DJ, Kikuchi S, Komuro H, et al. Mitochondrial fission augments capsaicin-induced axonal degeneration. Acta Neuropathol [Internet]. 2015 Jan [cited 2018 Mar 16];129(1):81–96. Available from: http://www.ncbi.nlm.nih.gov/pubmed/25322817
116. Touska F, Marsakova L, Teisinger J, Vlachova V. A "cute" desensitization of TRPV1. Curr Pharm Biotechnol [Internet]. 2011 Jan 1 [cited 2018 Mar 16];12(1):122–9. Available from: http://www.ncbi.nlm.nih.gov/pubmed/20932251
117. Mroczko B, Groblewska M, Litman-Zawadzka A, Kornhuber J, Lewczuk P. Amyloid β oligomers (AβOs) in Alzheimer's disease. J Neural Transm [Internet]. 2018 Feb 1 [cited 2018 Mar 11];125(2):177–91. Available from: http://www.ncbi.nlm.nih.gov/pubmed/29196815
118. Chen L, Huang Z, Du Y, Fu M, Han H, Wang Y, et al. Capsaicin Attenuates Amyloid-β-Induced Synapse Loss and Cognitive Impairments in Mice. Wang Y-J, editor. J Alzheimer's Dis [Internet]. 2017 Jul 17 [cited 2018 Mar 11];59(2):683–94. Available from:

http://www.ncbi.nlm.nih.gov/pubmed/28671132
119. Xu W, Liu J, Ma D, Yuan G, Lu Y, Yang Y. Capsaicin reduces Alzheimer-associated tau changes in the hippocampus of type 2 diabetes rats. Hu C, editor. PLoS One [Internet]. 2017 Feb 22 [cited 2018 Mar 11];12(2):e0172477. Available from: http://dx.plos.org/10.1371/journal.pone.0172477
120. Razavinasab M, Shamsizadeh A, Shabani M, Nazeri M, Allahtavakoli M, Asadi-Shekaari M, et al. Pharmacological blockade of TRPV1 receptors modulates the effects of 6-OHDA on motor and cognitive functions in a rat model of Parkinson's disease. Fundam Clin Pharmacol [Internet]. 2013 Dec [cited 2018 Mar 11];27(6):632–40. Available from: http://www.ncbi.nlm.nih.gov/pubmed/23216087
121. Nam JH, Park ES, Won S-Y, Lee YA, Kim KI, Jeong JY, et al. TRPV1 on astrocytes rescues nigral dopamine neurons in Parkinson's disease via CNTF. Brain [Internet]. 2015 Dec [cited 2018 Mar 11];138(Pt 12):3610–22. Available from: http://www.ncbi.nlm.nih.gov/pubmed/26490328
122. von Bohlen und Halbach O, Unsicker K. Neurotrophic support of midbrain dopaminergic neurons. Adv Exp Med Biol [Internet]. 2009 [cited 2018 Mar 11];651:73–80. Available from: http://www.ncbi.nlm.nih.gov/pubmed/19731552
123. Chung YC, Baek JY, Kim SR, Ko HW, Bok E, Shin W-H, et al. Capsaicin prevents degeneration of dopamine neurons by inhibiting glial activation and oxidative stress in the MPTP model of Parkinson's disease. Exp Mol Med [Internet]. 2017 Mar 3 [cited 2018 Mar 12];49(3):e298–e298. Available from: http://www.ncbi.nlm.nih.gov/pubmed/28255166
124. Sappington RM, Sidorova T, Long DJ, Calkins DJ. TRPV1: contribution to retinal ganglion cell apoptosis and increased intracellular Ca2+ with exposure to hydrostatic pressure. Invest Ophthalmol Vis Sci [Internet]. 2009 Feb 1 [cited 2018 Mar 11];50(2):717–28. Available from: http://iovs.arvojournals.org/article.aspx?doi=10.1167/iovs.08-2321
125. Ward NJ, Ho KW, Lambert WS, Weitlauf C, Calkins DJ. Absence of Transient Receptor Potential Vanilloid-1 Accelerates Stress-Induced Axonopathy in the Optic Projection. J Neurosci [Internet]. 2014 Feb 26 [cited 2018 Mar 11];34(9):3161–70. Available from: http://www.ncbi.nlm.nih.gov/pubmed/24573275
126. Ho KW, Lambert WS, Calkins DJ. Activation of the TRPV1 cation channel contributes to stress-induced astrocyte migration. Glia [Internet]. 2014 Sep 1 [cited 2018 Mar 11];62(9):1435–51. Available from: http://doi.wiley.com/10.1002/glia.22691
127. Han Z, Liu X, Luo Y, Ji X. Therapeutic hypothermia for stroke: Where to go? Exp Neurol [Internet]. 2015 Oct 1 [cited 2018 Mar 11];272:67–77. Available from: https://www.sciencedirect.com/science/article/pii/S0014488615300170?via%3Dihub
128. Cao Z, Balasubramanian A, Marrelli SP. Pharmacologically induced hypothermia via TRPV1 channel agonism provides neuroprotection following ischemic stroke when initiated 90 min after reperfusion. Am J Physiol Integr Comp Physiol [Internet]. 2014 Jan 15 [cited 2018 Mar 11];306(2):R149–56. Available from: http://www.physiology.org/doi/10.1152/ajpregu.00329.2013
129. Cao Z, Balasubramanian A, Pedersen SE, Romero J, Pautler RG, Marrelli SP. TRPV1-mediated Pharmacological Hypothermia Promotes Improved Functional Recovery Following Ischemic Stroke. Sci Rep [Internet]. 2017 Dec 15 [cited 2018 Mar 11];7(1):17685. Available from: http://www.ncbi.nlm.nih.gov/pubmed/29247238
130. Akpınar H, Nazıroğlu M, Övey İS, Çiğ B, Akpınar O. The neuroprotective action of

dexmedetomidine on apoptosis, calcium entry and oxidative stress in cerebral ischemia-induced rats: Contribution of TRPM2 and TRPV1 channels. Sci Rep [Internet]. 2016 Nov 22 [cited 2018 Mar 11];6:37196. Available from: http://www.ncbi.nlm.nih.gov/pubmed/27872485
131. Ren F, Zhang H, Qi C, Gao M, Wang H, Li X. Blockade of transient receptor potential cation channel subfamily V member 1 promotes regeneration after sciatic nerve injury. Neural Regen Res [Internet]. 2015 Aug [cited 2018 Mar 12];10(8):1324. Available from: http://www.ncbi.nlm.nih.gov/pubmed/26487864
132. Schampel A, Kuerten S. Danger: High Voltage—The Role of Voltage-Gated Calcium Channels in Central Nervous System Pathology. Cells [Internet]. 2017 Nov 15 [cited 2017 Nov 29];6(4):43. Available from: http://www.ncbi.nlm.nih.gov/pubmed/29140302
133. Eichler ME, Dubinsky JM, Rich KM. Relationship of intracellular calcium to dependence on nerve growth factor in dorsal root ganglion neurons in cell culture. J Neurochem [Internet]. 1992 Jan [cited 2017 Nov 29];58(1):263–9. Available from: http://www.ncbi.nlm.nih.gov/pubmed/1727434
134. Rich KM, Hollowell JP. Flunarizine protects neurons from death after axotomy or NGF deprivation. Science [Internet]. 1990 Jun 15 [cited 2017 Nov 29];248(4961):1419–21. Available from: http://www.ncbi.nlm.nih.gov/pubmed/2356470
135. Singh A, Verma P, Raju A, Mohanakumar KP. Nimodipine attenuates the parkinsonian neurotoxin, MPTP-induced changes in the calcium binding proteins, calpain and calbindin. J Chem Neuroanat [Internet]. 2018 Feb 7 [cited 2018 Mar 5]; Available from: http://www.ncbi.nlm.nih.gov/pubmed/29427747
136. Hui KKW, Liadis N, Robertson J, Kanungo A, Henderson JT. Calcineurin inhibition enhances motor neuron survival following injury. J Cell Mol Med [Internet]. 2010 Mar [cited 2017 Aug 22];14(3):671–86. Available from: http://www.ncbi.nlm.nih.gov/pubmed/19243469
137. Eichler ME, Dubinsky JM, Tong J, Rich KM. The Ability of Diphenylpiperazines to Prevent Neuronal Death in Dorsal Root Ganglion Neurons In Vitro After Nerve Growth Factor Deprivation and In Vivo After Axotomy. J Neurochem [Internet]. 1994 Jun 28 [cited 2017 Nov 29];62(6):2148–57. Available from: http://doi.wiley.com/10.1046/j.1471-4159.1994.62062148.x
138. Villegas R, Martinez NW, Lillo J, Pihan P, Hernandez D, Twiss JL, et al. Calcium release from intra-axonal endoplasmic reticulum leads to axon degeneration through mitochondrial dysfunction. J Neurosci [Internet]. 2014 May 21 [cited 2016 Jan 17];34(21):7179–89. Available from: /pmcc/articles/PMC4028495/?report=abstract
139. Mackay JP, Nassrallah WB, Raymond LA. Cause or compensation?-Altered neuronal Ca^{2+} handling in Huntington's disease. CNS Neurosci Ther [Internet]. 2018 Feb 9 [cited 2018 Mar 5]; Available from: http://www.ncbi.nlm.nih.gov/pubmed/29427371
140. Tan AR, Cai AY, Deheshi S, Rintoul GL. Elevated intracellular calcium causes distinct mitochondrial remodelling and calcineurin-dependent fission in astrocytes. Cell Calcium [Internet]. 2011 Feb [cited 2017 Aug 22];49(2):108–14. Available from: http://www.ncbi.nlm.nih.gov/pubmed/21216007
141. Shirakawa H, Yamaoka T, Sanpei K, Sasaoka H, Nakagawa T, Kaneko S. TRPV1 stimulation triggers apoptotic cell death of rat cortical neurons. Biochem Biophys Res Commun. 2008;377:1211–5.
142. Ren F, Zhang H, Qi C, Gao M-L, Wang H, Li X-Q. Blockade of transient receptor potential

cation channel subfamily V member 1 promotes regeneration after sciatic nerve injury. Neural Regen Res [Internet]. 2015 Aug [cited 2018 Mar 12];10(8):1324–31. Available from: http://www.ncbi.nlm.nih.gov/pubmed/26487864
143. Sappington RM, Sidorova T, Ward NJ, Chakravarthy R, Ho KW, Calkins DJ. Activation of transient receptor potential vanilloid-1 (TRPV1) influences how retinal ganglion cell neurons respond to pressure-related stress. Channels [Internet]. 2015 Mar 4 [cited 2018 Mar 11];9(2):102–13. Available from: http://www.ncbi.nlm.nih.gov/pubmed/25713995
144. Siesjö BK, Bengtsson F, Grampp W, Theander S. Calcium, excitotoxins, and neuronal death in the brain. Ann N Y Acad Sci [Internet]. 1989 [cited 2018 Mar 29];568:234–51. Available from: http://www.ncbi.nlm.nih.gov/pubmed/2576507
145. Deheshi S, Dabiri B, Fan S, Tsang M, Rintoul GL. Changes in mitochondrial morphology induced by calcium or rotenone in primary astrocytes occur predominantly through ros-mediated remodeling. J Neurochem. 2015;
146. Mattson MP. Calcium and neurodegeneration. Aging Cell [Internet]. 2007 Jun [cited 2018 Mar 16];6(3):337–50. Available from: http://www.ncbi.nlm.nih.gov/pubmed/17328689
147. Yang J, Weimer RM, Kallop D, Olsen O, Wu Z, Renier N, et al. Regulation of axon degeneration after injury and in development by the endogenous calpain inhibitor calpastatin. Neuron [Internet]. 2013 Dec 4 [cited 2018 Mar 29];80(5):1175–89. Available from: http://www.ncbi.nlm.nih.gov/pubmed/24210906
148. Hajnóczky G, Csordás G, Das S, Garcia-Perez C, Saotome M, Sinha Roy S, et al. Mitochondrial calcium signalling and cell death: approaches for assessing the role of mitochondrial Ca2+ uptake in apoptosis. Cell Calcium [Internet]. Jan [cited 2015 Nov 19];40(5–6):553–60. Available from: http://www.pubmedcentral.nih.gov/articlerender.fcgi?artid=2692319&tool=pmcentrez&rendertype=abstract
149. Salazar H, Llorente I, Jara-Oseguera A, García-Villegas R, Munari M, Gordon SE, et al. A single N-terminal cysteine in TRPV1 determines activation by pungent compounds from onion and garlic. Nat Neurosci [Internet]. 2008 Mar 24 [cited 2018 Mar 15];11(3):255–61. Available from: http://www.ncbi.nlm.nih.gov/pubmed/18297068
150. Kallenborn-Gerhardt W, Hohmann SW, Syhr KMJ, Schröder K, Sisignano M, Weigert A, et al. Nox2-dependent signaling between macrophages and sensory neurons contributes to neuropathic pain hypersensitivity. Pain [Internet]. 2014 Oct [cited 2014 Oct 20];155(10):2161–70. Available from: http://www.ncbi.nlm.nih.gov/pubmed/25139590
151. Cosentino-Gomes D, Rocco-Machado N, Meyer-Fernandes JR. Cell signaling through protein kinase C oxidation and activation. Int J Mol Sci [Internet]. 2012 [cited 2018 Apr 1];13(9):10697–721. Available from: http://www.ncbi.nlm.nih.gov/pubmed/23109817
152. Nazıroğlu M. Activation of TRPM2 and TRPV1 Channels in Dorsal Root Ganglion by NADPH Oxidase and Protein Kinase C Molecular Pathways: a Patch Clamp Study. J Mol Neurosci [Internet]. 2017 Mar 17 [cited 2018 Apr 1];61(3):425–35. Available from: http://www.ncbi.nlm.nih.gov/pubmed/28097492
153. Ibi M, Matsuno K, Shiba D, Katsuyama M, Iwata K, Kakehi T, et al. Reactive oxygen species derived from NOX1/NADPH oxidase enhance inflammatory pain. J Neurosci [Internet]. 2008 Sep 17 [cited 2018 Mar 16];28(38):9486–94. Available from: http://www.ncbi.nlm.nih.gov/pubmed/18799680
154. Gotoh Y, Cooper JA. Reactive oxygen species- and dimerization-induced activation of

apoptosis signal-regulating kinase 1 in tumor necrosis factor-alpha signal transduction. J Biol Chem [Internet]. 1998 Jul 10 [cited 2014 Nov 4];273(28):17477–82. Available from: http://www.ncbi.nlm.nih.gov/pubmed/9651337
155. Rosasco MG, Gordon SE. TRP Channels: What Do They Look Like? [Internet]. Neurobiology of TRP Channels. 2017 [cited 2018 Mar 14]. Available from: http://www.ncbi.nlm.nih.gov/pubmed/29356490
156. Salazar H, Llorente I, Jara-Oseguera A, García-Villegas R, Munari M, Gordon SE, et al. A single N-terminal cysteine in TRPV1 determines activation by pungent compounds from onion and garlic. Nat Neurosci [Internet]. 2008 Mar 24 [cited 2018 Mar 16];11(3):255–61. Available from: http://www.nature.com/articles/nn2056
157. Hilburger EW, Conte EJ, McGee DW, Tammariello SP. Localization of NADPH oxidase subunits in neonatal sympathetic neurons. Neurosci Lett [Internet]. 2005 Mar 22 [cited 2014 Oct 20];377(1):16–9. Available from: http://www.ncbi.nlm.nih.gov/pubmed/15722179
158. Cao X, Demel SL, Quinn MT, Galligan JJ, Kreulen D. Localization of NADPH oxidase in sympathetic and sensory ganglion neurons and perivascular nerve fibers. Auton Neurosci [Internet]. 2009 Dec 3 [cited 2014 Oct 20];151(2):90–7. Available from: http://www.pubmedcentral.nih.gov/articlerender.fcgi?artid=2783262&tool=pmcentrez&rendertype=abstract
159. Geiszt M, Lekstrom K, Witta J, Leto TL. Proteins homologous to p47phox and p67phox support superoxide production by NAD(P)H oxidase 1 in colon epithelial cells. J Biol Chem [Internet]. 2003 May 30 [cited 2014 Nov 8];278(22):20006–12. Available from: http://www.jbc.org/content/278/22/20006?ijkey=91d5f6e627439953162c9dbb6190b7cb29ee6142&keytype2=tf_ipsecsha
160. Lucke-Wold BP, Turner RC, Logsdon AF, Simpkins JW, Alkon DL, Smith KE, et al. Common mechanisms of Alzheimer's disease and ischemic stroke: the role of protein kinase C in the progression of age-related neurodegeneration. J Alzheimers Dis [Internet]. 2015 [cited 2017 Apr 27];43(3):711–24. Available from: http://www.ncbi.nlm.nih.gov/pubmed/25114088
161. Carrasco C, Naziroğlu M, Rodríguez AB, Pariente JA. Neuropathic Pain: Delving into the Oxidative Origin and the Possible Implication of Transient Receptor Potential Channels. Front Physiol [Internet]. 2018 Feb 14 [cited 2018 Mar 26];9:95. Available from: http://www.ncbi.nlm.nih.gov/pubmed/29491840
162. Liu M, Liu M-C, Magoulas C, Priestley J V, Willmott NJ. Versatile regulation of cytosolic Ca2+ by vanilloid receptor I in rat dorsal root ganglion neurons. J Biol Chem [Internet]. 2003 Feb 14 [cited 2016 Feb 4];278(7):5462–72. Available from: http://www.jbc.org/content/278/7/5462.full
163. Nassini R, Pedretti P, Moretto N, Fusi C, Carnini C, Facchinetti F, et al. Transient Receptor Potential Ankyrin 1 Channel Localized to Non-Neuronal Airway Cells Promotes Non-Neurogenic Inflammation. Guerrero-Hernandez A, editor. PLoS One [Internet]. 2012 Aug 14 [cited 2018 Mar 12];7(8):e42454. Available from: http://dx.plos.org/10.1371/journal.pone.0042454
164. Simon DJ, Weimer RM, McLaughlin T, Kallop D, Stanger K, Yang J, et al. A caspase cascade regulating developmental axon degeneration. J Neurosci [Internet]. 2012 Dec 5 [cited 2015 Nov 19];32(49):17540–53. Available from: http://www.scopus.com/inward/record.url?eid=2-s2.0-

84870481635&partnerID=tZOtx3y1
165. Öztürk G, Cengiz N, Erdoğan E, Him A, Oğuz EK, Yenidünya E, et al. Two distinct types of dying back axonal degeneration in vitro. Neuropathol Appl Neurobiol [Internet]. 2013 Jun [cited 2015 Nov 24];39(4):362–76. Available from: http://www.ncbi.nlm.nih.gov/pubmed/22845867
166. Unsain N, Bordenave MD, Martinez GF, Sami J, Von Bilderling C, Barabas FM, et al. Remodeling of the Actin/Spectrin Membrane-associated Periodic Skeleton, Growth Cone Collapse and F-Actin Decrease during Axonal Degeneration.
167. Ferrari G, Yan CY, Greene LA. N-acetylcysteine (D- and L-stereoisomers) prevents apoptotic death of neuronal cells. J Neurosci [Internet]. 1995 Apr [cited 2014 Nov 5];15(4):2857–66. Available from: http://www.ncbi.nlm.nih.gov/pubmed/7722634
168. Chao Yun IYLAG. Prevention of PC12 Cell Death by N-Acetylcysteine Requires Activation of the Ras Pathway. [cited 2014 Nov 5]; Available from: http://citeseerx.ist.psu.edu/viewdoc/summary?doi=10.1.1.328.671
169. Zareen N, Biswas SC, Greene LA. A feed-forward loop involving Trib3, Akt and FoxO mediates death of NGF-deprived neurons. Cell Death Differ [Internet]. 2013 Dec [cited 2014 Nov 12];20(12):1719–30. Available from: http://www.ncbi.nlm.nih.gov/pubmed/24212932
170. Altenhöfer S, Kleikers PWM, Radermacher KA, Scheurer P, Rob Hermans JJ, Schiffers P, et al. The NOX toolbox: validating the role of NADPH oxidases in physiology and disease. Cell Mol Life Sci [Internet]. 2012 Jul [cited 2018 Mar 24];69(14):2327–43. Available from: http://www.ncbi.nlm.nih.gov/pubmed/22648375
171. Wind S, Beuerlein K, Eucker T, Müller H, Scheurer P, Armitage M, et al. Comparative pharmacology of chemically distinct NADPH oxidase inhibitors. Br J Pharmacol [Internet]. 2010 Oct 1 [cited 2018 Mar 24];161(4):885–98. Available from: http://doi.wiley.com/10.1111/j.1476-5381.2010.00920.x
172. Wingler K, Altenhoefer SA, Kleikers PWM, Radermacher KA, Kleinschnitz C, Schmidt HHHW. VAS2870 is a pan-NADPH oxidase inhibitor. Cell Mol Life Sci [Internet]. 2012 Sep 9 [cited 2018 Mar 24];69(18):3159–60. Available from: http://www.ncbi.nlm.nih.gov/pubmed/22875281
173. Wakatsuki S, Furuno A, Ohshima M, Araki T. Oxidative stress-dependent phosphorylation activates ZNRF1 to induce neuronal/axonal degeneration. J Cell Biol [Internet]. 2015 Nov 23 [cited 2018 Jun 27];211(4):881–96. Available from: http://www.ncbi.nlm.nih.gov/pubmed/26572622
174. El-Benna J, Dang PM-C, Gougerot-Pocidalo M-A. Priming of the neutrophil NADPH oxidase activation: role of p47phox phosphorylation and NOX2 mobilization to the plasma membrane. Semin Immunopathol [Internet]. 2008 Jul [cited 2014 Nov 10];30(3):279–89. Available from: http://www.ncbi.nlm.nih.gov/pubmed/18536919
175. Zhao Y, Araki S, Wu J, Teramoto T, Chang Y-F, Nakano M, et al. An expanded palette of genetically encoded Ca^{2+} indicators. Science [Internet]. 2011 Sep 30 [cited 2018 Mar 24];333(6051):1888–91. Available from: http://www.ncbi.nlm.nih.gov/pubmed/21903779
176. Majima T, Funahashi Y, Takai S, Goins WF, Gotoh M, Tyagi P, et al. Herpes Simplex Virus Vector-Mediated Gene Delivery of Poreless TRPV1 Channels Reduces Bladder Overactivity and Nociception in Rats. Hum Gene Ther [Internet]. 2015 Nov [cited 2018 Mar 24];26(11):734–42. Available from:

http://www.ncbi.nlm.nih.gov/pubmed/26204493
177. Nishihara E, Hiyama TY, Noda M. Osmosensitivity of Transient Receptor Potential Vanilloid 1 Is Synergistically Enhanced by Distinct Activating Stimuli Such as Temperature and Protons. Barnes S, editor. PLoS One [Internet]. 2011 Jul 14 [cited 2018 Apr 4];6(7):e22246. Available from: http://dx.plos.org/10.1371/journal.pone.0022246
178. Wilkinson JA, Scragg JL, Boyle JP, Nilius B, Peers C. H2O2-stimulated Ca2+ influx via TRPM2 is not the sole determinant of subsequent cell death. Pflügers Arch - Eur J Physiol [Internet]. 2008 Mar 28 [cited 2018 Apr 4];455(6):1141–51. Available from: http://www.ncbi.nlm.nih.gov/pubmed/18043941
179. D'Amelio M, Cavallucci V, Cecconi F. Neuronal caspase-3 signaling: not only cell death. Cell Death Differ [Internet]. 2010 Jul [cited 2015 Nov 20];17(7):1104–14. Available from: http://dx.doi.org/10.1038/cdd.2009.180
180. Vogelbaum MA, Tong JX, Rich KM. Developmental regulation of apoptosis in dorsal root ganglion neurons. J Neurosci [Internet]. 1998 Nov 1 [cited 2014 Nov 9];18(21):8928–35. Available from: http://www.ncbi.nlm.nih.gov/pubmed/9786998
181. Chang LK, Schmidt RE, Johnson EM. Alternating metabolic pathways in NGF-deprived sympathetic neurons affect caspase-independent death. J Cell Biol [Internet]. 2003 Jul 21 [cited 2016 Feb 8];162(2):245–56. Available from: http://www.pubmedcentral.nih.gov/articlerender.fcgi?artid=2172806&tool=pmcentrez&rendertype=abstract
182. Stein AT, Ufret-Vincenty CA, Hua L, Santana LF, Gordon SE. Phosphoinositide 3-kinase binds to TRPV1 and mediates NGF-stimulated TRPV1 trafficking to the plasma membrane. J Gen Physiol [Internet]. 2006 Nov [cited 2018 Apr 5];128(5):509–22. Available from: http://www.ncbi.nlm.nih.gov/pubmed/17074976
183. Putney JW, Tomita T. Phospholipase C signaling and calcium influx. Adv Biol Regul [Internet]. 2012 Jan [cited 2018 Apr 5];52(1):152–64. Available from: http://www.ncbi.nlm.nih.gov/pubmed/21933679
184. Rohacs T, Thyagarajan B, Lukacs V. Phospholipase C Mediated Modulation of TRPV1 Channels. Mol Neurobiol [Internet]. 2008 Jun 5 [cited 2018 Apr 5];37(2–3):153–63. Available from: http://www.ncbi.nlm.nih.gov/pubmed/18528787
185. Chuang H, Prescott ED, Kong H, Shields S, Jordt S-E, Basbaum AI, et al. Bradykinin and nerve growth factor release the capsaicin receptor from PtdIns(4,5)P2-mediated inhibition. Nature [Internet]. 2001 Jun 21 [cited 2018 Apr 5];411(6840):957–62. Available from: http://www.ncbi.nlm.nih.gov/pubmed/11418861
186. Czeh G, Varga A, Sandor Z, Szolcsanyi J. Capsaicin-Induced Changes in the Cytosolic Calcium Level and Mitochondrial Membrane Potential. Neurophysiology [Internet]. 2005 Jan [cited 2016 Feb 4];37(1):76–87. Available from: http://link.springer.com/10.1007/s11062-005-0048-9